STANFORD RESEARCH INSTITUTE
MENLO PARK, CALIFORNIA

NASA 66275

December 1966

Final Report

USE OF THE LANGMUIR PROBE TO DETERMINE THE ELECTRON DENSITY AND TEMPERATURE SURROUNDING RE-ENTRY VEHICLES

Prepared for:

NATIONAL AERONAUTICS AND SPACE ADMINISTRATION
LANGLEY RESEARCH CENTER
LANGLEY STATION
HAMPTON, VIRGINIA 23365

CONTRACT NAS1-4872

By: W. E. SCHARFMAN H. R. BREDFELDT

SRI Project 5771

Approved: T. MORITA, MANAGER
ELECTROMAGNETIC SCIENCES LABORATORY

D. R. SCHEUCH, EXECUTIVE DIRECTOR
ELECTRONICS AND RADIO SCIENCES

Copy No. .....

ABSTRACT

The operation of a probe consisting of an electrode wire supported by a wedge-shaped dielectric structure, which was designed to fly on board the Langley Research Center RAM-C vehicle, was checked by comparison with wire probes and microwave interferometers in an arc-driven shock tube. Measurements were performed over a wide range of electron densities and at initial shock-tube pressures of 0.1 and 1.0 torr. The effect of yaw angle of up to 15 degrees was also checked. The measurements showed that the RAM-C probe could be interpreted in the same manner as a cylindrical-wire probe.

A theory has been developed, and measurements which confirm the theory have been performed, for a wedge-shaped electrode structure. This probe can be made to operate in an interpretable manner at altitudes for which the structure is large compared to the mean-free path. The theory assumes that the flow across the oblique shock formed around the probe is frozen. This assumption is analyzed theoretically for several simple cases.

Electron temperature measurements were made in the shock tube under conditions that were not free-molecular. Good agreement was obtained between the measured electron temperatures and the gas temperature.

An experiment was conducted to estimate how the probes would operate in an environment that includes water droplets. This sort of environment may be encountered during the RAM-C flight when water is injected into the flow field, upstream of the probes.

In this experiment, the electron density inferred from the probe current was compared to that measured by a microwave interferometer both before and during water-droplet injection into a seeded ethylene-oxygen flame. The relative changes in electron density, as inferred by both techniques,

followed each other closely. It was concluded that for the environment studied, the probe was not affected by the presence of water droplets. More refined experiments are required to ensure that this conclusion will apply to the flight-test environment.

ACKNOWLEDGMENTS

It is a pleasure to acknowledge the many stimulating discussions with H. Guthart of this laboratory. The shock tube measurements were all capably performed by J. Granville, as were the water droplet experiments by S. Dixon.

This report was prepared by Stanford Research Institute, Menlo Park, California and is the Final Report on NASA Contract NAS1-4872. This work was administered under the direction of Langley Station, Langley Research Center. Mr. Linwood Jones was the technical monitor.

CONTENTS

ILLUSTRATIONS

ILLUSTRATIONS (Continued)

TABLES

I INTRODUCTION

It is highly desirable to be able to measure the electron density in the flow field surrounding a re-entry vehicle in order to check the electron density calculations. The calculations depend in a complicated manner on a number of reactions that occur in the flow field, and uncertainties in the rates of these reactions are reflected as uncertainties in electron density. Measurements of electron density to a factor of 2 would significantly reduce the uncertainty.

There are a number of possible techniques for measuring electron density in an on-board flight experiment. The electrostatic probe technique is an attractive candidate for these measurements because of its wide dynamic range, good spatial resolution, and simple instrumentation. Previous work at SRI has demonstrated the usefulness of this technique for diagnosing supersonic, ionized flow fields with the required accuracy. In the work discussed in this report, the operation of a probe consisting of an electrode wire supported by a wedge-shaped dielectric structure, which was designed to fly on board the Langley Research Center RAM-C vehicle, was checked by comparison with wire probes and microwave interferometers in an arc-driven shock tube. Measurements were performed over a wide range of electron densities and at initial shock-tube pressures (p_1) of 0.1 and 1.0 torr. The effect of yaw angles up to 15 degrees was also measured.

In addition, measurements were made on another form of wedge-shaped probe which may prove useful in circumventing possible difficulties with the RAM-C probe. A theory has been developed for the interpretation of this probe operation, and it is consistent with the measured results.

Electrostatic probes can be used to measure electron temperature under free-molecular conditions, however, until recently the applicability of probes for measurement of electron temperature under conditions which are not strictly free-molecular, and in the presence of a supersonic

neutral gas flow, had not been verified. In the work reported herein, electron temperature measurements under these conditions have been made in the shock tube. Good agreement was obtained between the measured electron temperature and the gas temperature.

Section IV of this report describes an experiment that was conducted to determine the operation of the probes in an environment containing water droplets of the order of 100 microns in diameter. This sort of environment may be encountered during the RAM-C flight when water is injected into the flow field upstream of the probes.

In this experiment the electron density inferred from the probe current was compared to that measured by a microwave interferometer, both before and during water-droplet injection into a seeded ethylene-oxygen flame. The relative changes in electron density, as inferred by both techniques, showed close agreement. Since the microwave technique was not affected by the water droplets, the agreement between the probe and microwave inferred electron densities showed that the probes were operating correctly.

II ELECTROSTATIC PROBE THEORY

A. OPERATION OF CYLINDRICAL PROBES

Much of the probe theory used in inferring electron density from measured currents was outlined in Ref. 1.* That discussion will not be repeated here, but reference will be made to several of the figures in that report which summarize the results of the analysis.

Under free-molecular conditions, the curves of Fig. 1 describe the relation between probe current, electron density and temperature, flow velocity, and sheath-to-probe size for cylindrical probes in the ion saturation region. This region is defined by potentials between the probe and the plasma which are sufficiently negative that the electron current to the electrode is less than ten percent of the ion current.

The applicable symbols are defined as follows:

i_n = ratio of the measured current to the random current density times the physical area of the probe = I/AJ

I = measured current

A = Physical area of the probe = $2\pi r_p L$

J = random ion current density = $n_+ e v_{th}/4$

v_{th} = thermal velocity of the ions = $(8kT_-/\pi M_+)^{1/2}$

T = electron temperature

η = ratio of potential to kinetic energy = eV/kT_-

V = probe-to-plasma potential = applied voltage + $5kT_-/e$

γ = ratio of sheath-to-probe radii = a/r_p

---

* References are given at the end of this report.

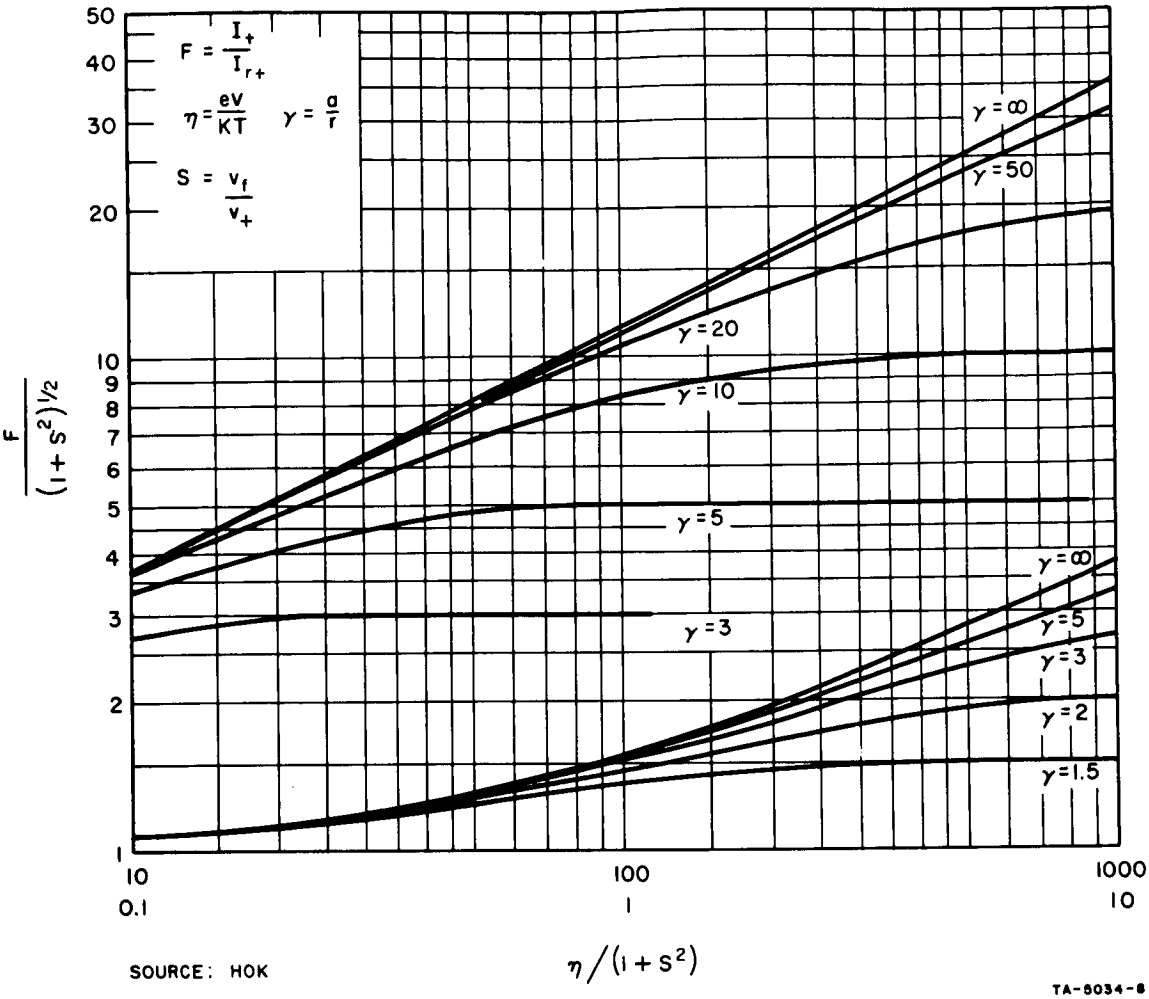

FIG. 1 NORMALIZED PROBE CURRENT AS A FUNCTION OF η, WITH a/r_p AS A PARAMETER

S = ratio of the normal component of the flow velocity to

$$(2kT_-/M_+)^{1/2} = \frac{v_f \sin\theta}{(2kT_-/M_+)^{1/2}}$$

θ = angle between the flow velocity and the cylinder axis.

The effect of angle θ was not discussed in Ref. 1, but analysis of the effects of flow velocity for different values of θ can be found in the work of Smetana and Kanal.[2,3] Figure 1 was calculated by Hok for a static plasma,[4] but when normalized as shown, it fits quite well with a

theory developed by Smetana for flowing plasmas. As discussed in Ref. 1, we demonstrated the applicability of Fig. 1 in supersonic plasma flows when a/r_p is not much greater than 1 and when $r_p \approx 2\lambda_{n-n}$ (neutral-neutral mean-free paths). The flow was not strictly free-molecular, and yet the theory still gave good results. In this report we extend these results to the case of large a/r_p.

Recently Laframboise[5] published a very sophisticated solution, which utilizes computer techniques, to solve the problem of a cylindrical probe under free-molecular, static conditions. He included as a variable the ratio of the ion-to-electron temperature (T_i/T_-). If his results for $T_i/T_- = 0$ are compared to the curves in Fig. 1, the results agree to about 10% for all values of η. For $T_i/T_- = 1$, his results change only slightly when $a/r_p > \sqrt{\eta + 1}$, but they are about 40% higher than the $T_i/T_- = 0$ results when $a/r_p \approx 1$. For the shock-tube case, $T_i/T_- \approx 1$; therefore, from Laframboise's results, use of Fig. 1 could give errors of up to 40%. However, since his analysis is applicable only to static plasmas, it is not clear that this correction will apply to the supersonic flowing plasma problem with which we are concerned in this report. All data in this report were interpreted using Fig. 1 and the gas temperature for T_-.

To determine the electron density from a measurement of current, an estimate of the ratio a/r_p is required. This can be obtained by manipulating the space-charge-limited diode equation in terms of the measured current and the other measurable parameter of length, probe radius, and probe voltage. The results are shown in Fig. 2.

B. THEORY OF RAM-C PROBE

In order to fly a cylindrical probe on a flight test, some support must be designed for the electrode and electrical leads to the instrumentation. The manner in which this is accomplished for the probes to be flown on the RAM-C flights is illustrated in Fig. 3. The ion-collecting electrode is mounted at the leading edge of a wedge structure. The wedge forms the mechanical support for the probe. If the wedge angle is sufficiently small and the Mach number sufficiently high, the shock is attached

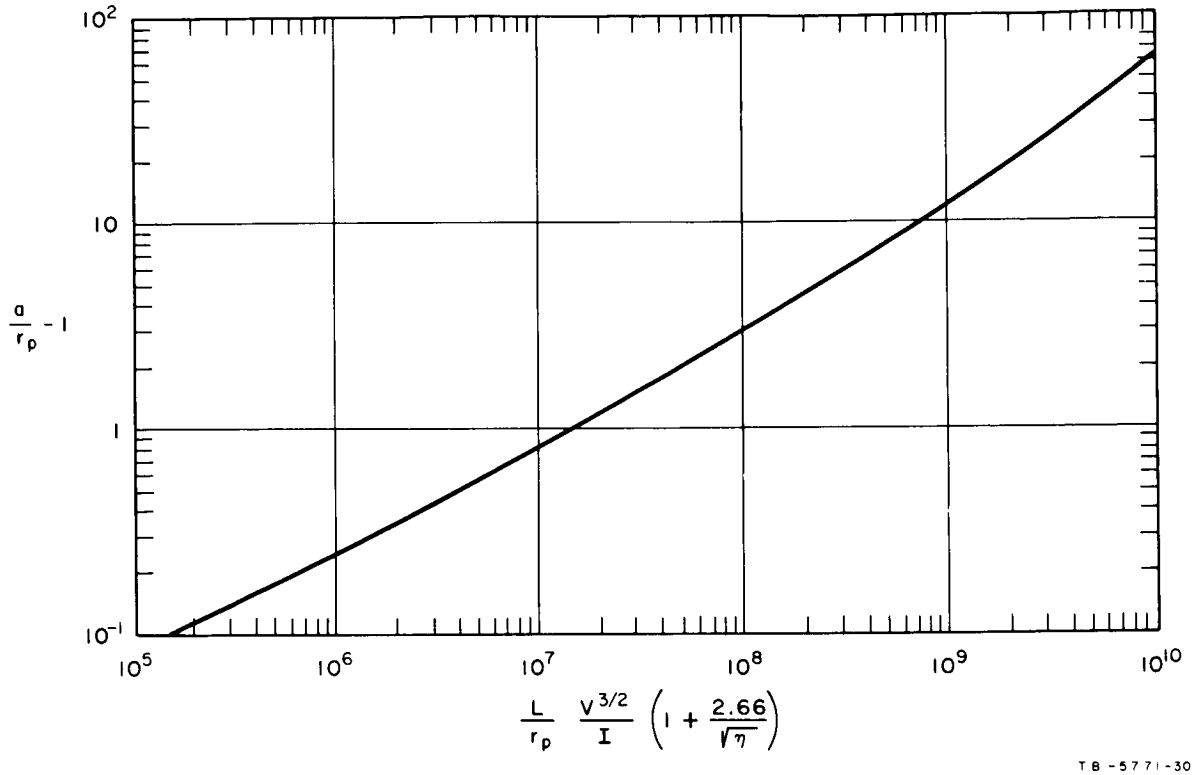

FIG. 2 a/r_p AS A FUNCTION OF THE MEASURED PARAMETERS

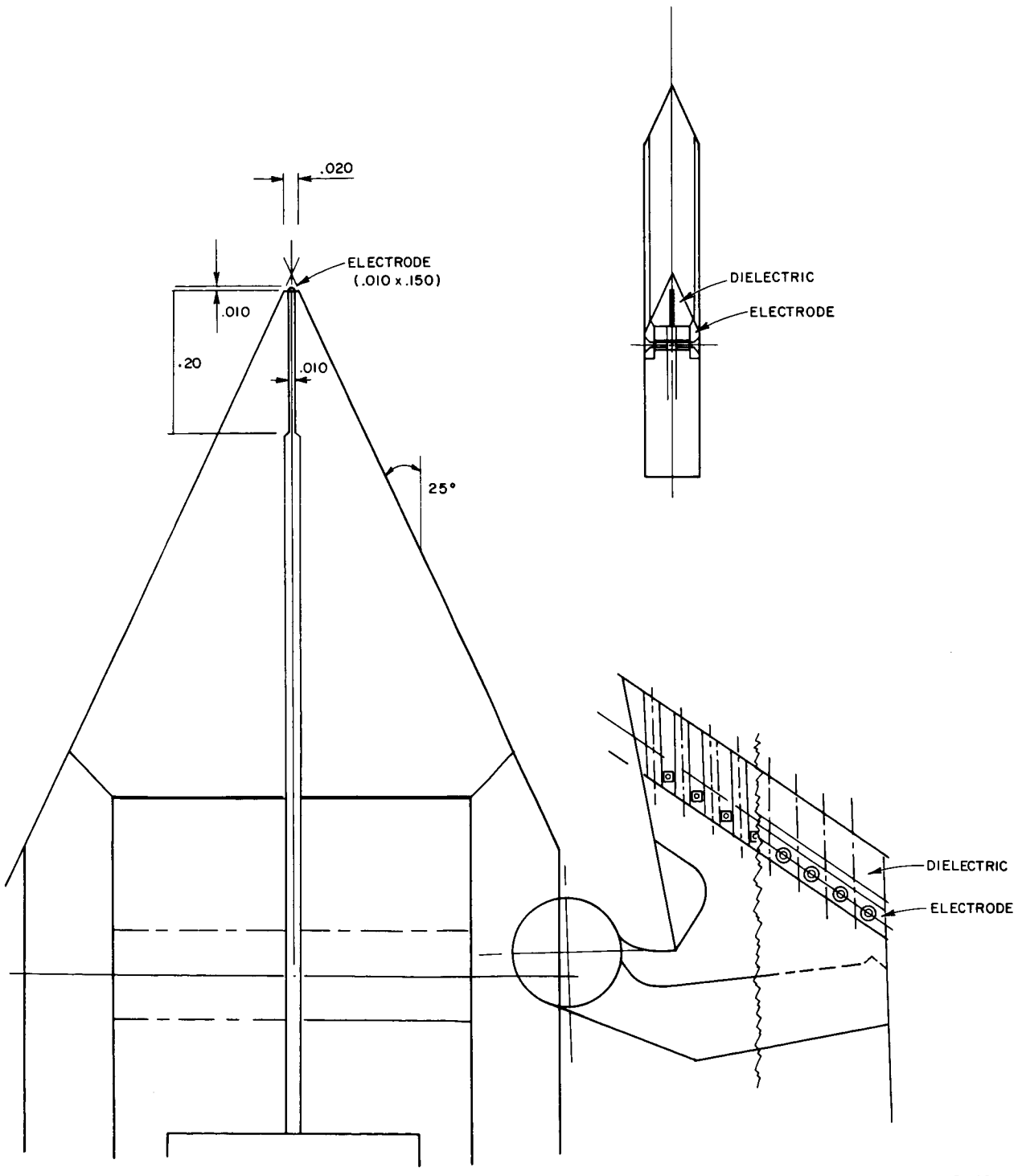

FIG. 3 DRAWING OF RAM-C PROBE

to the structure with no stagnation region. For the RAM-C probe, with a wedge half-angle of 25 degrees normal to the flow, the shock will remain attached if the Mach number is greater than about 2.2.

The importance of maintaining an attached shock is that as long as that condition holds and the leading edge is free-molecular, there is no stagnation region in which electron production mechanisms can operate to change the electron density at the electrode from the incident value. Although the electron density downstream of the leading edge may be changed due to the wedge structure, the electron density at the leading edge is unaffected. The electron density surrounding the downstream electrode does not determine the current collected by the leading-edge electrode as long as the area of the leading-edge electrode is smaller than the downstream electrode and both electrodes are immersed in plasmas of similar electron densities. If the electron density surrounding the downstream electrode is significantly lower than that surrounding the leading-edge electrode, it is possible for the downstream electrode to control the collected current. If the downstream electron density is higher, the leading-edge electrode controls the collected current.

When the mean-free path becomes much smaller than the leading-edge radius, a stagnation region can form near the leading edge. Then the possibility exists that electron production in the stagnation region will mask the incident plasma properties, and (if this is not correctly taken into account) large errors can be made in the inferred plasma properties. However, consideration of these effects involves an analysis of the ionization process behind the stagnation region, which depends upon the very rate constants that are in doubt. Therefore, unless it can be shown that the relaxation times for ionization in the stagnation region are much longer than the flow times, the usefulness of probes will be greatly diminished when shocks form around the electrodes.

The radius of the leading-edge electrode is 5 mils. This is equal to the ambient neutral-neutral mean-free path at an altitude of about 170 kft. At the probe station, the gas density in the flow field is approximately three times the ambient density; therefore, the leading

edge will be free-molecular down to an altitude of about 190 kft. Since the probe radius must be many times the mean-free path before significant shock-heating occurs, it is to be expected that serious effects of shocks formed around the leading-edge electrode will not be detected until the vehicle has descended another 50 kft to an altitude of about 140 kft.

When a cylindrical wire is placed in a supersonic flow, almost all of the flux it collects comes from the windward side. Covering the leeward side will introduce only a small error. Therefore, placing the electrode as in Fig. 3, with the back portion of the electrode embedded in dielectric, will not introduce a serious error.

The effect of placing a cylindrical electrode at an angle to the flow is taken into account in the curves of Fig. 1, where the term $v_f \sin \theta$ appears in the value of S.

There is one difference between the cylindrical wire probe and the RAM-C probe that could introduce some error; this is the width of the dielectric structure at the leading edge, which is 0.020-inch across. It will be significant in determining when a stagnation region forms around the electrode, but since it is only twice the electrode diameter, it can at most raise the altitude at which a stagnation region forms by about 15 kft.

On the basis of the above discussion, it is expected that the interpretation of the RAM-C probe will be similar to that for a cylindrical probe so long as the shock is attached. This will be the case throughout the entire altitude range of interest (down to 160 kft). Small differences may occur because of the 0.020-inch dielectric leading edge. That this expectation is borne out will be shown in the section on experimental results.

C. WEDGE SURFACE PROBE THEORY

The RAM-C wedge-shaped dielectric probe with cylindrical wire electrode uses the wedge structure mainly as a mechanical support for the electrode. Since the electrode radius must be less than a mean-free path for the probe to operate in the strictly free-molecular region, the wires must be relatively small, limiting the collected current. This

can be an important consideration if there is a leakage current due to the finite conductivity of the dielectric. All dielectrics become poorer insulators when they are heated, and in the high-temperature environment surrounding a re-entry vehicle, the leakage currents may become larger than the electrode-collected current, making the measurements uninterpretable. Furthermore, for operation at low altitudes, the wire size required to ensure that the electrode is free-molecular may be impracticably small.

An alternative approach is to use the entire wedge surface as an electrode, not just the leading edge. This would increase the collected current and simplify probe fabrication. If the wedge angle is made small, the oblique shock formed by the incident flow striking the probe will be weak. The incident flow will be turned through a small angle but will continue with almost the incident flow velocity. If the time it takes the flow to transit the probe is small compared to the time it takes additional ionization to form, the ionization is frozen and the effect of the oblique shock will be mainly to compress the gas and electron density by a calculable factor.

Since the flow behind the oblique shock has no component normal to the wedge surface, the current collected by it is proportional to the random velocity of the particles, not the directed velocity. If the sheath were free-molecular, the current density collected by the probe would be $n\ e\ v_{th}/4$. We have found that even when many collisions occur in the sheath, flush probes collect as though they were free-molecular.[6] Therefore, we assumed that this was the case and verified this assumption experimentally. As will be seen from the experimental results (Sec. III); this was a good assumption for all of the conditions under which the measurements were made.

Under the assumptions that flow was frozen and that the collected current density was $n\ e\ v_{th}/4$, the following analysis was used to interpret the wedge probes. Consider the current to one side of the wedge shown in Fig. 4. The wedge is inclined to the flow at an angle δ. The

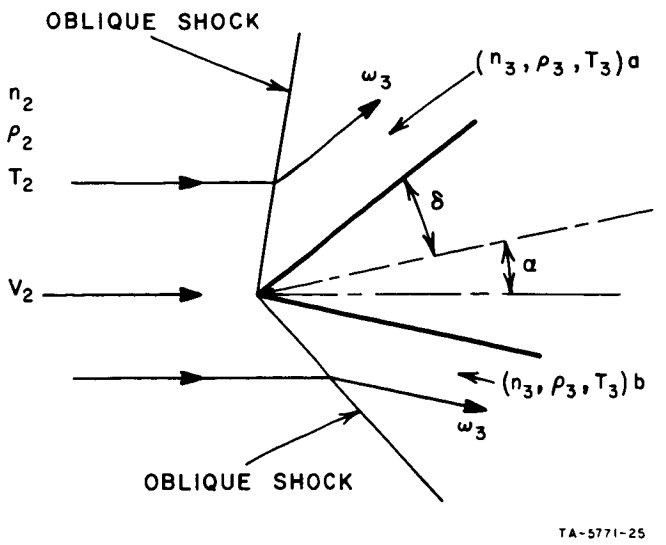

FIG. 4 WEDGE WITH AN ATTACHED OBLIQUE SHOCK

incident parameters have a subscript 2; the properties behind the oblique shock have a subscript 3. The current collected by the probe surface is

$$I = \frac{n_3 \, e \, v_{th3} \, A_3}{4} \quad , \tag{1}$$

where A_3 = surface area of the electrode.

By the assumption of frozen flow we may relate n_3 to n_2 as

$$n_3 = n_2 \rho_3 \rho_2 \quad ,$$

where ρ_3/ρ_2 = gas density increase across the oblique shock. Similarly,

$$v_{th3} = v_{th2} \, (T_3/T_2)^{1/2} \quad ,$$

where T_3/T_2 = temperature ratio across the oblique shock.
Therefore,

$$I = \frac{n_2 \, e \, v_{th2}}{4} \frac{\rho_3}{\rho_2} \, (T_3/T_2)^{1/2} A_3 \quad , \tag{2}$$

The factors ρ_3/ρ_2 and $(T_3/T_2)^{1/2}$ are functions of the incident Mach number and the wedge inclination angle. The values of these factors for frozen flow across the shock have been calculated for δ equal to 10, 20, and 30 degrees and have been plotted in Fig. 5. The ratio of

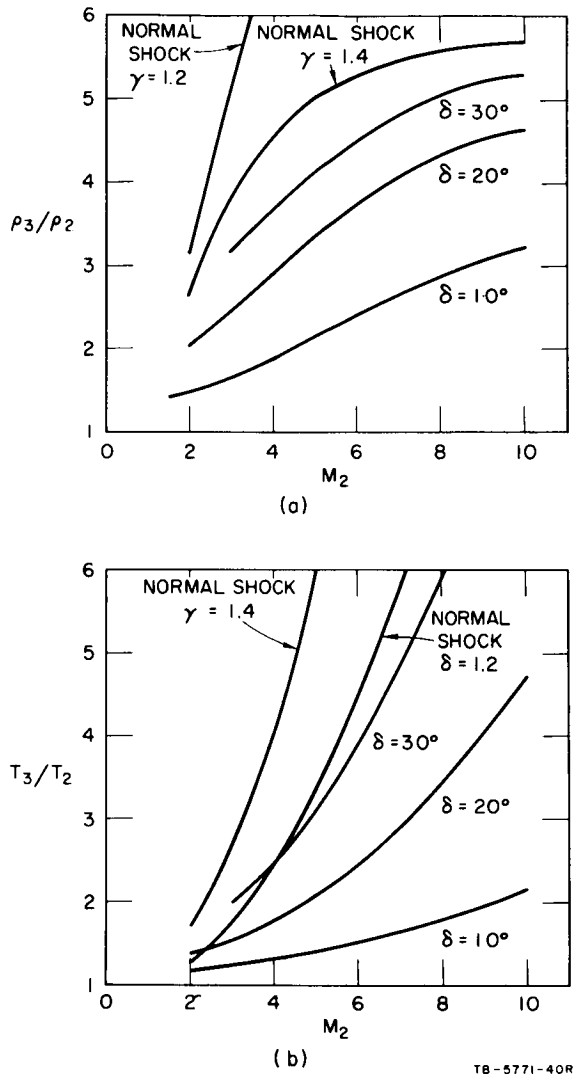

FIG. 5 GAS DENSITY AND TEMPERATURE JUMPS ACROSS AN OBLIQUE SHOCK AS A FUNCTION OF MACH NUMBER OF THE INCIDENT FLOW

specific heats was taken as 1.4. The results change only slightly for a value of specific heat equal to 1.2. In the shock-tube experiments, the Mach number varied from about 2.5 to 3.3. In the RAM flight, the Mach number near the RAM-C probe will be about 4.5.

Feldman[7] has calculated the gas density and temperature in region 3 in terms of the incident shock velocity in a shock tube. His results agree quite well with those presented in Fig. 5. His calculations were down to initial shock-tube pressures of 1.0 torr, but the results change only slightly with initial pressure.

Also shown in Fig. 5 are the values of the gas density and temperature jump across a normal shock for a ratio of specific heats of 1.2 (an average value for the shock-tube flows). These are the values that were used when the wedge angle became so large that a detached shock was formed. Under these conditions, the frozen flow assumption is more questionable.

Since the flow past one side of a two-sided wedge is independent of the other side, the gas density and temperature changes across the oblique shock may be calculated separately for each side. The total current collected by a two-sided wedge is simply the sum of the current collected on each side. For a wedge of half-angle δ, at zero-degrees angle of attack, the total current would be simply twice the value given by Eq. (2). For angles of attack α other than zero, the gas density and temperature jump for each side must be computed separately. The inclination angle of the wedge is then the wedge half-angle δ, plus and minus the angle of attack θ (see Fig. 4).

Denoting one side of the wedge by subscript a and the other side by b, the total current is then

$$I = \frac{n_2 \, e \, v_{th2}}{4} \left[\left\{ A \, \rho_3/\rho_2 \left(\frac{T_3}{T_2} \right)^{1/2} \right\}_a + \left\{ A \, \rho_3/\rho_2 \left(\frac{T_3}{T_2} \right)^{1/2} \right\}_b \right] . \quad (3)$$

In order to estimate the reasonableness of the frozen flow assumption, several simple asymptotic cases were considered. The rate of change of electron density in high-temperature air, where the main production and recombination processes involve the reaction $N + O \rightleftharpoons NO^+ + e$, is given by

$$\frac{dn}{dt} = \langle N \rangle \langle O \rangle \quad K_f - K_r \langle n \rangle^2 \quad , \tag{4}$$

where

$\langle N \rangle$ = concentration of atomic nitrogen

$\langle O \rangle$ = concentration of atomic oxygen

K_f = forward rate constant

K_r = backward rate constant.

If the frozen flow assumption is not applicable, the current collected by the probes will be a function of K_f and K_r, making the probe interpretation dependent upon a knowledge of these rate constants. This is undesirable, since it is these very rate constants that must be verified in flight tests. It is therefore important to establish that frozen flow conditions prevail in the region where the probes are operating. To perform an exact calculation of the electron production process behind the oblique shock is beyond the scope of this contract; however, several simple asymptotic cases have been analyzed to show the plausibility of the frozen flow assumption for the shock-tube case wherein the flow is equilibrium. When the flow is nonequilibrium (where the electron density is greater than the equilibrium value), the frozen flow assumption is easier to justify.

In the actual case, all of the parameters in Eq. (4) are functions of time of travel behind the oblique shock. To simplify the analysis we shall consider those cases wherein all parameters are constant except the electron density.

1. Frozen Flow Dissociation

If the dissociation of the molecular nitrogen and oxygen behind the oblique shock does not have time to occur, the concentration of atomic nitrogen and oxygen in region 3 will be simply ρ_3/ρ_2 times the incident concentrations. Under these conditions, the gas temperature will remain at the level which one would calculate with a constant ratio of specific heats for the given shock conditions. Since K_f is an increasing function of temperature, this will give the maximum value of K_f. It will also correspond to the minimum values of the atomic species, since it is assumed that no additional dissociation occurs. The assumption of frozen flow dissociation is consistent with the assumption of a constant specific heat calculation of the temperature behind the shock.

Under the assumption of constant values for the atomic species and for the temperature, Eq. (4) can be directly integrated. The electron density behind the oblique shock may be expressed as

$$n_3 = n_2 \rho_3/\rho_2 + (C_1/K_r)^{1/2} \left\{ \frac{\exp\left[2(C_1K_r)^{1/2}t\right] - 1}{\exp\left[2(C_1K_r)^{1/2}t\right] + 1} \right\} , \quad (5)$$

where

$$C_1 = (\rho_3/\rho_2)^2 \langle N\rangle_2 \langle O\rangle_2 K_f$$

$\langle N\rangle_2$ = Equilibrium concentration of atomic nitrogen in region 2

$\langle O\rangle_2$ = Equilibrium concentration of atomic oxygen in region 2.

Subscript 2 denotes incident properties; subscript 3 denotes properties behind the shock.

The first term on the right represents the frozen compression of the incident electrons; the second term on the right represents additional ionization behind the oblique shock and therefore the error in assuming frozen flow. These terms have been evaluated for the shock-tube case at an initial shock-tube pressure of 1.0 torr for a wedge of

half-angle equal to 10 degrees with a 1/8-inch-long electrode. Values of K_f and K_r were taken from Lin.[8] The results are shown in Fig. 6 for a range of shock velocities. It can be seen that if frozen flow dissociation holds, the assumption of frozen flow ionization will also hold to an accuracy of better than a factor of 2.

2. Equilibrium Dissociation

Another asymptotic case is to assume that the concentrations of atomic nitrogen and oxygen reach their equilibrium values in region 3 immediately behind the oblique shock. The assumption of equilibrium gas temperature beyond the point is consistent with the assumption of equilibrium dissociation. Equation (5) has been solved with these assumptions and with

$$C_1 = \langle N \rangle_3 \langle O \rangle_3 K_f \quad ,$$

where

$\langle N \rangle_3$ = Equilibrium concentration of atomic nitrogen in region 3

$\langle O \rangle_3$ = Equilibrium concentration of atomic oxygen in region 3.

The solution is plotted in Fig. 7 for a 10-degree half-angle wedge, a 1/8-inch-long electrode, and an initial pressure of 1.0 torr. Once again, the assumption of frozen flow compression gives an accuracy better than a factor of 2.

3. Equilibrium Electron Density

In Ref. 7 Feldman gives values for the equilibrium temperature and gas density in region 3 for shock-tube flows incident on wedges. From these values we have determined the equilibrium electron density. In Fig. 8, this value is compared to the value for frozen compression for a 10-degree half-angle wedge, at $p_1 = 1.0$ torr. The equilibrium values are about twice the values for frozen compression.

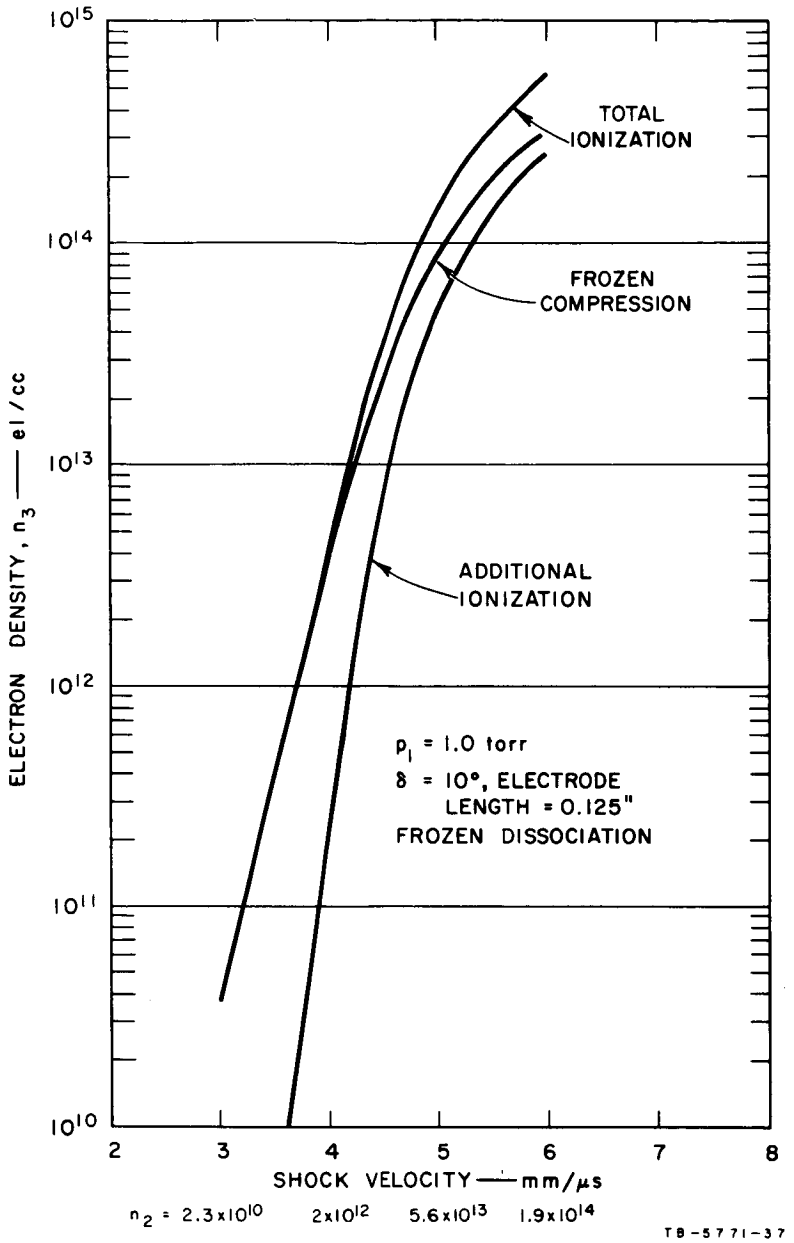

FIG. 6 ADDITIONAL IONIZATION PRODUCED BEHIND AN OBLIQUE SHOCK, ASSUMING FROZEN DISSOCIATION

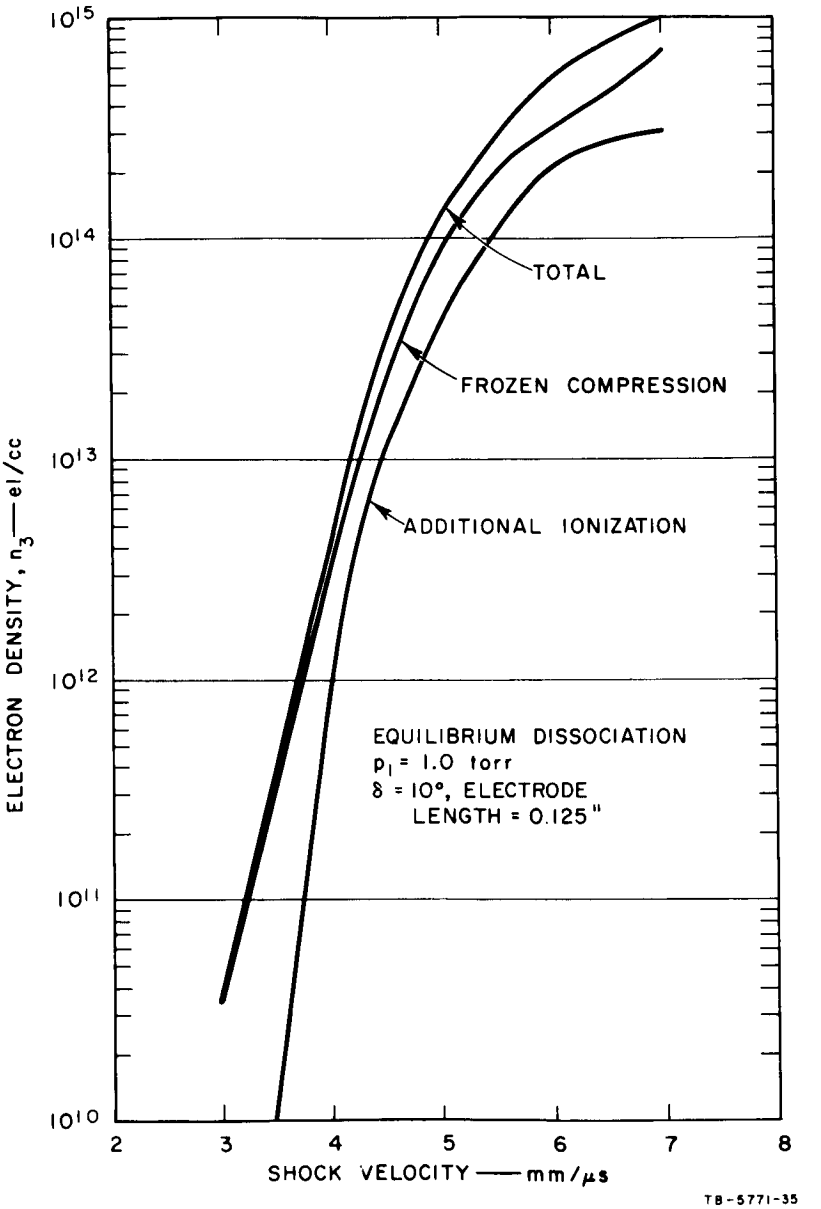

FIG. 7 ADDITIONAL IONIZATION PRODUCED BEHIND AN OBLIQUE SHOCK, ASSUMING EQUILIBRIUM DISSOCIATION IMMEDIATELY BEHIND THE SHOCK

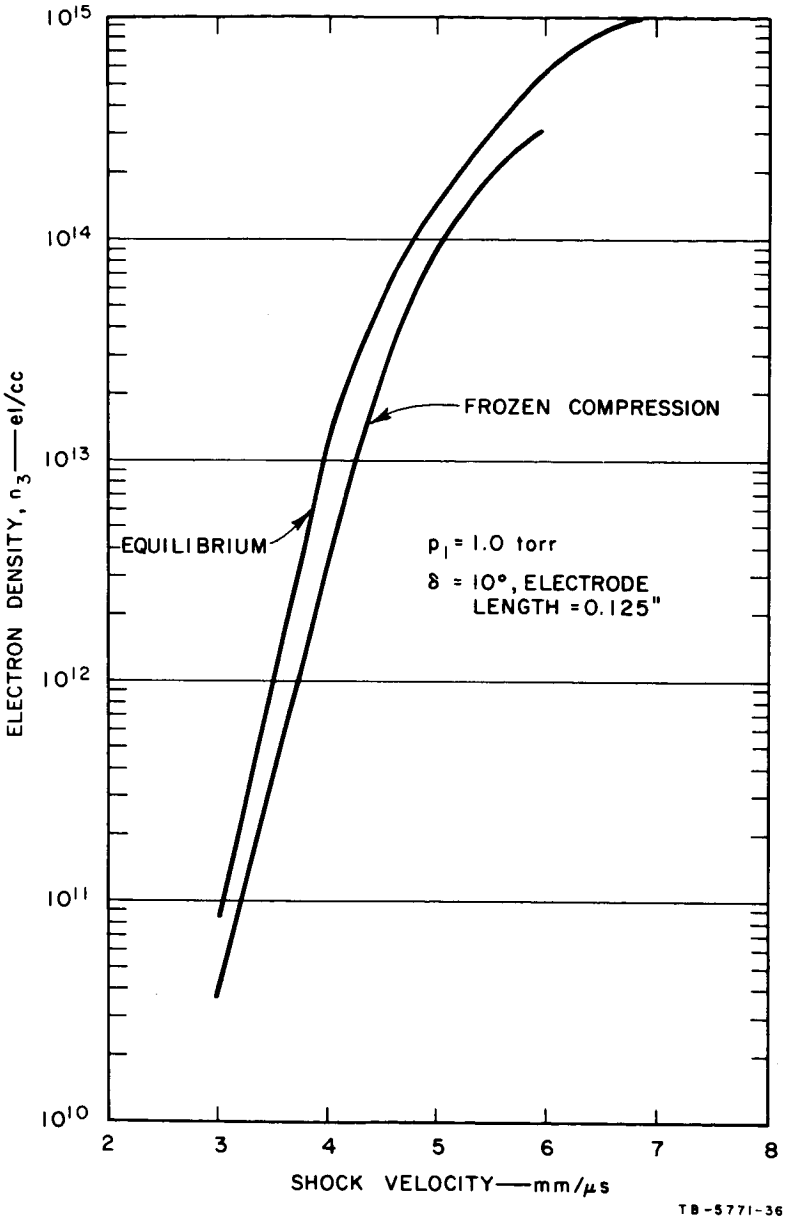

FIG. 8 EQUILIBRIUM ELECTRON DENSITY BEHIND AN OBLIQUE SHOCK

From these three sets of computations it is clear that for the 10-degree half-angle wedge, the electron density in region 3 will not deviate by more than a factor of 2 from the value obtained from the frozen flow compression calculation.

D. THEORY OF ELECTRON TEMPERATURE MEASUREMENT

Langmuir[9] developed a theory which related electron temperature to the currents measured as a function of voltage on a probe with unequal-area electrodes. Johnson and Malter[10] further developed this theory so that it was applicable to any value of area ratio for the two electrodes. Both theories are applicable for the free-molecular, nonflowing plasma condition. We shall not take the space to summarize the theories, but only quote a result from Johnson and Malter's work. They show that under the assumed plasma conditions

$$T_{-} = 11{,}600 \frac{\sigma}{(\sigma + 1)^2} \left[\Sigma I_p \frac{dV}{dI} \right]_{V_d=0} \quad {}^{\circ}K \quad , \tag{6}$$

where

σ = $A_1 J_1 / A_2 J_2$, the ratio of the probe area times the current density at each electrode,

$\frac{dV}{dI}$ = slope of the voltage-current plot

I_p = sum of the saturated ion currents from each electrode

V_d = potential difference between electrodes.

Note that the quantity in the brackets is to be evaluated at $V_d = 0$. These quantities are illustrated in Fig. 9 for an equal-area probe in a uniform plasma. Under these conditions, $\sigma = 1$ and

$$T_{-} = 2900 \left[\Sigma I_p \frac{dV}{dI} \right]_{V_d=0} \quad {}^{\circ}K \quad . \tag{7}$$

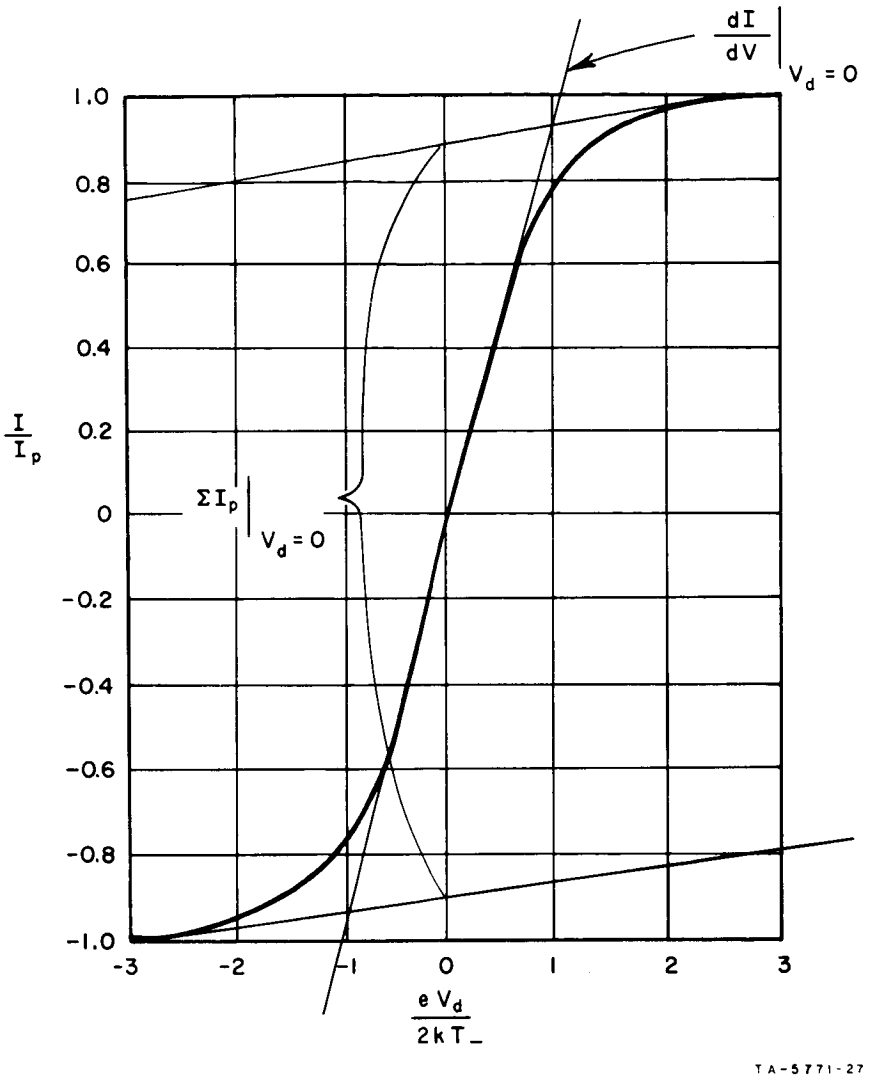

FIG. 9 CURRENT-VOLTAGE CHARACTERISTIC FOR EQUAL-AREA LANGMUIR PROBES

For a flowing plasma, this analysis should be applicable as long as the flow velocity is small compared to the thermal velocity of the electrons. Since the electron thermal velocity is of the order of 10^5 m/s at temperatures of several thousand degrees Kelvin, the effect of flow velocity can be ignored for all of the conditions of interest for re-entry and satellite vehicles.

The effect of deviation from free-molecular flow may be more significant. This problem has been considered, with respect to stationary plasmas, by Zhakarova,[11] who shows that the current voltage characteristic is distorted by collisions; however, the error is small if $r_p/\lambda \exp(\eta) \ll 1$. Thus, operation near zero net current, where $\eta \approx -5$, would still yield accurate measurements of T_- for r_p/λ as large as 20. With an equal-area probe, when $I = 0$, $\eta \approx -5$; therefore, this type of probe can be operated in an optimum region for making electron temperature measurements where the mean-free path is short compared to the probe radius. On the other hand, the usual "single" or unequal-area probe technique would give a poor indication of electron temperature as the probe potential approached the plasma potential ($\eta = 0$). Of course, the unequal-area probe could be used in the region of $I = 0$, but then there would be no point in making a "single" rather than an equal-area probe.

In a flowing continuum plasma, the main effect of the flow velocity on the electron temperature measurement will be the heating of electrons due to shock formation around the probe. Under these conditions, and if $r_p/\lambda \exp(\eta) \ll 1$, the probe will measure the electron temperature behind the shock formed around the probe.

III ELECTROSTATIC PROBE MEASUREMENTS

A. INTRODUCTION

In order to check the probe theories outlined in the previous section, a series of measurements were made in an arc-driven shock tube. This device is capable of producing supersonic, ionized plasma flows over a wide range of electron and gas densities. The shock tube was described in some detail in Ref. 1. Table I shows the equilibrium electron density,

Table I

SHOCK-TUBE PARAMETERS FOR EQUIVALENT FLIGHT ALTITUDES

U_s (mm/μs)	n_{eq} (elec/cc)	λ_{n-n} (mils)	Altitude With Same Ambient Gas Density (kft)	Altitude With Same Gas Density Near the Probe (kft)	r_p/λ_{n-n}
p_1 = 0.1 torr					
3	1.2×10^{9}	2.4	155	178	2.1
4	1.9×10^{11}	2.0	150	173	2.5
5	4.8×10^{12}	1.8	148	171	2.7
6	1.4×10^{13}	1.6	144	167	3.2
7	3.2×10^{13}	1.4	142	165	3.6
p_1 = 1.0 torr					
3	2.3×10^{10}	0.26	103	126	19.5
4	1.9×10^{12}	0.21	99	122	23
5	5.6×10^{13}	0.20	98	121	25
6	2.0×10^{14}	0.17	95	118	30
7	4.3×10^{14}	0.14	92	115	37

the neutral-neutral mean-free path, the ratio of probe radius to mean-free path, and the equivalent flight altitude (assuming that the gas density around the probe in flight is three times the ambient density) for different shock velocities.

Tests were made to determine whether equilibrium electron densities were obtained. The actual electron density was inferred from microwave interferometer measurements. The tests showed that at an initial pressure of 0.1 torr, the electron density could be as much as an order of magnitude below equilibrium. These results were obtained when the tube had not been cleaned for many shots. At p_1 = 1.0 torr, equilibrium densities were obtained (plus or minus a factor of 2) except at the very low electron densities, where the results were erratic.

Because of space limitations, the tests with the RAM-C probe and the interferometer could not be run simultaneously. It was therefore decided to try to calibrate the 10-mil-diameter wire probes against the interferometer and use the 10-mil probes as a standard of comparison with the RAM-C probe. This would also serve to check the theory of probe operation in supersonic flows for this probe. If the inferred electron density, using the theory for cylindrical probes given in Sec. II, agreed with the interferometer data, this would confirm that theory. Some confirmation had been obtained in the previous contract, but the confirmation was for only a limited range of free-stream electron density.

In all of the measurements presented in this report, except for the electron temperature measurements, the circuit shown in Fig. 10 was used. A fixed bias of -15 volts was applied to the electrode to draw saturation ion current. "Saturated" is used in the sense that negligible electron current was collected by the negatively biased electrode. This does not imply that the current would not change if the voltage changed. The current would change for certain plasma conditions, but this change would entirely result from changes in the sheath structure.

Referring to Fig. 10, the probe current produced a voltage across the resistor, and this in turn was fed into about 30 feet of RG 58/U cable, which has about 30 $\mu\mu$fd/ft capacitance. The RC time constant

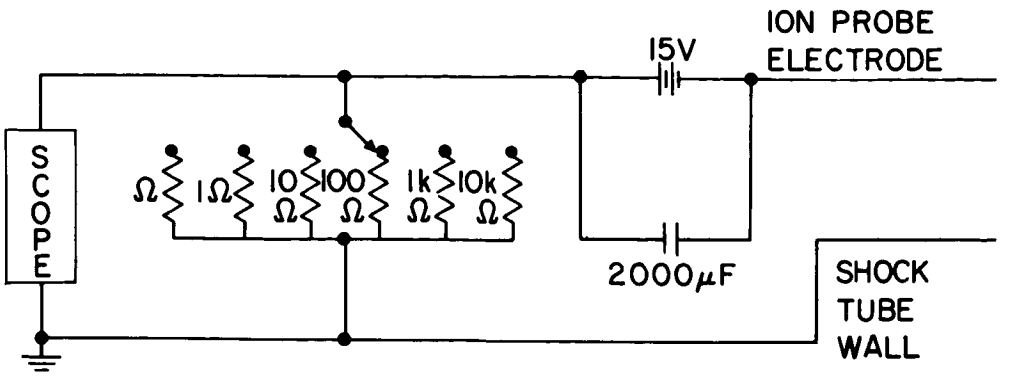

FIG. 10 ION PROBE CIRCUITRY

resulting from this combination of resistance and capacitance was always less than a microsecond, and most of the time it was less than 0.1 μs.

Often several probes were mounted at the same station, and tests were made. As reported in Ref. 1, these tests demonstrated that there was no detectable coupling between the probes.

B. TESTS OF A 10-MIL-DIAMETER WIRE PROBE AT 0.1 TORR

The measurements on the 10-mil-diameter wire probes were made with the wires supported in a "harp" structure shown in Fig. 11. This structure kept the probes from bending in the flow and was designed so that any shocks formed on the wire holder would not influence the currents collected. This probe and several others like it were tested at the same time an X-band (9.6 GHz) interferometer was measuring the phase shift due to the plasma. Interferometer data had been taken at K-band (30 GHz) in previous work but could not be used for the lower electron densities. The probe and interferometer locations are given in Fig. 12.

The results obtained with this setup are shown in Fig. 13. The abscissa is the electron density inferred from interferometer measurements. Above about 10^{12} elec/cc these interferometer data were no longer usable, and we have therefore substituted the equilibrium electron density determined from the measured shock velocity. It is not known how accurate these values of electron density are, but at the higher shock

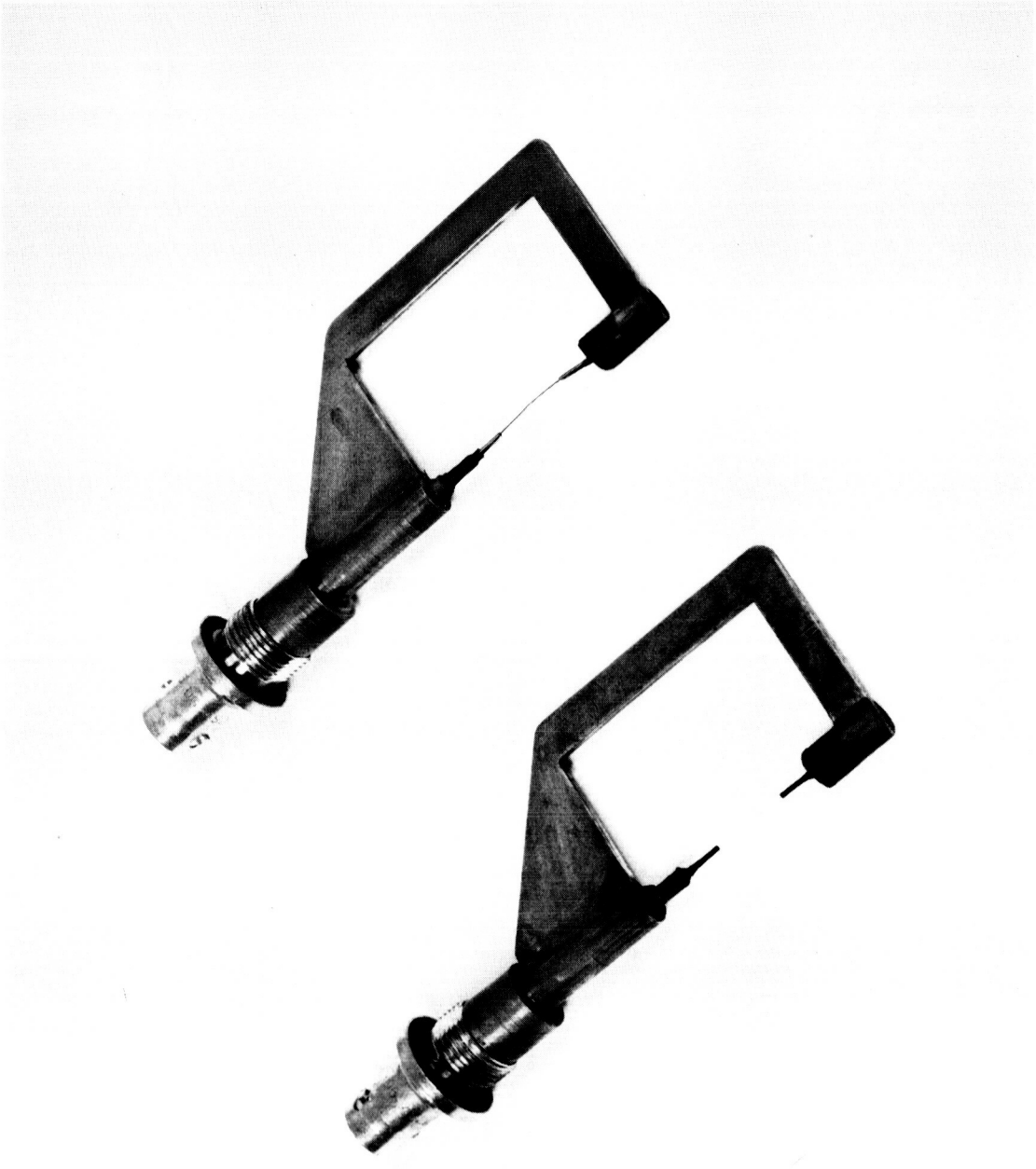

TA-5771-18

FIG. 11 PHOTOGRAPH OF HARP STRUCTURE SUPPORTING 10-mil-diameter PROBE WIRE

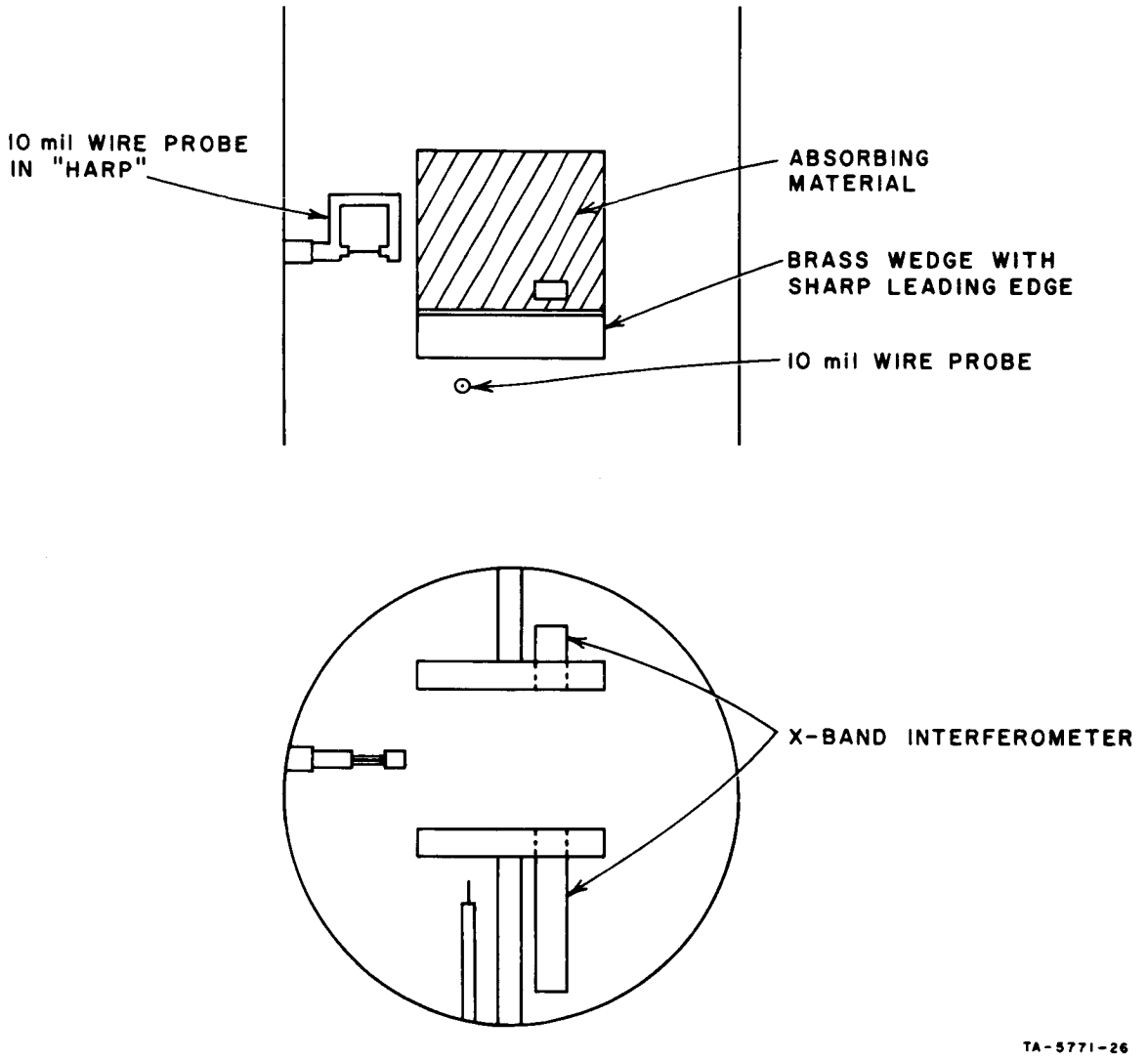

FIG. 12 SKETCH SHOWING X-BAND MICROWAVE INTERFEROMETER AND HARP STRUCTURE MOUNTED IN THE SHOCK TUBE

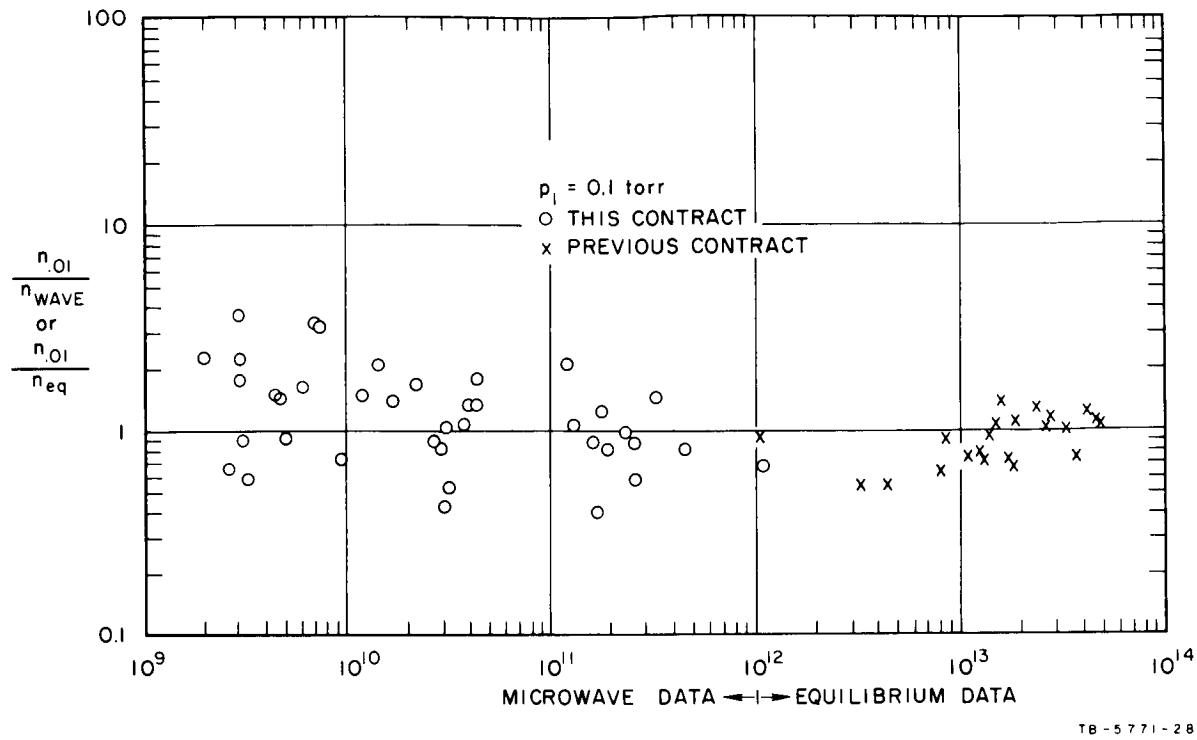

FIG. 13 RATIO OF ELECTRON DENSITIES INFERRED FROM 10-mil WIRE PROBES AND FROM MICROWAVE DATA AS A FUNCTION OF ELECTRON DENSITY INFERRED FROM MICROWAVE DATA

velocities the effects of impurities should be smaller than at lower shock velocities. The data also showed little scatter at high electron densities, which is not in accordance with the nonequilibrium effects noted previously.

The ordinate is the ratio of the electron density inferred from the 10-mil probe to the electron density indicated on the abscissa. A value of this ratio of unity would indicate that the probe was accurately measuring the charge density.

The data from 10^{10} to 10^{14} elec/cc scatter fairly evenly about the unity ratio line. The spread is about a factor of ± 2. Previous measurements had shown electron density variations of this same factor from point to point across a tube diameter, therefore it is concluded that the data scatter is characteristic of the shock-tube facility. Since

the average value of the ratio is close to unity, the probe theory is confirmed to a factor of better than 2. We can therefore use this probe as a measure of the free-stream electron density over this range of electron densities with an accuracy better than a factor of 2.

C. TESTS OF A 90° MOCKUP OF THE RAM-C PROBE

In order to see whether the currents from the RAM-C probe could be interpreted as though the probes were freely suspended wires, a mockup of the probe was made with only three of the eight electrodes. To determine if the swept-back angle had any effect, the first mockup was constructed so that the wires were perpendicular to the flow. A photograph of the probe is shown in Fig. 14. The leading edge electrodes were 10-mil-diameter wires, 0.15 inch long. The probe was mounted in the shock tube, and the electron density inferred from the probe was compared with the results from the 10-mil-diameter "harp" probe under the same conditions. The results are shown in Fig. 15 for electron densities of from 6×10^9 to 2×10^{13} elec/cc at $p_1 = 0.1$ torr. This figure shows that the two probes are reading identically, with a scatter about the mean of a factor that is approximately ± 2. It was concluded that the wedge support structure was not influencing the results and that the data from the RAM-C mockup could be interpreted in the same manner as when a wire probe is used.

D. TESTS OF A 45° MOCKUP OF THE RAM-C PROBE AT p_1 = 0.1 TORR

Next, a mockup of the RAM-C probe that included the swept-back leading edge, shown in Fig. 16, was inserted into the shock tube, and the data were compared to the electron density inferred from the 10-mil harp probe. The RAM-C probe measurements were interpreted using the factor S sin θ, discussed in Sec. II, with $\theta = 45°$. The results are shown in Fig. 17. Once again, the electron density inferred from both probes agreed to within the data-scatter factor of ± 2. The results show that the 45° swept-back leading edge did not introduce any significant uninterpretable phenomena and that at least down to the equivalent altitude at which these tests were run (170 kft), the RAM-C probes can be interpreted as wire probes with errors less than a factor of 2.

FIG. 14 MOCKUP OF THE RAM-C PROBE WITH NO SWEEP-BACK OF LEADING EDGE

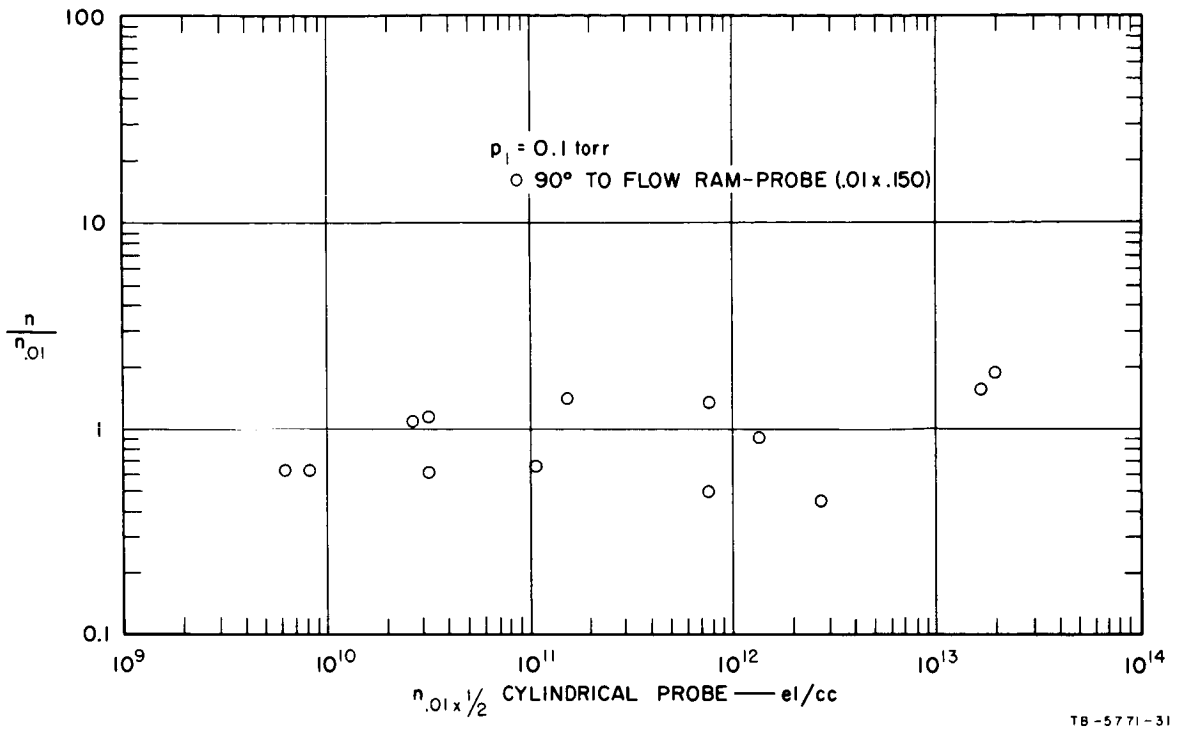

FIG. 15 RATIO OF ELECTRON DENSITY INFERRED FROM 90° RAM-C MOCKUP TO THAT INFERRED FROM 10-mil WIRE PROBE AS A FUNCTION OF THE ELECTRON DENSITY INFERRED FROM 10-mil WIRE PROBE

FIG. 16 MOCKUP OF RAM-C PROBE WITH 45° SWEPT-BACK LEADING EDGE

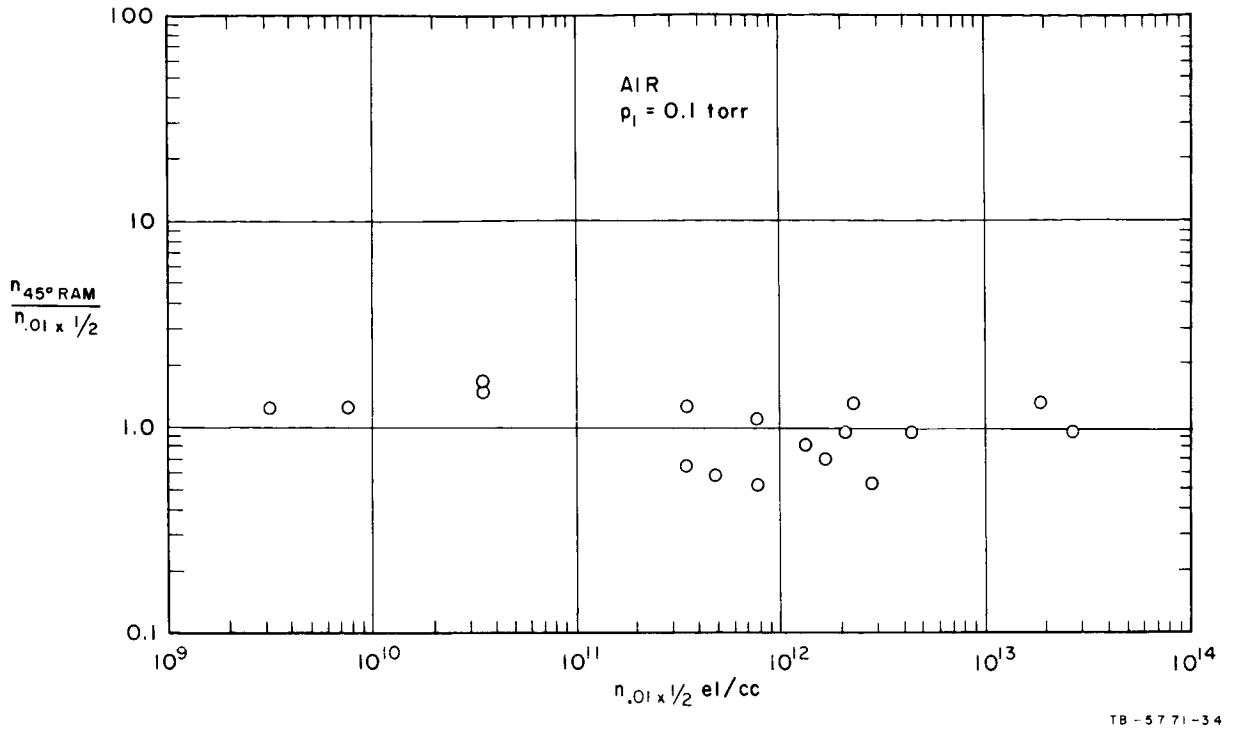

FIG. 17 RATIO OF ELECTRON DENSITY INFERRED FROM 45° RAM-C MOCKUP TO THAT INFERRED FROM 10-mil WIRE PROBE AS A FUNCTION OF THE ELECTRON DENSITY INFERRED FROM 10-mil WIRE PROBE

E. TESTS OF A 45° MOCKUP OF THE RAM-C PROBE AT p_1 = 1.0 TORR

Since the actual probes will begin melting at altitudes higher than 170 kft, testing at lower altitudes was unnecessary. However, for a better understanding of the limits of the free-molecular assumption of probe operation and the effects of the supporting wedge structure, some tests were run at p_1 = 1.0 torr (equivalent to an altitude of 120 kft).

It was previously established, by means of a microwave interferometer, that values of electron density close to equilibrium are obtained at p_1 = 1.0 torr, at least down to about 10^{10} elec/cc. On the other hand, it was also established that 10-mil wire probes do not give results that agree with free-stream data because of shock formation around the probes. This effect has been reported in Ref. 1 for electron densities between 10^{11} and 10^{14} elec/cc.

In order to check 10-mil wire probe operation at electron densities below 10^{11}, and also to determine how well the RAM-C probe configuration followed the wire probe data, tests with both probes were made at $p_1 = 1.0$ torr. The results are shown in Fig. 18. Above 10^{11} elec/cc, the abscissa is the equilibrium electron density. Below 10^{11}, the electron density inferred from a 10^{0} half-angle wedge probe was used as a standard. The performance of the wedge probe at these electron densities was checked against equilibrium values in other tests described below. The reason equilibrium values were not used at the lower electron densities was because of the shock deceleration effects, discussed in the following paragraphs.

The RAM-C and 10-mil wire probes were mounted at the station furthest from the driver (station 1094). At the low electron densities, the current rise did not exhibit a step-function rise with a flat level corresponding to the test gas, but was "smeared out," with a long, slow increase. We attribute this to the effects of shock deceleration down the tube. To illustrate, suppose the shock velocity is 3.3mm/μs at station 918; the equilibrium electron density will then be 8×10^{10} elec/cc. If in traveling down the tube to station 1094 the shock velocity decreases to 3.0 mm/μs, the new equilibrium electron density will be only 2.3×10^{10} elec/cc. Now, if the time to travel from station 918 to 1094 is not sufficient for the electrons formed at station 918 to recombine, some of them will be left over, giving an electron density higher than the equilibrium value at station 1094. Since the recombination time is inversely proportional to the electron density, this effect tends to become important at low electron densities.

Under these conditions, only the portion of the slug near the current rise will be near the equilibrium value. At later times in the slug, the electron densities will be higher and cannot be inferred from the local shock velocity. Furthermore, because of the "smearing out" of the current trace, it becomes difficult to make accurate velocity measurements with ion probes, since these depend upon accurate knowledge of the

arrival of the shock at a given station. Since the equilibrium electron density is a sensitive function of shock velocity, a small error in this quantity will lead to larger errors in equilibrium electron density. Another type of sensor, such as a pressure probe, would not be susceptible to this difficulty.

The shock deceleration effect was not as serious at stations closer to the driver, where the 10^0 half-angle wedges were tested. However, since both tests of the wedges and the RAM-C probe were run concurrently to gather the most data per shot, it was necessary to place the RAM-C mockup downstream of the wedge probes to avoid interference. The solid wedges being quite small, they could be placed upstream of the RAM-C probes and would produce only a small disturbance in the flow by the time it reached the RAM-C station.

Figure 18 shows that the electron densities indicated by the 10-mil wire probe and the RAM-C probe were similar. Above 10^{12} elec/cc the RAM-C probe indicated electron densities about one-half those of the wire probe. The width of the leading edge of the RAM-C probe is 20 mils. Previous measurements with 10-mil, 1/16-inch and 1/4-inch-diameter rods showed that the largest probe indicated a lower electron density.[1] This is consistent with the result presented here.

Below about 10^{11} elec/cc, both probes approached an accurate measurement of the free-stream properties. Without a detailed analysis of the problem little can be said with confidence, but one possible explanation is that at the lower electron densities, although a shock is still formed around the probe, the ionization relaxation times are longer than the flow times.

The results shown in Fig. 18 are based on the interpretation that the probes were collecting flux at a Mach number of about 3. Actually, since there is a shock, the velocity at which the current was collected is lower by about a factor of 3, but since the ionization is compressed by a factor of about 4, the two effects cancel and yield inferred electron densities close to the incident values.

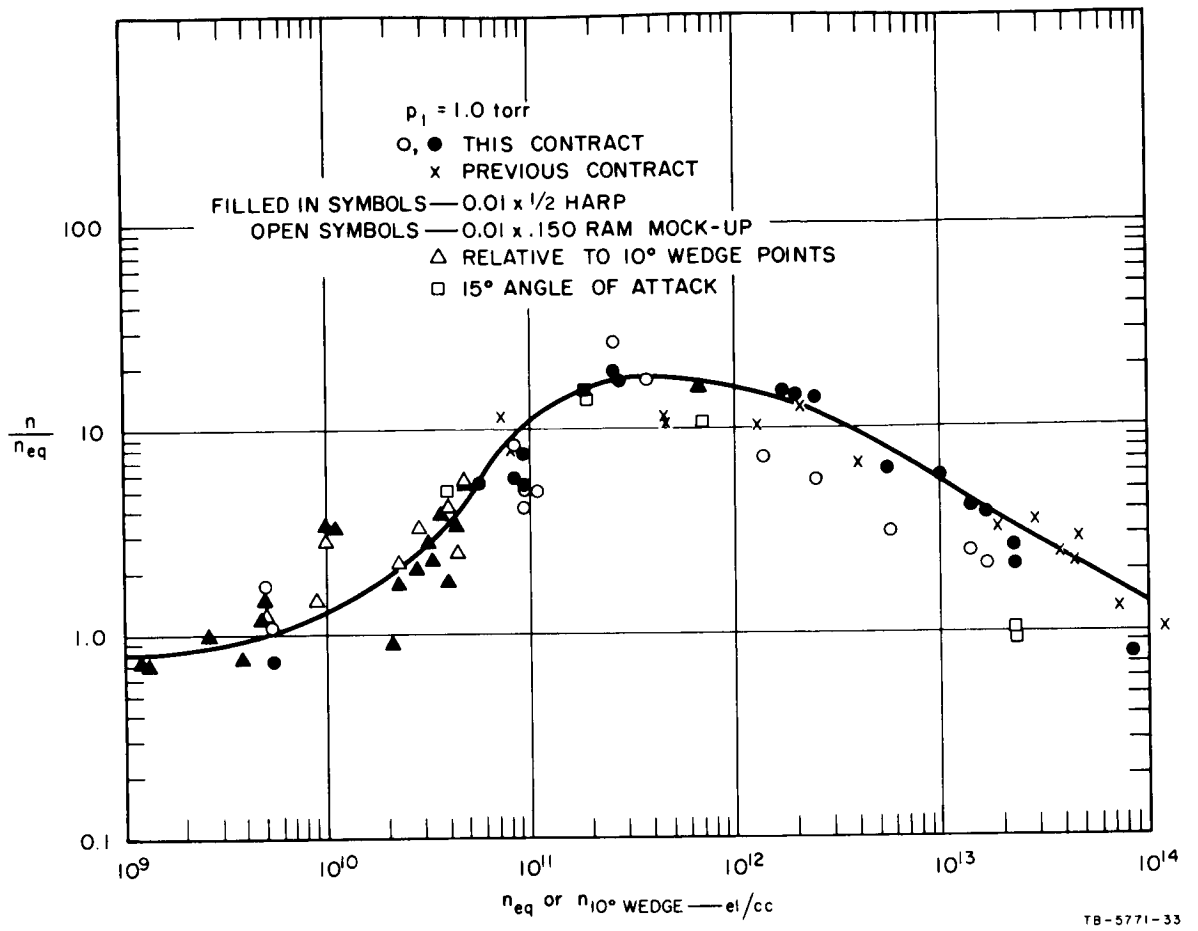

FIG. 18 RATIO OF ELECTRON DENSITY INFERRED FROM 10-mil WIRE PROBE AND FROM 45° RAM-C MOCKUP TO EQUILIBRIUM ELECTRON DENSITY AS A FUNCTION OF THE EQUILIBRIUM ELECTRON DENSITY

It was also found that even at incident electron densities of up to 10^{11} elec/cc, if this value were far back in the slug where it was out of equilibrium with the gas properties, the inferred electron densities would be equal to the incident electron densities. Thus, the inferred electron densities would vary by an order of magnitude, depending upon the state of the gas in the incident slug. This is not a surprising result; it merely illustrates the dependence of the ionization produced in the shock surrounding the probe upon the incident gas properties. However, it also emphasizes that when probes are used in plasma environments where the state of the gas is not well known, the probe inferred densities can be in error by as much as an order of magnitude when

shocks are formed around the probe. Thus, a calibration of the RAM-C probe in an equilibrium plasma may lead to erroneous deductions if the probe is subsequently used in a nonequilibrium plasma and the leading-edge electrode is in a stagnation region.

F. EFFECTS OF YAW ANGLE

The square boxes in Fig. 18 are the results of measurements with the RAM-C probe yawed at 15^{o}. The data fall within the scatter of the 0^{o} yaw points. It is concluded that small yaw angles of up to 15^{o} will not affect the inferred electron density.

G. WEDGE SURFACE PROBE MEASUREMENTS

1. Measurements at Zero Angle of Attack

In order to check the theory of ion current collection by wedge-shaped electrodes in supersonic flow, measurements were made in the arc-driven shock tube with a set of wedge probes. To study the effect of wedge half-angle, a series of three probes with half-angles of 10, 20, and 30 degrees was made. The nose dimension was between 2 and 3 mils across in each case. A sketch of the probes, with dimensions, is shown in Fig. 19, and a photograph is shown in Fig. 20.

The wedges were all mounted at station 918 at different positions around the circumference of the tube. A 10-mil wire probe was also mounted at this station to measure the free-stream electron density.

The results of measurements at initial pressures of both 0.05 and 0.10 torr are shown in Fig. 21. The wedges were mounted at zero-degrees angle of attack. The ordinate is the ratio of the electron density inferred from the wedges to the electron density inferred from the 10-mil wire. Once again, the data scatter about a value of unity for this ratio, with a spread of about ± 2. At this pressure the wedge structure was large compared to the mean-free path. In Ref. 1, measurements on 1/16-inch-diameter rods, which are smaller than the base dimension of the smallest wedge, showed significant deviations from the free-stream electron density. Therefore, shaping the electrode into a narrow wedge can be advantageous, since measurements on a probe that is large compared to the mean-free path are easily interpreted.

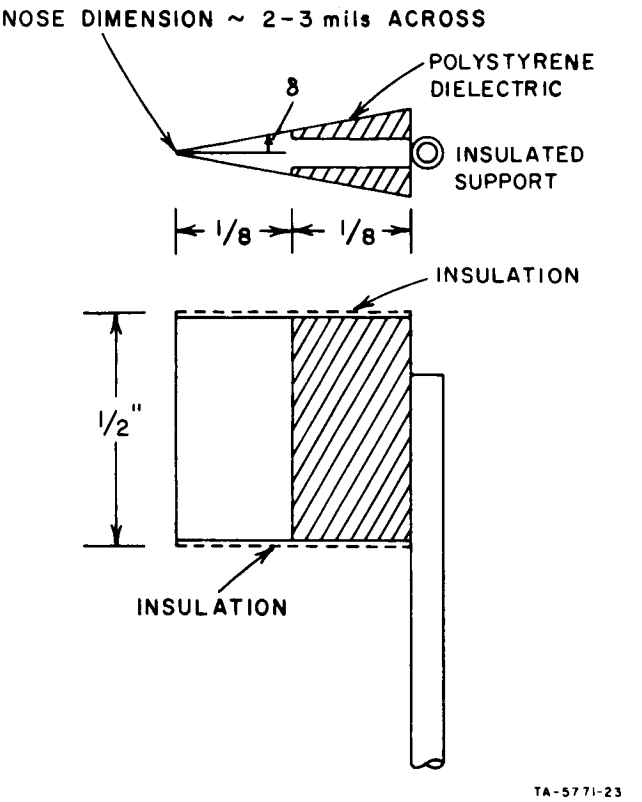

FIG. 19 SKETCH OF WEDGE PROBES

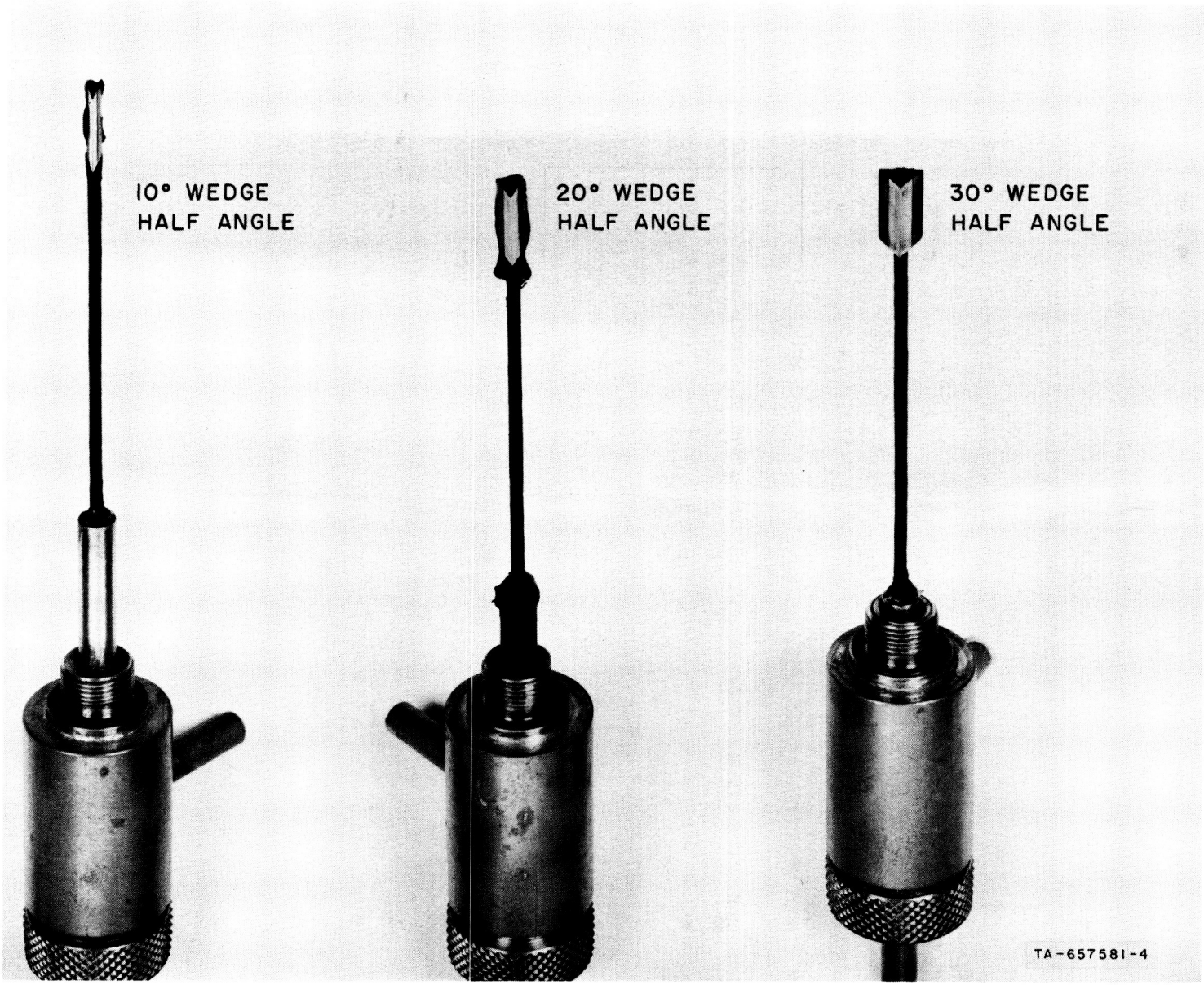

FIG. 20 THE 10, 20, AND 30-DEGREE HALF-ANGLE WEDGE PROBES

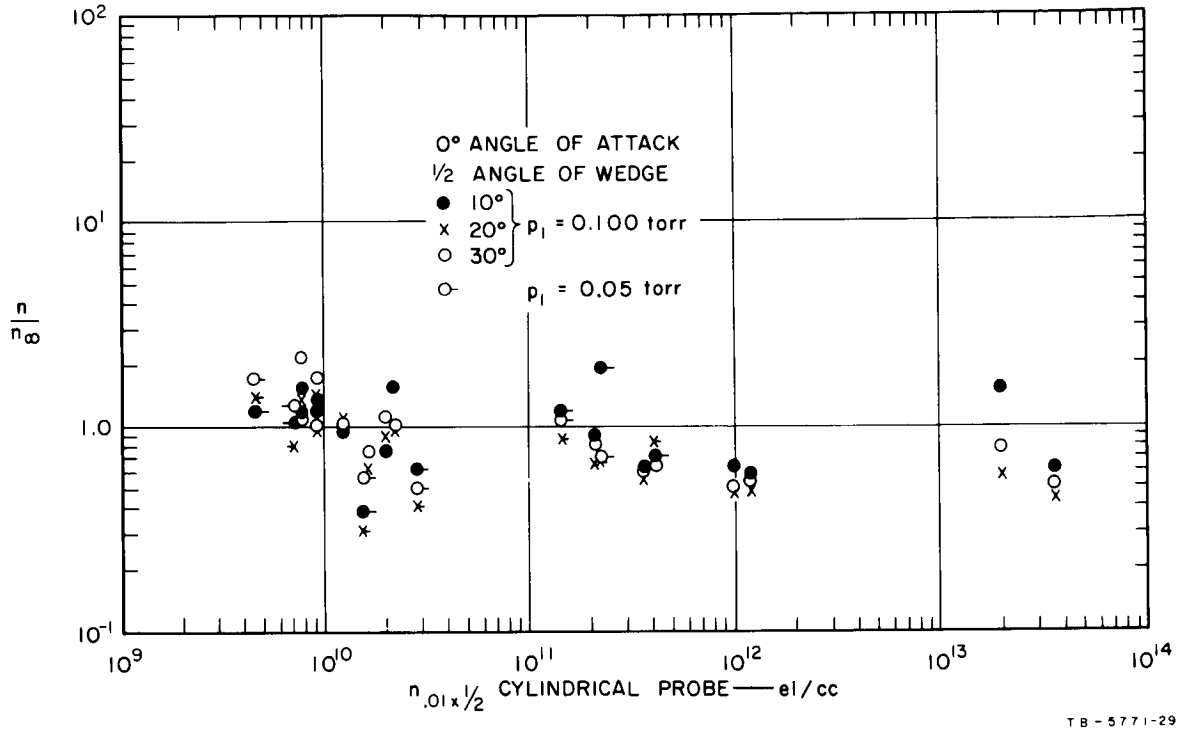

FIG. 21 RATIO OF ELECTRON DENSITY INFERRED FROM WEDGE PROBES TO THAT INFERRED FROM 10-mil WIRE PROBE AS A FUNCTION OF THE ELECTRON DENSITY INFERRED FROM 10-mil WIRE PROBE (p_1 = 0.1 torr)

Similar measurements were made at p_1 = 1.0 torr with the 10^0 wedge. The electron density inferred from this wedge is compared to the equilibrium electron density computed from measured values of shock velocity in Fig. 22. The data scatter about a value of unity for the ratio, with a spread of ±2, except at the highest electron densities. The wedge indicates densities that are somewhat lower than equilibrium. Without an independent measurement of electron density it is difficult to say whether this is due to the fact that equilibrium electron density is not achieved at these high densities or to the operation of the probe. At the lower electron densities, microwave measurements showed that equilibrium electron densities are achieved within a factor less than 2.

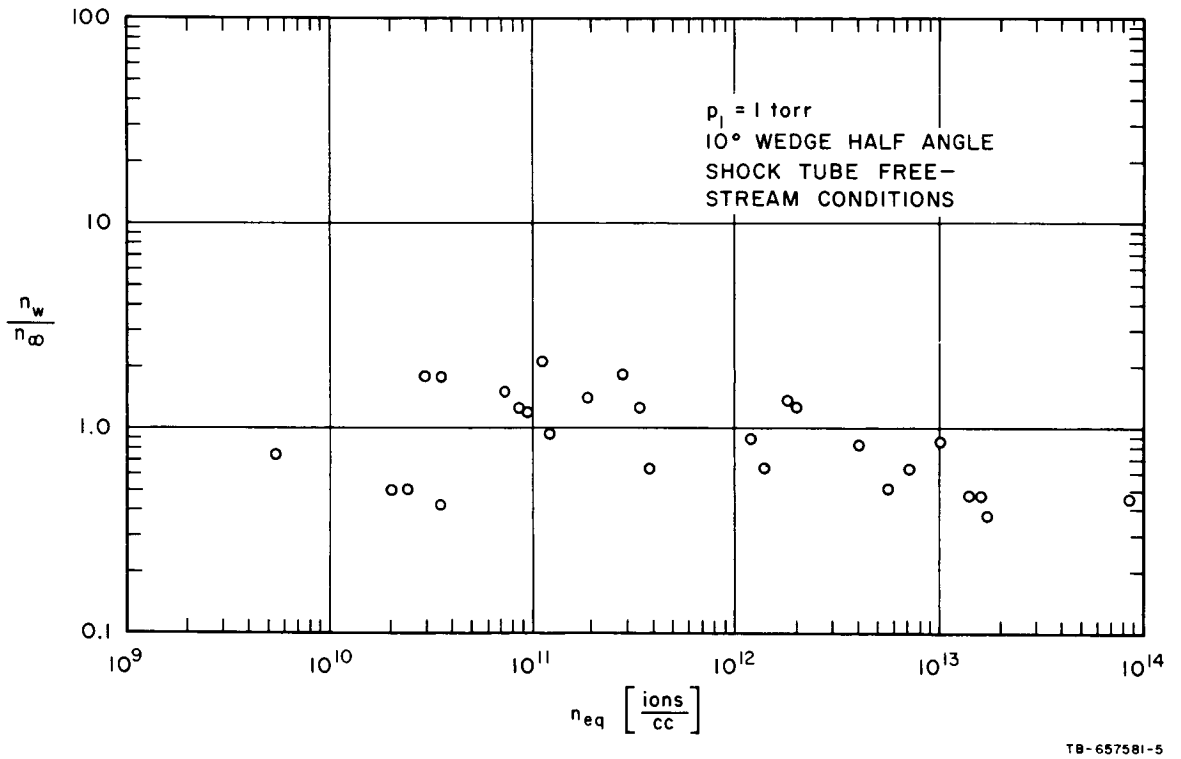

FIG. 22 RATIO OF ELECTRON DENSITY INFERRED FROM 10-DEGREE HALF-ANGLE WEDGE PROBE TO THAT INFERRED FROM 10-mil WIRE PROBE AS A FUNCTION OF THE ELECTRON DENSITY INFERRED FROM 10-mil WIRE PROBE (p_1 = 1.0 torr)

2. Angle-of-Attach Studies with Wedge Surface Probes

The effect of changing the angle of attack from zero degrees was studied at $p_1 = 0.10$ torr and an electron density of about 10^{10} elec/cc. The results are shown in Fig. 23 for angles of attack, α, up to 20 degrees.

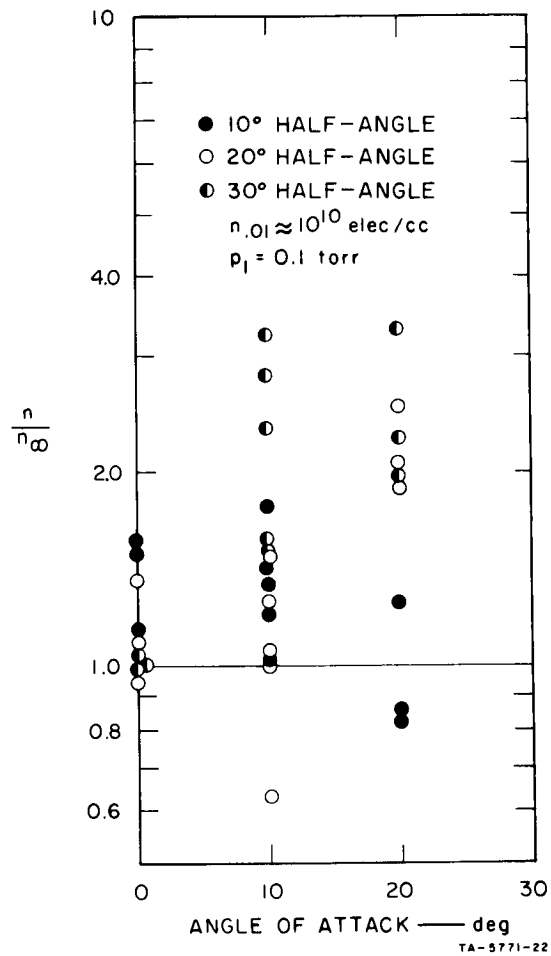

FIG. 23 RATIO OF ELECTRON DENSITY INFERRED FROM WEDGE PROBES TO THAT INFERRED FROM 10-mil WIRE PROBE AS A FUNCTION OF THE WEDGE ANGLE OF ATTACK

At $\alpha = 0^o$, an attached shock is formed on all wedges. The results show an electron density within the usual scatter for all probes. At $\alpha = 10^o$, a detached shock forms around the 30^o wedge. Under these conditions a stagnation region is formed and the gas flows past the electrode more

slowly, allowing the ionization process to proceed further towards equilibrium. This effect is clearly shown in Fig. 23. The 30^{o} wedge indicates electron densities on the average of twice the value of those on the other probes.

At $\alpha = 20^{o}$, both the 20^{o} and 30^{o} wedges form detached shocks; this again is clearly seen in Fig. 23. Both probes indicate electron densities higher than the 10^{o} wedge by a factor of about 2.5.

These results demonstrate that when a wedge probe is operated such that a detached shock forms, the possibility of producing additional ionization in the shock formed around the probe is increased. It should be noted, though, that the effect of detached shocks is not catastrophic.

H. MEASUREMENTS OF ELECTRON TEMPERATURE

In order to check the theories discussed in Sec. II on the measurement of electron temperature, experiments were performed with sets of equal-area probes mounted in the shock tube. One probe consisted of a pair of 10-mil-diameter wires 1/2-inch long, while the other pair consisted of 1/16-inch-diamter rods, 5/8-inch long. The probe configuration and circuitry are shown in Fig. 24. The probes were mounted with the cylindrical axis perpendicular to the flow.

The probes were driven by a triangular wave generator at a frequency of either 25 or 50 kc, so that a complete current-voltage characteristic could be measured in either 20 or 10 μs, respectively. Isolation of the probes from the shock-tube ground was accomplished by isolation transformers. Short cables were used between the probe circuitry and the oscilloscope to keep the response time down to a few tenths of a microsecond.

The results of measurements at $p_1 = 0.10$ torr are shown in Fig. 25(a) for the 10-mil-diameter probes and in Fig. 25(b) for the 1/16-inch-diameter probes. The results are plotted as the ratio of the inferred electron temperature to the equilibrium gas temperature (calculated from the shock velocity) as a function of equilibrium gas temperature.

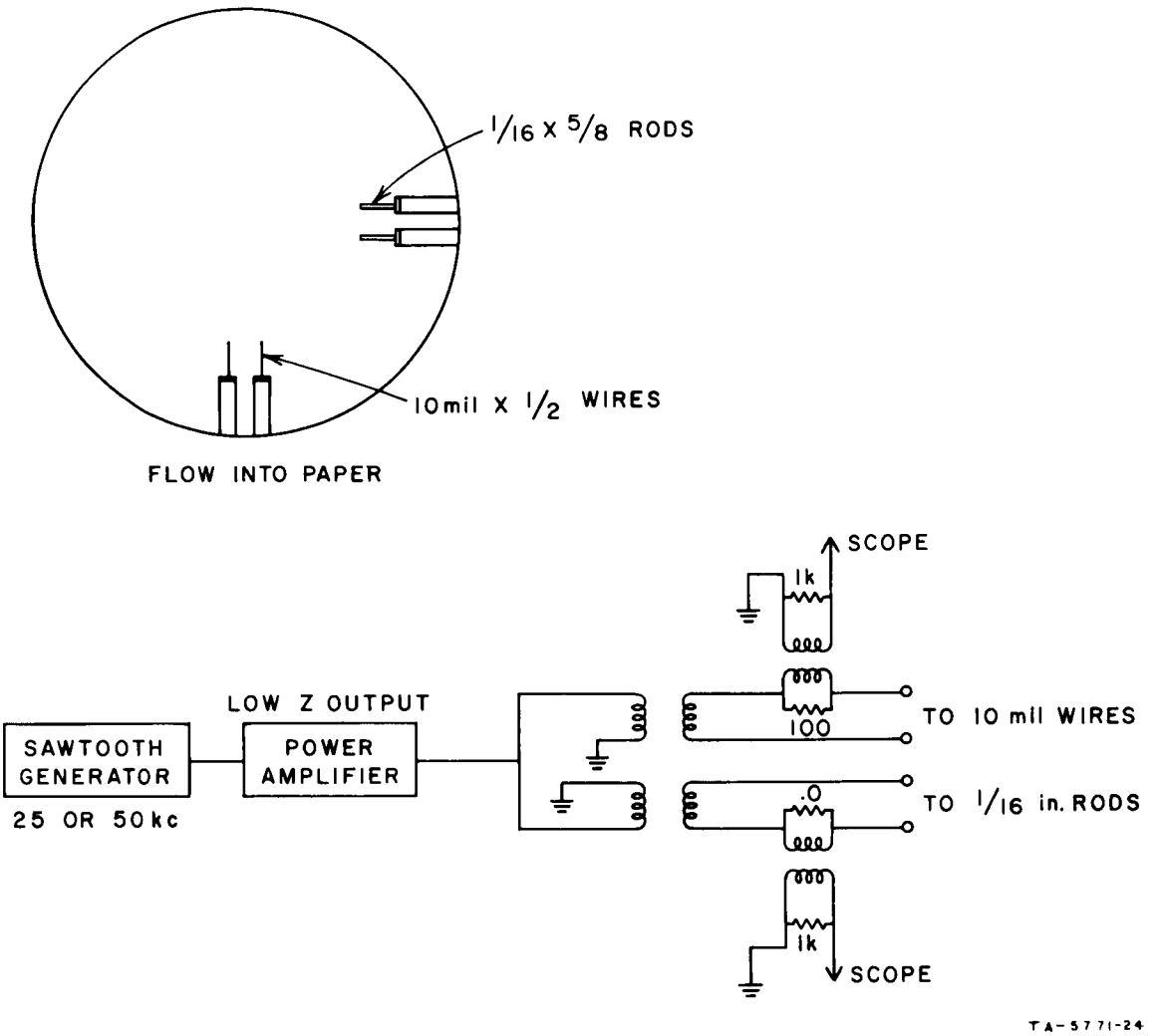

FIG. 24 CIRCUITRY USED FOR MEASURING ELECTRON TEMPERATURE AND LOCATION OF EQUAL-AREA PROBES IN THE SHOCK TUBE

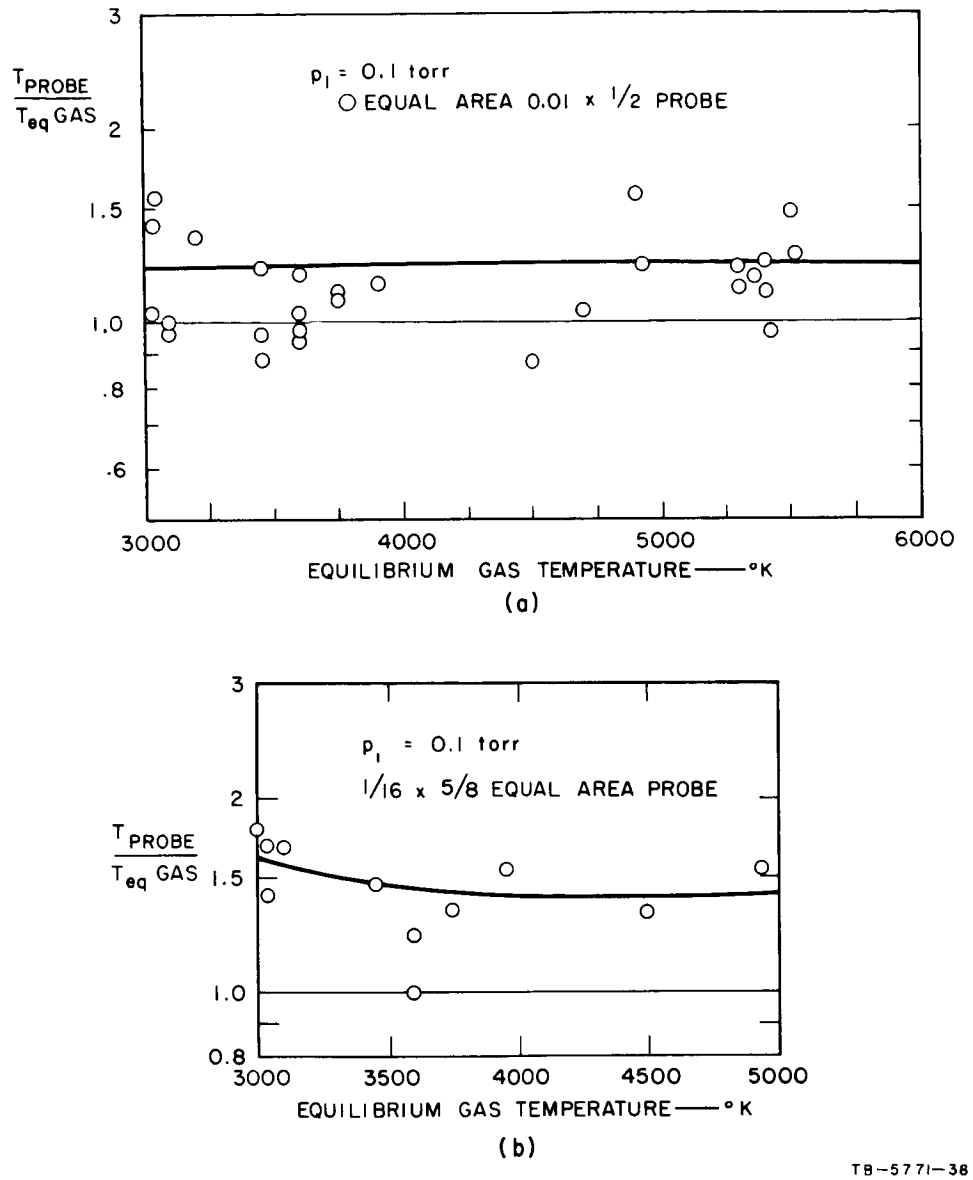

FIG. 25 RATIO OF INFERRED ELECTRON TEMPERATURE TO CALCULATED EQUILIBRIUM GAS TEMPERATURE AS A FUNCTION OF THE GAS TEMPERATURE

a. Probe Diameter = 10 mils
b. Probe Diameter = 1/16 inch

The results for the 10-mil-diameter probes indicate electron temperatures about 20% higher than the gas temperature throughout the slug length. We have no calculations of what the electron temperature behind the shock should be, but the following is an argument which suggests that the higher electron temperature is real and not an error introduced by the measurements.

The translational temperature of the gas decreases from a large value immediately behind the shock to the equilibrium value many mean-free paths behind the shock. This decrease is due to the translational energy being transferred to dissociation and ionization. From Ref. 7, the maximum ionization rate occurs when the gas temperature is about twice the equilibrium value. If it is true that the electrons are made with an average energy equal to the temperature at which they are made, the average electron temperature at this point would be about twice the equilibrium gas temperature. It might be thought that the electrons made further back in the slug at lower gas temperatures would have lower electron temperatures; however, the high thermal conductivity of the electron gas makes it difficult to maintain strong gradients in electron temperature. The higher temperature electrons provide energy to heat the cooler electrons. The temperature distribution for our conditions can only be determined by a detailed calculation. The above argument is intended only to suggest the plausibility of an electron temperature greater than the equilibrium gas temperature.

The results with the 1/16-inch probes indicates an electron temperature about 50% higher than the gas temperature. These probes are almost in continuum flow, and it is likely that a shock forms around them. The probes are therefore measuring the temperature of the electrons behind the shock surrounding the probe.

To see if this is plausible, we have calculated the ratio of the stagnation temperature to incident temperature as a function of the incident temperature. The results are shown in Fig. 26. The ratio of

the temperature measured by the 1/16-inch probes to that measured by the 10-mil probes is also plotted. Although there is considerable scatter, the assumption that the 1/16-inch probes were measuring the stagnation temperature is consistent with the data.

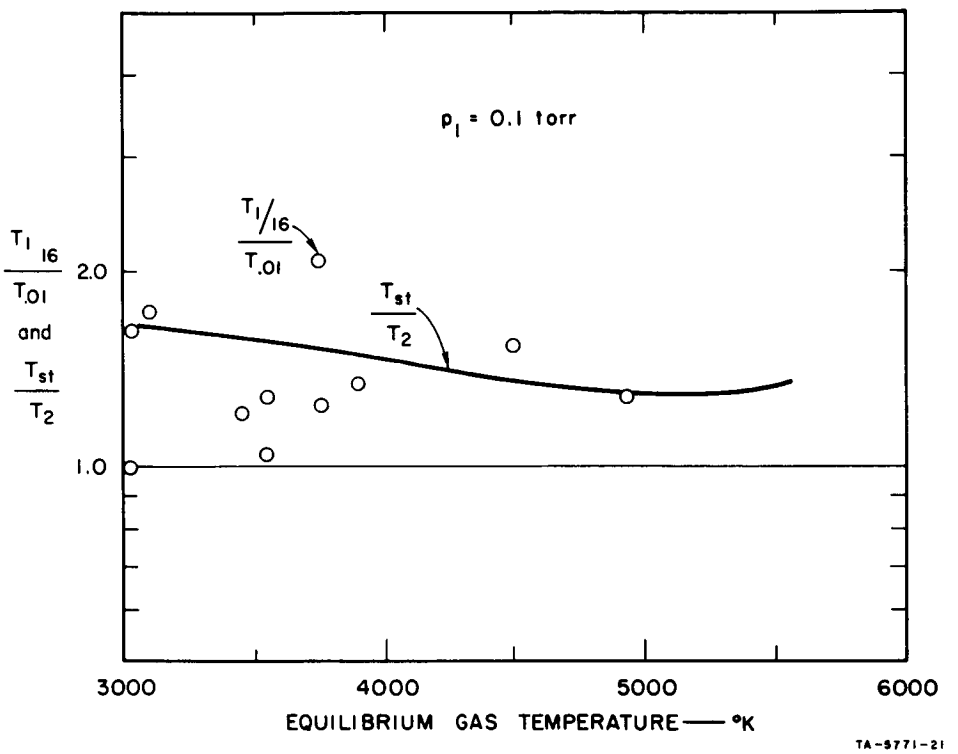

FIG. 26 RATIO OF ELECTRON TEMPERATURE INFERRED FROM 1/16-inch-diameter PROBES TO THAT INFERRED FROM 10-mil-diameter PROBES AND RATIO OF STAGNATION TEMPERATURE TO INCIDENT GAS TEMPERATURE AS A FUNCTION OF THE INCIDENT GAS TEMPERATURE

IV WATER INJECTION EXPERIMENT

A. INTRODUCTION

Recent experimental[12] and flight test[13] data indicate that the problem of re-entry communications blackout can be at least partially solved by water injection into the flow field about the vehicle. The injection of water serves two purposes: (1) evaporation cools the hot compressed air about the re-entry body, and (2) the droplet spray provides a large surface area within the plasma to enhance ion-electron recombination.[14] One major consideration in regard to water injection is the effect of water droplets on the operation of instruments located external to or on the vehicle surface. Of particular interest in the RAM experiments is the question of how the electrostatic probes will operate when they are immersed in a two-phase flow environment. Obviously, the answer to this question will depend strongly on the particular re-entry conditions, such as heating rate, altitude, and water flow rate.

The experiments to be discussed represent a preliminary investigation of electrostatic probe operation when probes are exposed to a mixture of flame plasma and water droplets. In view of the limited time available for the experiments (4 months) and the many inherent uncertainties involved, it was felt that a few simple qualitative experiments would serve best as pilot experiments and indicate areas requiring further study.

Two simple methods were employed to check electrostatic probe operation. A microwave interferometer was used to verify both the absolute and the relative response characteristics of the electrostatic probes. Additional verification was obtained by comparing the response characteristics of two electrostatic probes in the same plasma vicinity. One probe was exposed directly to the water spray, while the other probe was located in the water-cooled plasma but outside the region of direct droplet impingement. An existing seeded-flame facility was used as a plasma source, and an impinging jet atomizer served as the water spray

source. Three types of electrostatic probes were tested: (1) a single cylindrical probe using the burner as the second electrode; (2) a coaxial probe; and (3) a mockup of the RAM probe, i.e., a wedge-shaped dielectric block with a wire probe at the leading edge and the other electrode at the terminal end of the wedge.

In all experiments, water injection produced a drastic reduction in plasma charge density. However, while several experimental observations confirmed that water droplets were wetting the probes, the excellent relative response correlation between microwave interferometer and electrostatic probes indicated that water injection in these experiments did not adversely affect probe operation.

B. EXPERIMENTAL FACILITY

1. Flame Facility

The experiments were carried out in a low-pressure flame facility. The low pressure chamber is shown in Fig. 27 and described in detail in Ref. 15. The ethylene-oxygen burner is located at the bottom center of the vacuum chamber; the vacuum pump connection is vertically above the burner at the top of the chamber.

All experiments were conducted at 10-torr ambient pressure and at an initial flame charge density of about 10^{11} ions/cc. The charge density level in the flame was maintained by seeding with potassium-chloride salt.

Two types of burners were used in the experimental work. The initial instrumentation checkout was conducted using a flat carbon burner 10 cm in diameter, which gave rise to a laminar flame exhaust. The RAM mockup was tested in a high-velocity turbulent exhaust jet from a low-pressure combustion chamber with a 1-inch-diamter exit nozzle. Diagrams of the two types of burner geometries are shown in Fig. 28.

In the low-velocity laminar flame experiment, the water spray was injected diametrically across the exhaust jet, splitting the exhaust into three distinct regions: (1) a hot region below the water injection station, (2) a water spray and flame interaction region, and (3) a cooled exhaust region above the extent of the water spray.

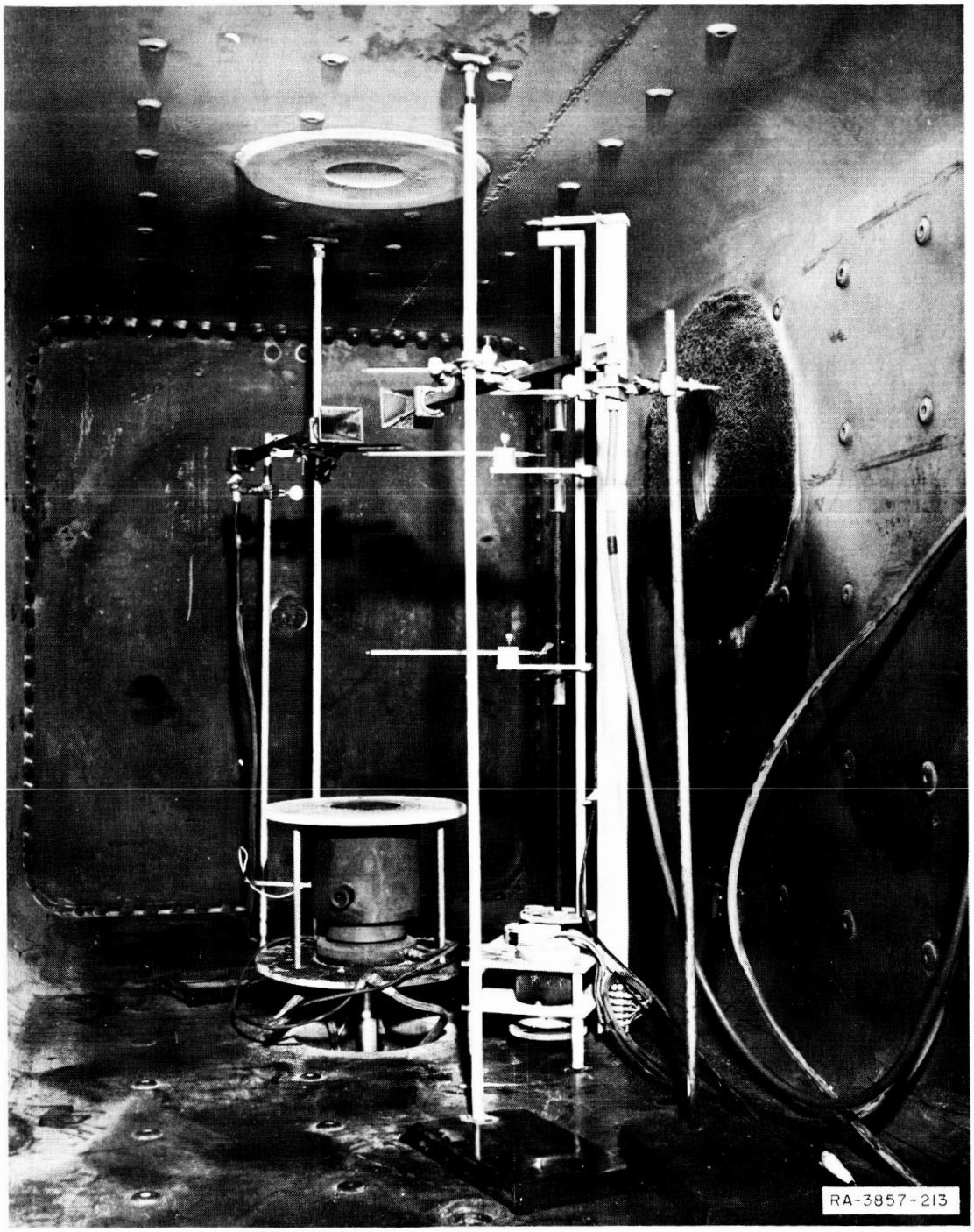

FIG. 27 PHOTOGRAPH OF EXPERIMENTAL APPARATUS WITHIN LOW-PRESSURE CHAMBER

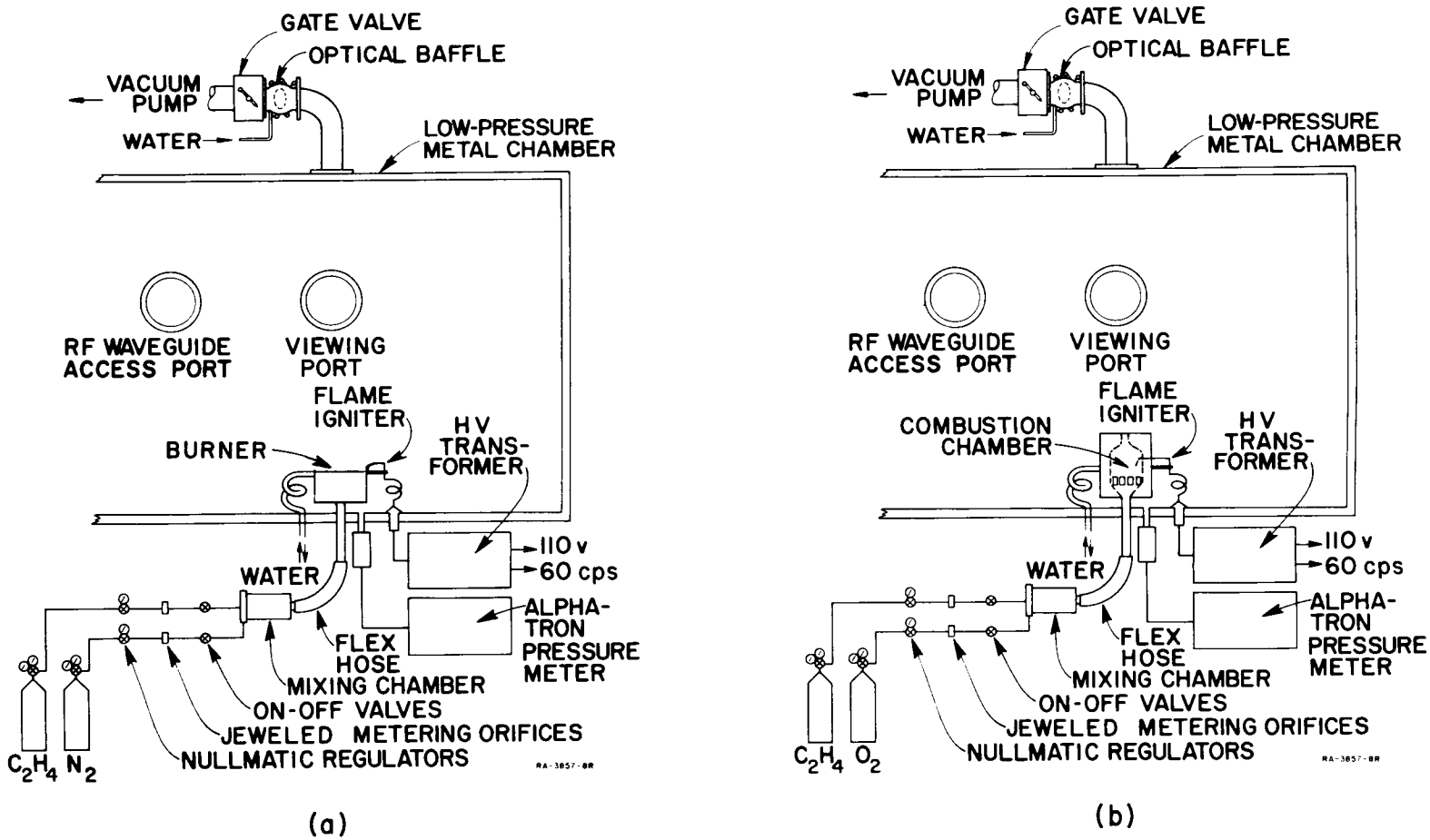

FIG. 28 SCHEMATICS OF THE LOW-PRESSURE CARBON BURNER
(a) Low-pressure laminar flame burner arrangement
(b) Low-pressure turbulent flame burner arrangement

The laminar flame experiments provided a more closely controlled experimental environment than the turbulent flame experiments, in that the velocity and charge density profiles across a jet diameter were relatively uniform, the exhaust charge density level before water injection was steady, and the spatial extent of the droplet spray was more clearly defined. On the other hand, two disadvantages of the laminar flame setup, the very low exhaust velocity (20 m/s) and the orthogonal orientations of the spray fan and exhaust jet, made it difficult to test the mockup of the RAM probe. Most experiments testing the wedge type electrostatic probe were therefore conducted in the high-velocity (230 m/s) turbulent flame. The laminar flame was used for the initial instrumentation checkout and for extensive testing on the cylindrical single electrostatic probe. The probe served later as a standard for comparison with other electrostatic probe geometries.

In the high-velocity turbulent flame, the water spray was injected approximately along the exhaust axis in order to simulate flight conditions more closely. In all experiments, water injection was continuous once injection was begun.

2. Water Injection

The water spray was produced by means of an impinging jet atomizer of the type used in liquid-rocket combustion chambers. A diagram of the injector is shown in Fig. 29. The impinging jet produces a finely atomized spray fan of elliptical cross section. The droplets in the spray have a directed forward velocity proportional to the jet velocity at the orifice. Considerable experimental work has been done on the impinging injector at atmospheric pressure,[16-21] permitting at least an estimate of the mean droplet size to be made from a knowledge of the injector geometry and the injector flow rates alone. In addition, the impinging jet atomization process introduces a desirable modulation of the water concentration in the plasma. The mass density across the spray fan varies approximately as a cosine function[20] across both the major and minor axes of the ellipse.

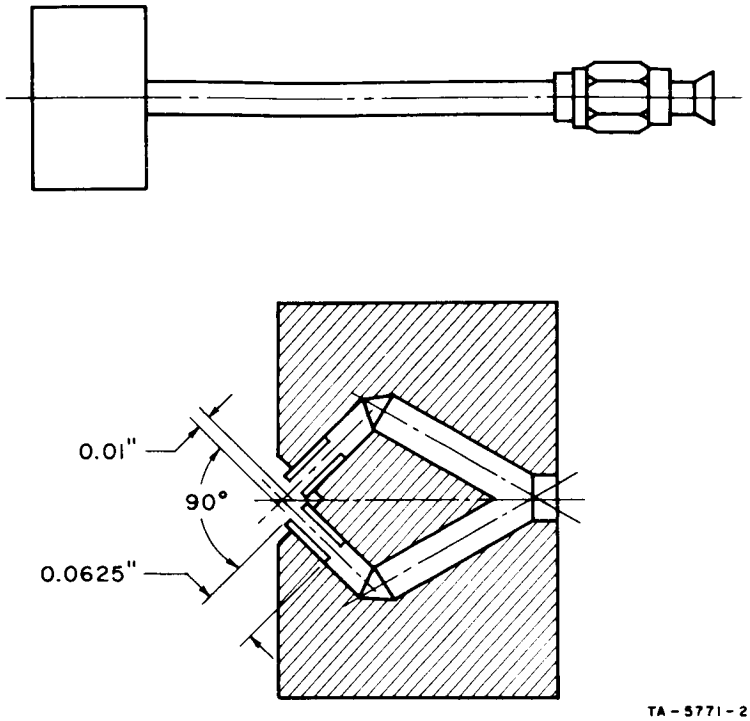

FIG. 29 DIAGRAM OF THE IMPINGING JET ATOMIZER

The impinging injector used in this experiment consisted of two jet orifices of 0.25-mm diameter. The jets impinged at a 90^0 impingement angle. The droplet spray velocity was varied from about 20 to 60 m/s. The modulation of water droplet density in the plasma included frequency components up to about 1300 cycles/s. It is estimated that for the presently used injector, the mean droplet diameter is about 100 μ when injection takes place at atmospheric pressures.[22]

For the present experimental conditions, the injector was preheated to about 100^0F to prevent freezing of the orifices. At this temperature the water vapor pressure is about 48 torr, or roughly five times the ambient pressure. Under these injection conditions, it is necessary to investigate the existence of two-phase flows in the orifices, the droplet and impingement sheet instabilities, and the changes in droplet size due to evaporation losses.

Since the water stagnation pressure for all injection conditions was well above the water vapor pressure, metastable single-phase flow was assumed to exist within the orifice tubes,[14] although the orifice exit pressure of the water was probably not the ambient pressure but rather the liquid vapor pressure. Upon emergence from the orifice tubes, the water jet is assumed to further expand until the jet pressure equals the ambient pressure, while evaporation of the liquid takes place simultaneously.[14] However, the high latent heat of vaporization of water and the cold ambient atmosphere limit the amount of water that can be evaporated before the droplets reach the flame plasma. For the present experimental conditions, only about 6% of the droplet mass can be evaporated before the droplet vapor pressure is reduced to values compatible with ambient flow conditions. This would correspond to a change of less than 2% in droplet diameter. Kurzius and Ellison,[23] in preliminary investigations regarding droplet instabilities, could find no measurable difference in droplet diameters between cold water injection and heated water injection. They concluded that small initial evaporation losses cooled the droplets fast enough to prevent the appearance of droplet instabilities.

It is not thought that the overall liquid sheet at the point of impingement was changed significantly relative to the overall sheet characteristics at atmospheric pressure. This was confirmed from experimental observation, which indicated that the usual impinging jet-spray pattern existing at atmospheric pressure was repeated at the low ambient pressures. It was also observed that without the flame plasma present, the droplet spray would impinge on the opposite wall of the vacuum chamber about 2-1/2 ft from the injector. In view of the absence of gross changes in the injector spray characteristics, it was assumed that the estimates of droplet size obtained at atmospheric pressures could be used for the low ambient pressures present in these experiments, at least as a first approximation.

Since the water droplets would flash into vapor either in the flame plasma or upon impingement on the chamber walls, the additional mass of gas in the vacuum chamber taxed the capacity of the pumping

system and generally caused the chamber pressure to rise. Correspondingly, a typical experimental run was restricted to less than 8-s duration. Changes in the chamber pressure were generally accompanied by changes in the measured maximum flame charge density. In a few runs, the rise in chamber pressure was disregarded and water was injected for longer periods of time to see whether one could in fact coat the probes with water in the hot flame environment.

3. Instrumentation

The charge density in the flame was monitored by two electrostatic probes and an X-band microwave interferometer. The general characteristics of the X-band microwave interferometer system are described in Ref. 1. The electrostatic probe located immediately below the microwave horns was called Probe B (see Fig. 30); the probe above the microwave horns was called Probe C. An electrostatic Probe A was often used to monitor the initial flame charge density below the spray injection station.

Microwave measurements were made with the electrostatic probes in place at the flame center. The close proximity of the probes to the microwave horns was shown to have only negligible effect on the microwave interferometer readings. The effect of the presence of water spray alone between the microwave interferometer horns was also checked and was shown to have a negligible effect on microwave interferometer operation. From the microwave interferometer data, the maximum charge density at the flame centerline before water injection could be inferred by assuming plane-wave propagation and integrating the phase shift due to the nonuniform charge density distribution across the transmission path. The nonuniform charge density profile across a flame diameter was determined by means of electrostatic probe traverses.

The normalized charge density profiles for both the laminar and turbulent flames are shown in Fig. 31. The maximum charge density for both laminar and turbulent flow conditions was held to about 10^{11} ions/cc.

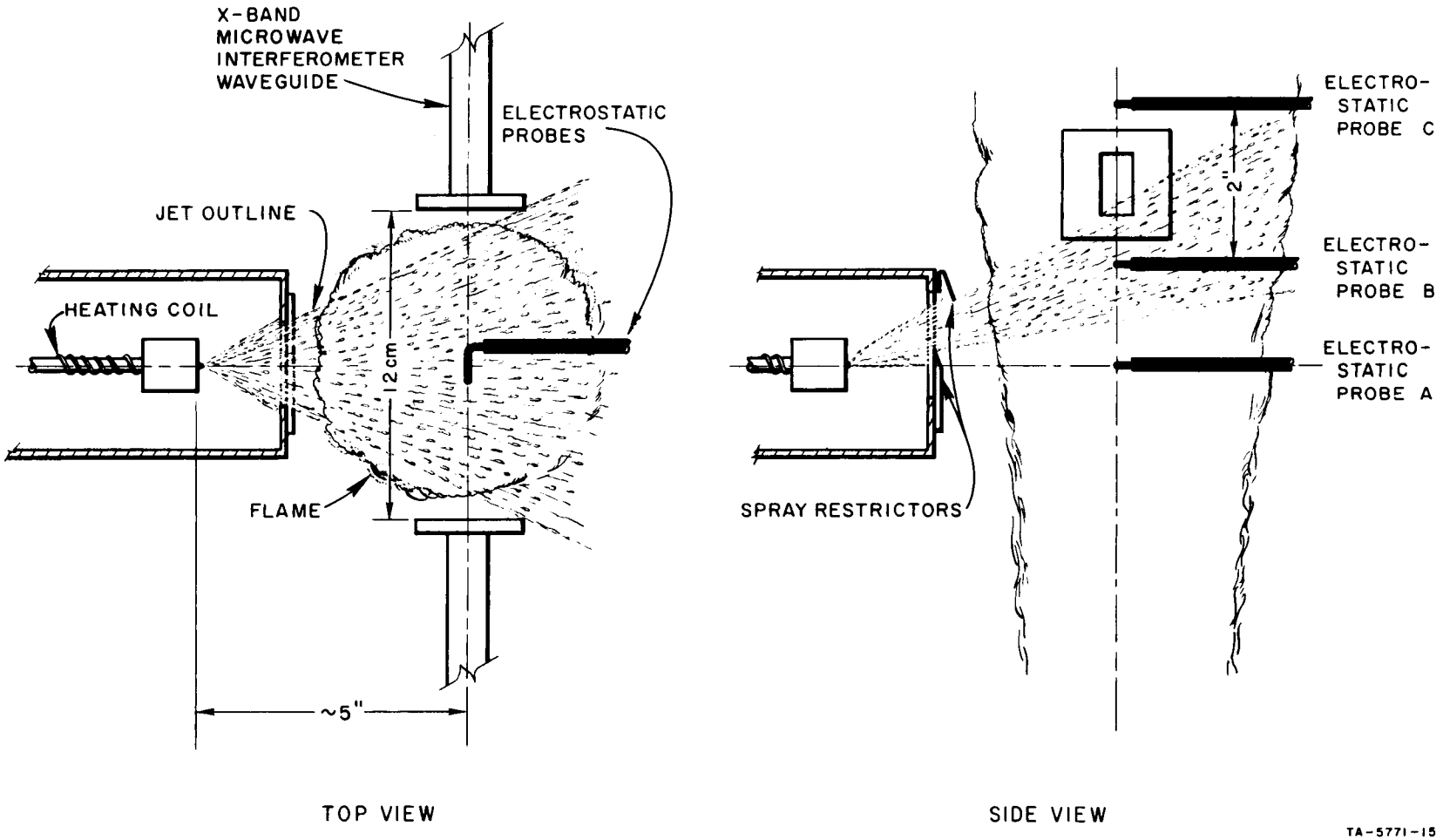

FIG. 30 DIAGRAM OF THE INSTRUMENTATION IN THE LAMINAR FLAME EXPERIMENT

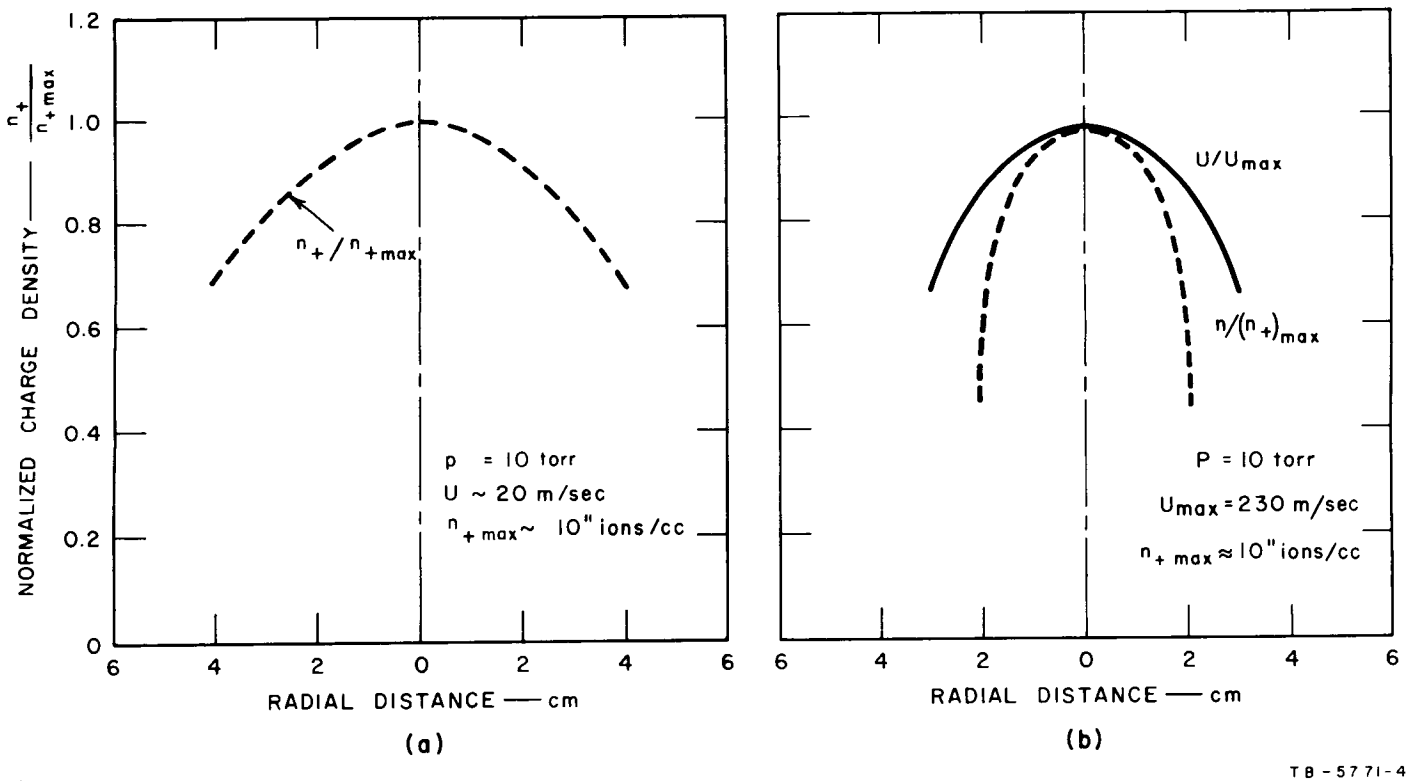

FIG. 31 FLAME CHARGE DENSITY PROFILES
(a) Laminar flame
(b) Turbulent flame

Different probe geometries were substituted for the electrostatic B and C probes in some of the experiments. The probe geometries tested are shown in Fig. 32. In most experiments the single electrostatic probe was used. For this probe the burner was used as the second electrode. The coaxial probe was tested because the two electrodes are in close proximity, and it would therefore be more likely to short out quickly when exposed to the water spray. The wedge probe was a mockup of the RAM probe configuration. All electrostatic probes were biased at -6V for the collection of ion saturation current.

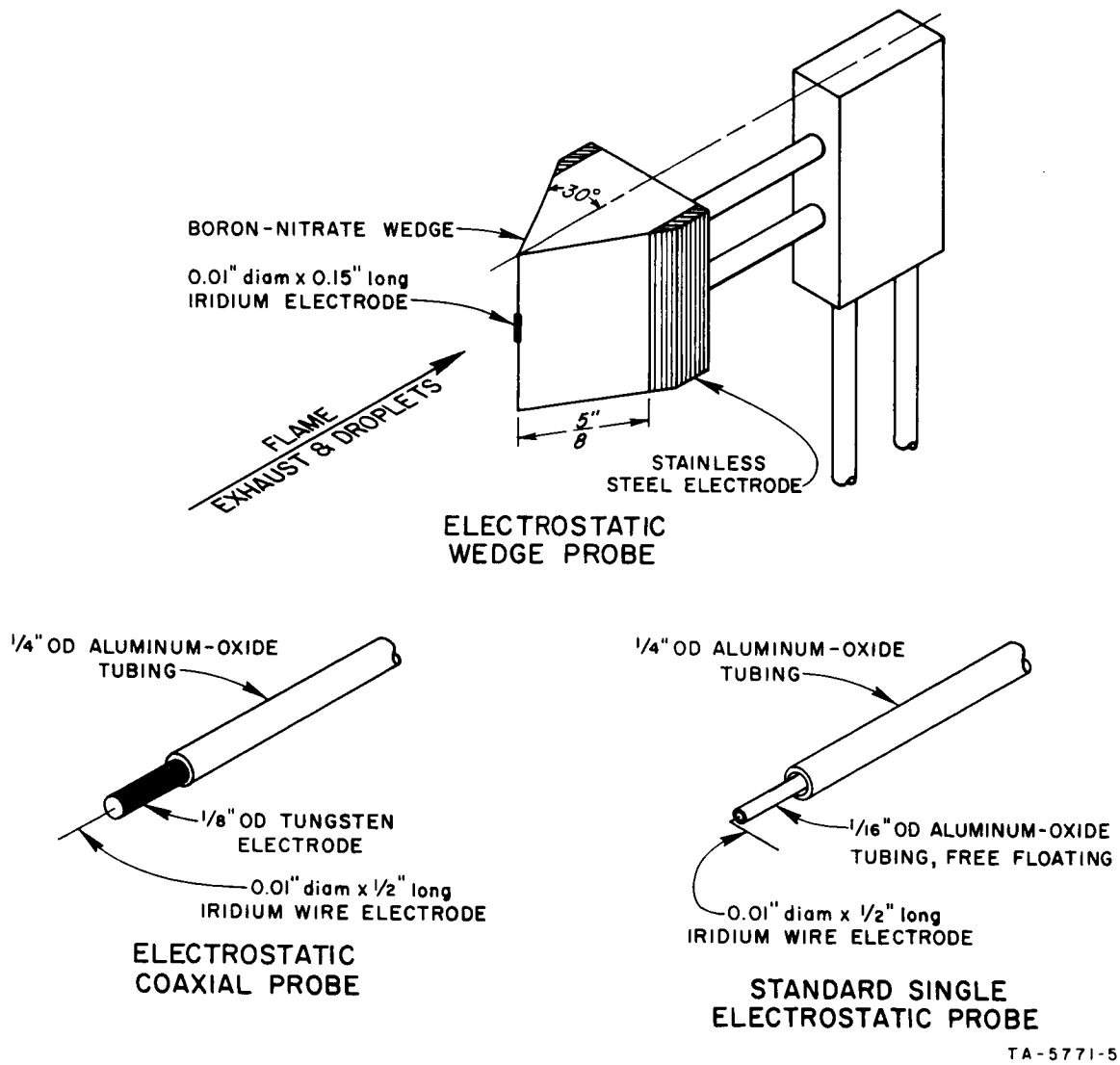

FIG. 32 ELECTROSTATIC PROBE GEOMETRIES USED

C. EFFECTS OF WATER SPRAY ON PROBE OPERATION

1. Water Injection Into Laminar Flame Exhaust

The laminar exhaust jet flame was produced by an open flame burner 10 cm in diameter. The gas flow rate was 0.5 gr/s. At the test station, about 30 cm above the burner, the exhaust jet was 12 cm in diameter and the exhaust velocity was about 20 m/s. The velocity was assumed to be uniform across a jet diameter. Actual velocity measurements in the laminar flame were not made because of the low flame velocity and low neutral gas density. Water was injected horizontally by means of an electrically heated impinging jet injector. The total water mass flow rates were generally held constant at 1.5 gr/s; however, apertures on the injector restricted the amount of spray passing through the flame to about 0.3 gr/s. Higher water flow rates would totally cool the flame above the water injection station, so that no measurable charge densities were left. The maximum water mass flux at the spray center was estimated to be about 10^{-2} gr/cm^2/s. This meant that about 3.22×10^{-4} gr/s of water were incident on the electrostatic probe cross section. Assuming the initial mean droplet diameter to be about 100 μ, the number of drops striking the probe was 615 droplets/s, obtained from $n_p = 6\,\dot{m}/\pi d^3 \rho$. Furthermore, an estimate of the droplet number density can be obtained if one considers that the droplets move with a transverse velocity of about 20 m/s. Then, assuming a uniform droplet distribution across a unit area at the probe station, the droplet number density is given by

$$n_p = 6\,\dot{m}/V_d \rho \pi d^3 = 10 \text{ droplets/cm}^3 \quad .$$

a. Water Injection Without Flame

To verify that the probes were indeed exposed to a high water droplet flux, cold tests were run at 10-mmHg chamber pressure. The injector was in the same position as in the laminar flame experiment. Injector flow rates were held to 1.5 gr/s. Probe C was out of reach of the spray, but on Probe B, small accumulations of water appeared at various circumferential positions. Probe B was totally covered in about 2 s.

To simulate the effect of the flame velocity, which might carry droplets downstream of Probe B, cold oxygen was injected while the spray was turned on. Essentially no difference in spray characteristics relative to injection into the cold stationary gas, was observed. For the 10-torr ambient pressure and cold-flow chamber condition, the spray would impinge in about the same general area on the opposite chamber wall, whether or not the oxygen gas jet was turned on. This is to be expected, since the drag force on the droplets is very small at this low ambient pressure.

b. Water Injection With Flame

Visual observation of the standard single electrostatic probe behavior in the laminar flame provided some interesting results. Before water was added, both electrostatic Probes B and C glowed brightly due to flame heating. The probe response monitored on a brushrecorder exhibited a steady-state dc response at this time, corresponding to the steady charge density in the flame.

Immediately upon water injection, the flame exhaust characteristics changed. The faintly violet color of the flame exhaust became completely invisible above the water injection section. In addition, Probe C, located in the cooled gas region, lost all color (probably because of cooling), while sections of Probe B, located at the spray center, seemed to fluctuate in color. By marking the ion-current response trace on the brush recorder when particularly eminent color fluctuations occurred, a correlation between no color and low currents, and bright color and high currents became evident. Since the correlation marks on the brush recorder were made manually, however, only gross features can be compared (owing to the inherent time lag involved).

The color fluctuations on Probe B cannot be explained on the basis of probe flame cooling and heating alone. The time required for the 0.01-inch-diameter iridium probe to reach 1000°C is estimated to be on the order of 1 s. The fluctuations in probe color were observed to be more rapid, on the order of 0.1 s.

In view of the high droplet vapor pressure relative to the ambient pressure, a possible explanation could be that the droplets flatten out upon impingement on the hot probe surface, increasing the efficiency of the thermal contact and absorbing sufficient energy from the surface to flash into vapor. The transient absorption of heat energy from the probe cools only the probe surface, which becomes red hot again after the impinged droplet has evaporated. The possibility of these processes are indicated by the following considerations.

The total heat content of the iridium probe, estimated to be at 1400°K in the uncooled flame, was 2.35×10^{-3} Btu. The heat transfer rate to Probe B in the partially cooled flame was estimated at 4×10^{-4} Btu/s. Neglecting any droplet mass loss due to evaporation as the droplets move through the flame, the energy required for evaporation of the total water mass flux incident on the probe ($\sim 3.22 \times 10^{-4}$ gr/s) is 7.8×10^{-4} Btu/s. Considering the high heat content of the probe, the rate of heat transfer to the probe, and the fact that droplet evaporation in the flame has been neglected, it becomes evident that more than sufficient energy is available at the probe for evaporation of the total incident water flux.

Figure 33 shows a typical brush recording of the probe current and the microwave interferometer phase shift during a laminar flame experiment with water injection. The bottom channel corresponds to Electrostatic Probe B, located just below the horns in the center of the spray. Probe C, on the top channel, is located just above the horns and is presumed to be above the droplet spray. The two middle channels correspond to the microwave measurements. One channel records the signal amplitude level transmitted through the plasma, while the other records the phase shift. Time increases from left to right at the rate of 0.2 s/div.

Note that in the laminar flame, the probe responses indicate a steady level on all instruments before water injection. Immediately upon initiation of water injection, the instrument response indicates a decrease in flame charge density. The difference in average response

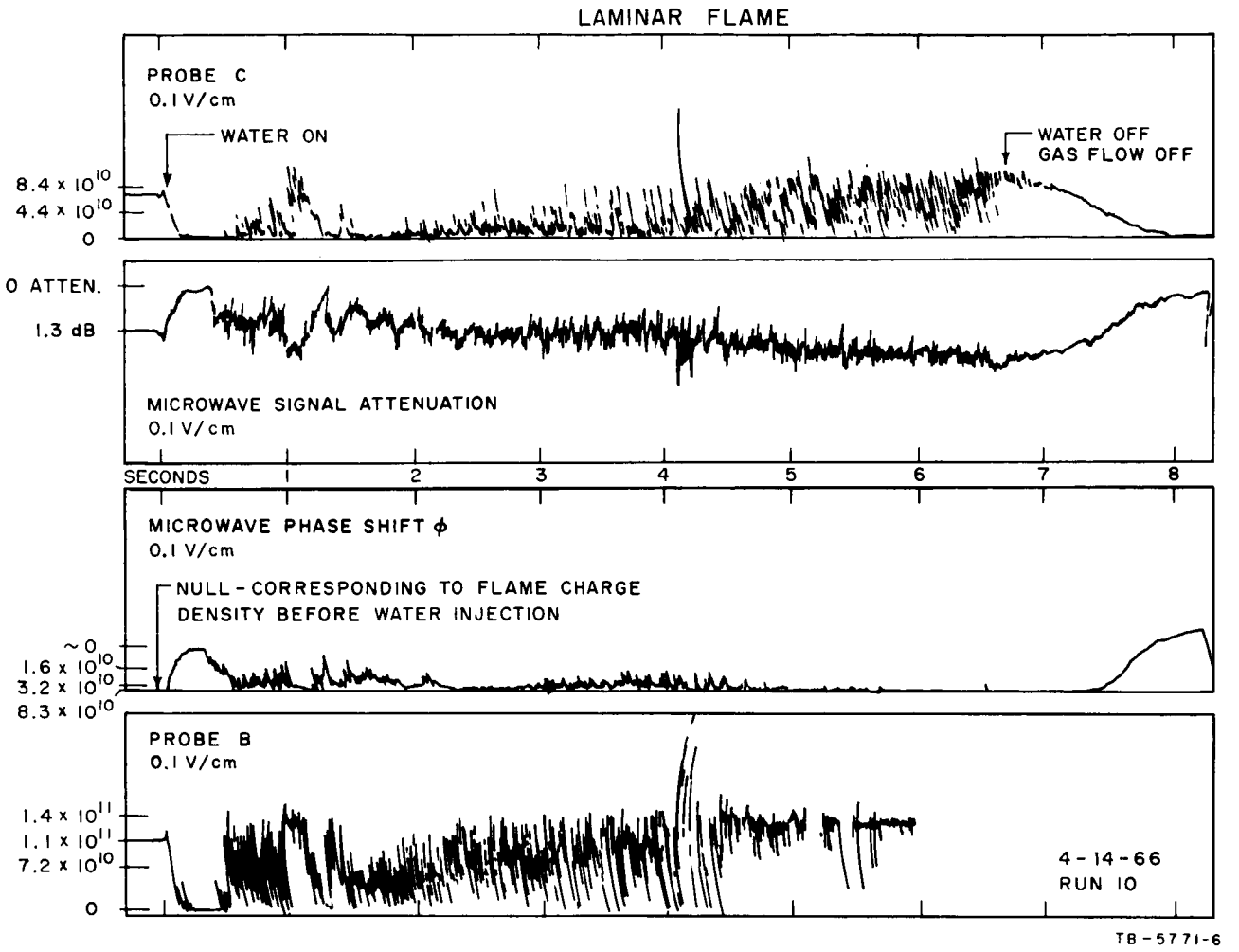

FIG. 33 TYPICAL LAMINAR FLAME RECORD INDICATING EFFECT OF WATER INJECTION
($P_\infty \approx$ 10 Torr, $U_{Gas} \sim$ 20 m/sec, P_{inj} = 40 Psig)

level between Probes B and C indicates that the average charge density level rapidly decreases with increasing distance from the water injection station. Also note that when the probes are operating properly, the relative responses of the microwave system and the probes are reversed. The microwave phase-measurement signal is nulled just before water injection, so that any signal deviation from the null denotes a change in charge density. Similarly, the maximum signal on the attenuation channel corresponds to zero charge density, or no attenuation (i.e., the presence of a plasma between the horns will decrease the signal level). The electrostatic probe signals are proportional to charge

density. The discontinuous decrease in charge density at the beginning of water injection is associated with transients in the injector starting process. Note that whatever the transient process, all instruments confirm the phenomenon. Since the microwave interferometer system is not sensitive to the presence of droplets but only responds to changes in charge density, correlation between microwave and probe fluctuations implies that these fluctuations are due to real changes in the flame charge density and not necessarily to droplets hitting the probe.

Note the rapid fluctuations. Since the microwave response is integrated across the flame cross section, it is to be expected that the frequency content of the microwave signal would not be identical to that of the electrostatic probes; however, it seems that all gross fluctuations that have durations longer than say 50 ms show up simultaneously on all channels.

Figure 34 shows a comparison of the absolute charge-density level variations after water injection was initiated, as measured by the microwave interferometer and the electrostatic Probes B and C. The data in Fig. 34 correspond to the first 2.6 s of the raw data in Fig. 33. Only gross variations in charge density are indicated. The restricted time interval of 2.6 s demonstrates sufficiently the observed typical characteristics associated with water injection into the laminar flame. Note that there is good correlation in both the frequency and amplitude of the microwave interferometer and electrostatic probe responses, and also that the average level of charge density can be decreased easily by simply increasing the water mass flow rate. In fact, the data in Fig. 33 are somewhat atypical, in that the average response level of the Probe C was increased so that the correlation between the various instruments regarding the fluctuations in charge density could be demonstrated more easily.

In Fig. 35, the relative probe current levels have been superimposed to confirm the excellent temporal response correlations between the various instruments and to compare the changes in relative response magnitude.

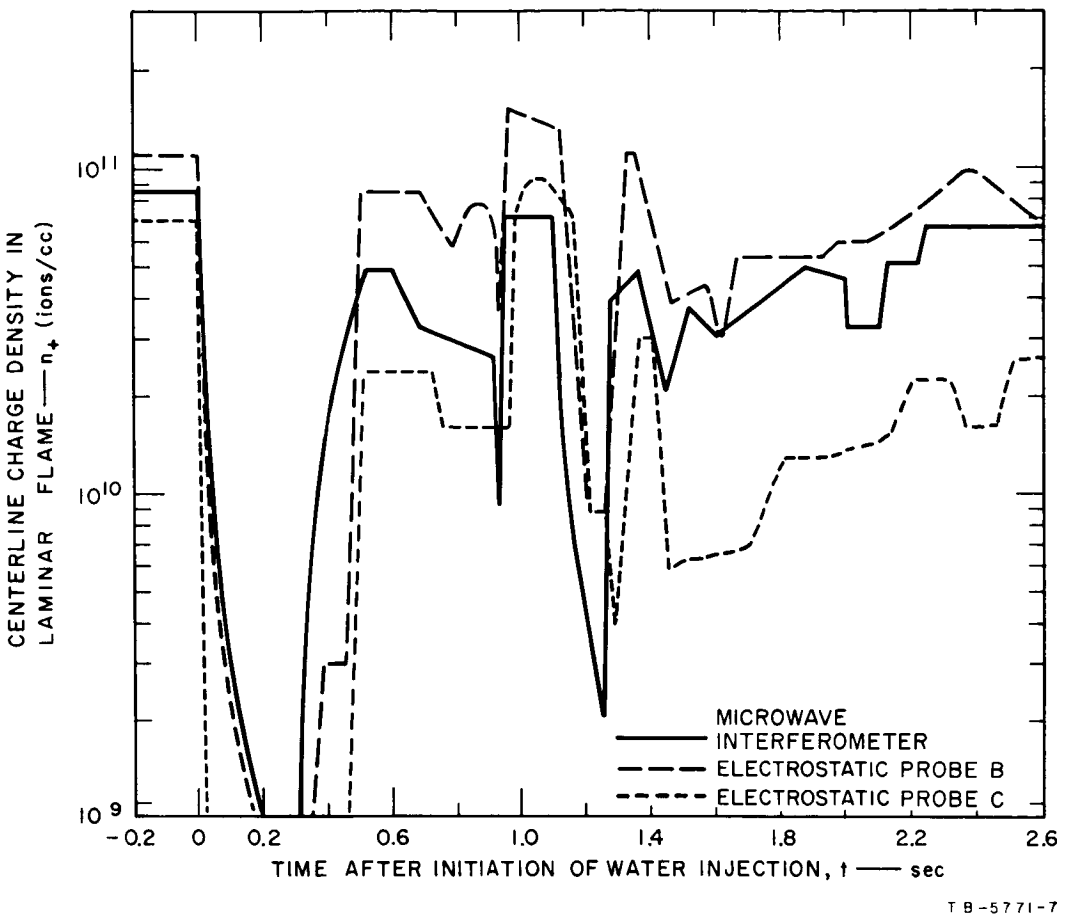

FIG. 34 ABSOLUTE CHARGE DENSITY LEVELS IN THE LAMINAR FLAME AFTER WATER INJECTION AS INFERRED FROM MICROWAVE INTERFEROMETER MEASUREMENTS AND ELECTROSTATIC PROBES ($P_\infty \approx 10$ Torr, $U_{Gas} \sim 20$ m/sec, $P_{inj} = 40$ Psig)

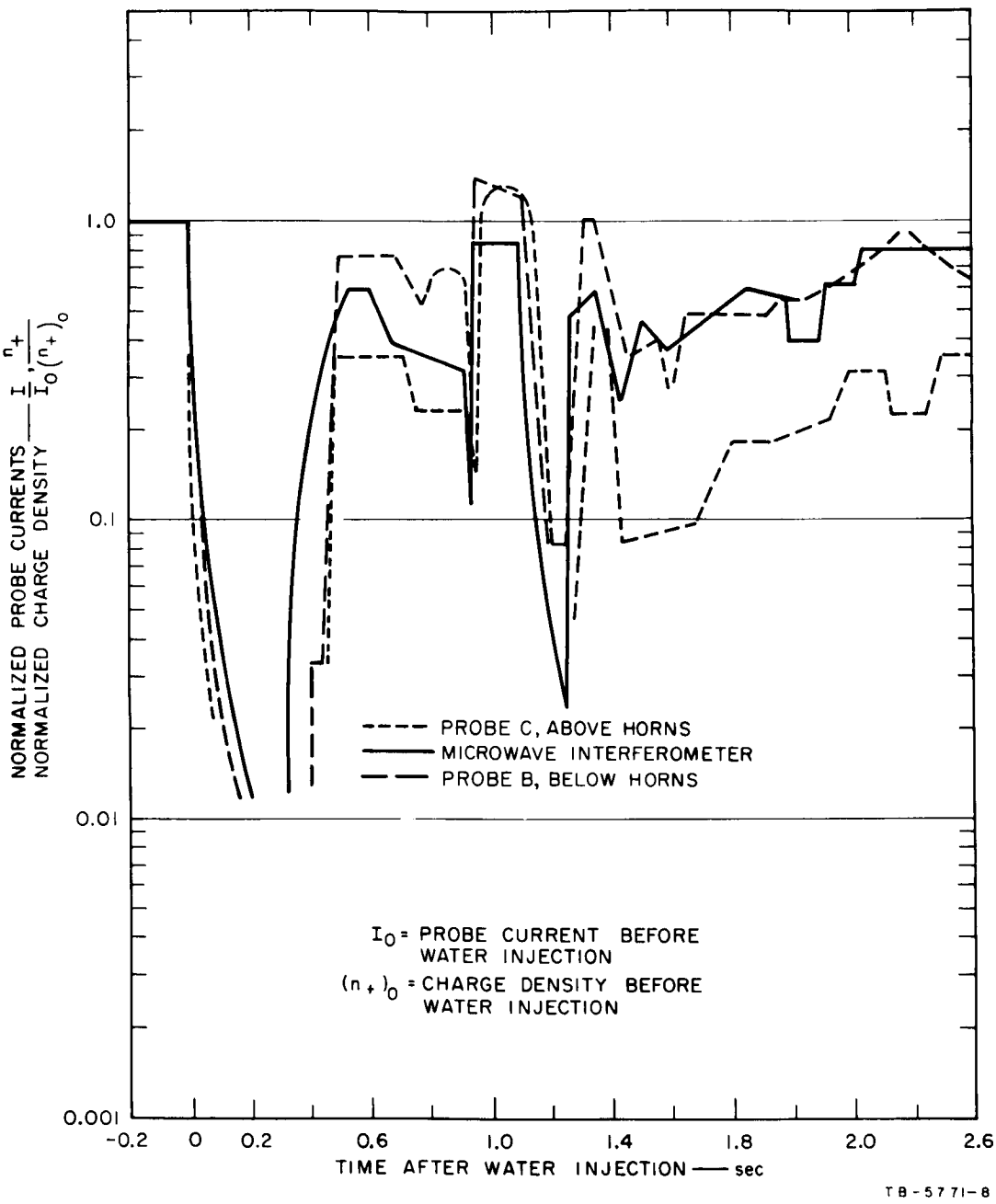

FIG. 35 COMPARISON OF NORMALIZED MICROWAVE INTERFEROMETER INFERRED CHARGE DENSITIES WITH THE NORMALIZED CHARGE DENSITIES INFERRED BY MEANS OF THE ELECTROSTATIC 'B' AND 'C' PROBE ($P_\infty \sim 10$ Torr, $U_{Gas} \sim 20$ m/sec, $P_{inj} = 40$ Psig)

It is necessary at this point to consider the uncertainties involved in the data reduction process. The large axial gradients in charge density in the laminar flame experiment after water injection invalidate the assumptions used in interpreting the microwave interferometer data. The magnitude of the resulting error is difficult to assess correctly and has not been evaluated. In Fig. 34 this error is not assumed to be serious, since the axial gradient in charge density variation is moderate. However, in the present experiments, generally, higher water mass flux rates produced steeper axial gradients in charge density.

Uncertainties in the electrostatic probe interpretation arise because the cylindrical probe radius is larger than the local mean-free path. Experiments in the flame facility which empirically verified electrostatic probe operation when the probe radius was larger than a mean-free path were conducted by Weissman, et al.[24] Weissman found that over a large variation in probe Knudsen number and over several orders of magnitude in charge density, the probe current was proportional to the local charge density: $(I_+)_{sat} = Kn_+$, where K was found empirically by substituting the charge density obtained from the microwave interferometer data into the above formula for the electrostatic probe current. The assumption was then made that the constant of proportionality K applied to the flame plasma after water injection, i.e., in the presence of water droplets.

The fluctuating response of the Probe B, i.e., the probe response after water injection, has been recorded on a spectrum analyzer. A typical spectrum record is shown in Fig. 36. The abscissa denotes frequency and the ordinate denotes the relative magnitude of the fluctuations, in dB. Note that at 1000 cycles/s, the amplitude decrease is about 10 dB. The peak signal on the right results from 60 cycles ac. The presence of similar fluctuations on the microwave interferometer data indicate that the fluctuations do not result from individual droplets hitting the probes, but rather from gross modulations of the spray fan. These modulations of the water spray density within the plasma cause local fluctuations of charge density. Comparing the frequencies

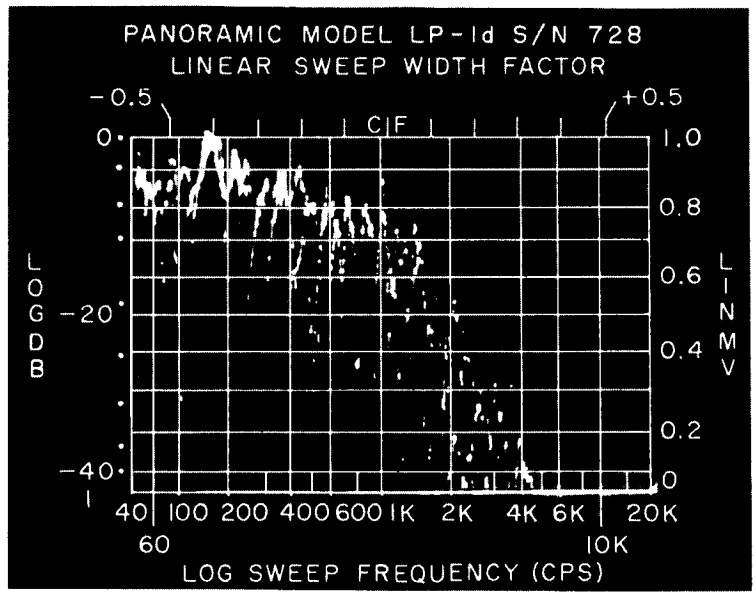

SENSITIVITY: .005 V/cm

TA-5771-9

FIG. 36 SPECTRUM ANALYZER RECORD OF ELECTROSTATIC 'B' PROBE RESPONSE

observed in our experiments to frequencies found characteristically in impinging jets,[18] it is found that for our experimental conditions (i.e., jet diamter, jet velocities, and impingement angles), our observed frequencies appear low by a factor of 2. This might be due to the low pressure environment, but it is more probable that it is attributable to the different type of impinging injector we used.

Figure 37 shows a typical vertical electrostatic probe traverse moving along the flame exhaust centerline. The ordinate denotes the normalized probe current, while the abscissa indicates the vertical distance from the centerline of the microwave interferometer horns. The injector apertures limit the vertical extent of the spray fan under cold-flow test conditions at the flame exhaust axis to a width of about ±1 inch. Note that there is a rapid variation in charge density in the spray region, and also that some water evidently reached the flame below the actual extent of the spray. The curve labeled "Run #1" corresponds to the first run, and the large shift in profile probably relates to the fact that the injector water feed lines were initially partially empty of liquid water. In these experiments a single electrostatic probe was moved vertically along the flame axis, and the extent of the probe movement was primarily limited by the time it took the chamber pressure to rise significantly and thus distort the charge density profile. A better experiment would use several probes at various axial stations in the flame simultaneously.

2. Water Injection Into Turbulent Flame Exhaust

A substantial increase in flame exhaust jet velocity was obtained by increasing the gas flow rate and using a combustion chamber with a 1-inch-diameter exit nozzle instead of an open-flame burner. The maximum centerline gas velocity was about 230 m/s; the gas mass flow rate was 1.2 gr/s.

To ensure a sufficiently uniform plasma region between the microwave interferometer horns, the centerline of the horns was located 30 cm above the nozzle exit. At this point the jet diameter was approximately 10 cm

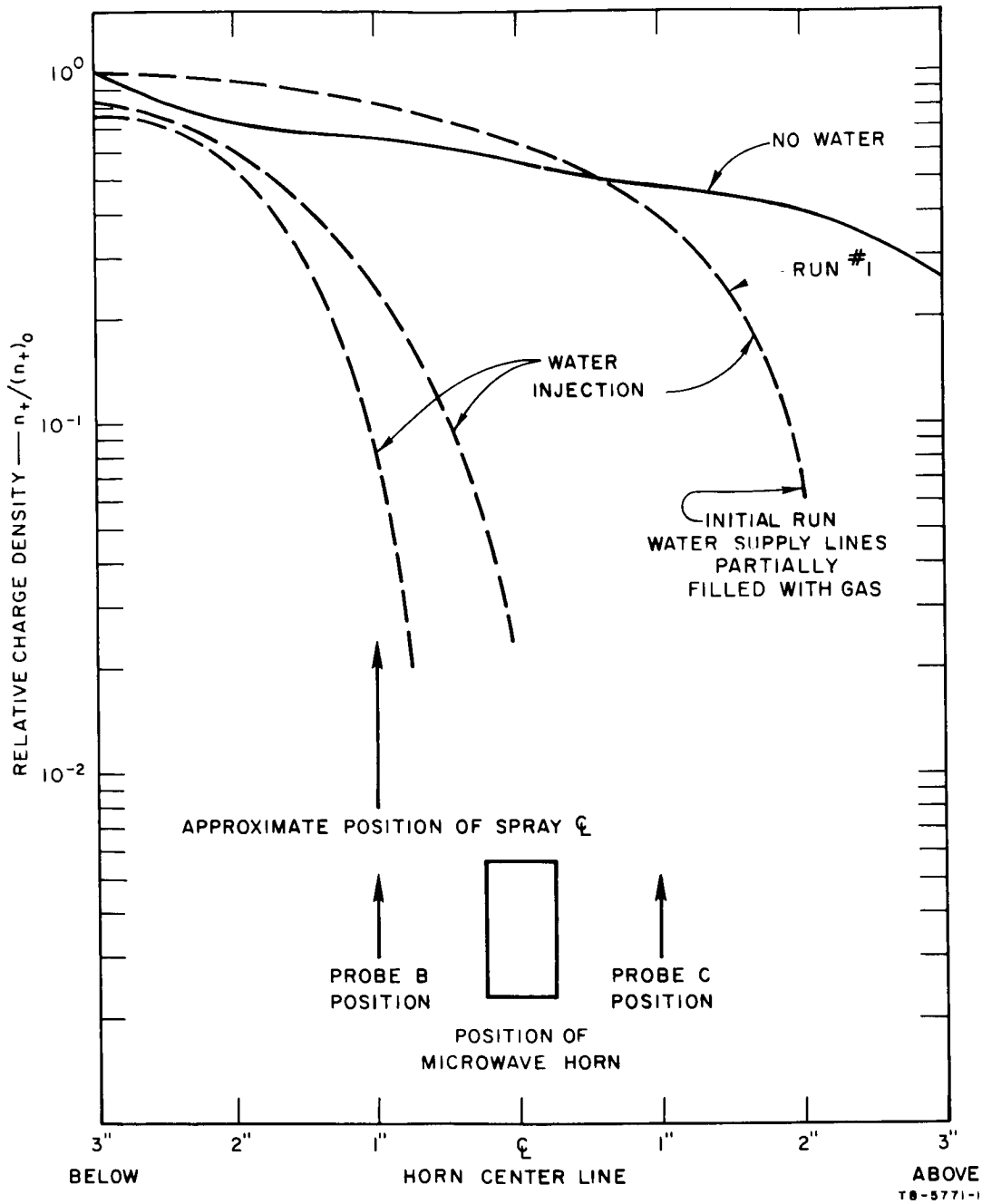

FIG. 37 AXIAL CHARGE DENSITY VARIATION IN THE LAMINAR FLAME

and the jet had become highly turbulent. A typical velocity and charge density profile across a jet diameter is shown in Fig. 31.

As mentioned previously, the direction of spray injection was changed to coincide approximately with the jet velocity (See Fig. 38). Under cold-flow conditions, the spray fan center passed through the centerline between the horns, 21 cm from the point of impingement. The same injector was used as in previous tests, but without restraining apertures. The injector mass flow rate was varied from 1.5 to 5 gr/s. This corresponded to a variation in water mass flow flux from 0.1 $gr/cm^2/s$ to 0.3 $gr/cm^2/s$. The spray velocity varied from 20 to 60 m/s.

Three sets of experiments were conducted, testing different types of probe configurations:

(1) The standard single electrostatic probes
(2) Coaxial electrostatic probes
(3) A wedge probe in the Probe C position.

a. Standard Single Electrostatic Probes

In order to compare the turbulent and laminar flame results, the standard electrostatic probes were used initially to analyze the turbulent flame exhaust. Since this flame was substantially cooler ($\sim$1000°C) the probes did not heat up as much as before, and visual observation of probe color changes was not possible. In addition, as seen in Fig. 39, the turbulent nature of the exhaust jet, i.e., the large random fluctuations of charge density before water injection, limited the observation of water injection effects to observation of gross phenomena.

It was again found that the electrostatic probes, and also the microwave interferometer, indicated a substantial discontinuity in signal level when the water injection process was initiated. The correspondence between the fluctuations on the microwave signal and the electrostatic probe signal indicated that these fluctuations were associated with fluctuations in charge density. However, in the high-velocity flame experiment, the decrease in the average level of the

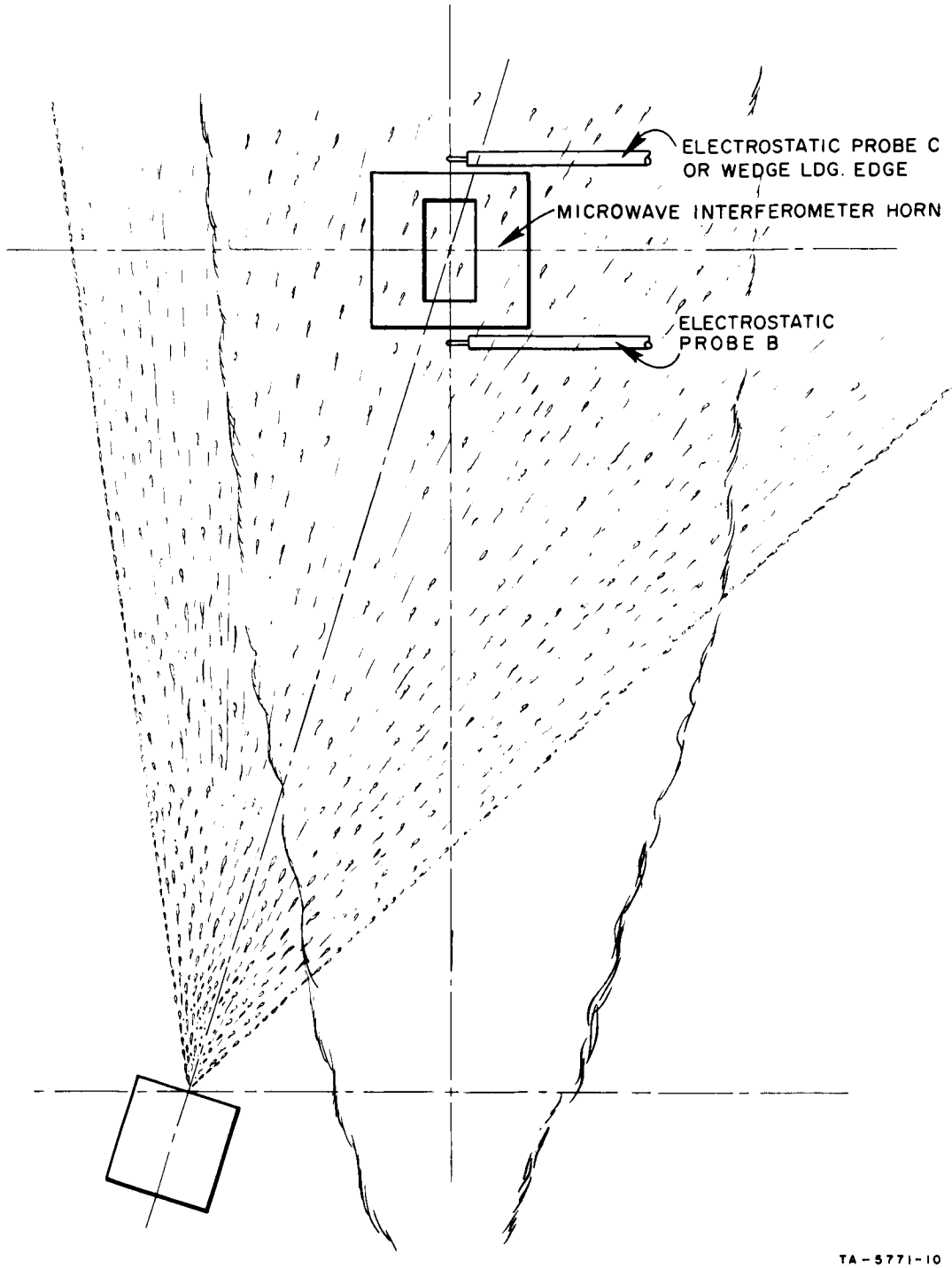

FIG. 38 EXPERIMENTAL ARRANGEMENT IN THE TURBULENT FLAME SET-UP

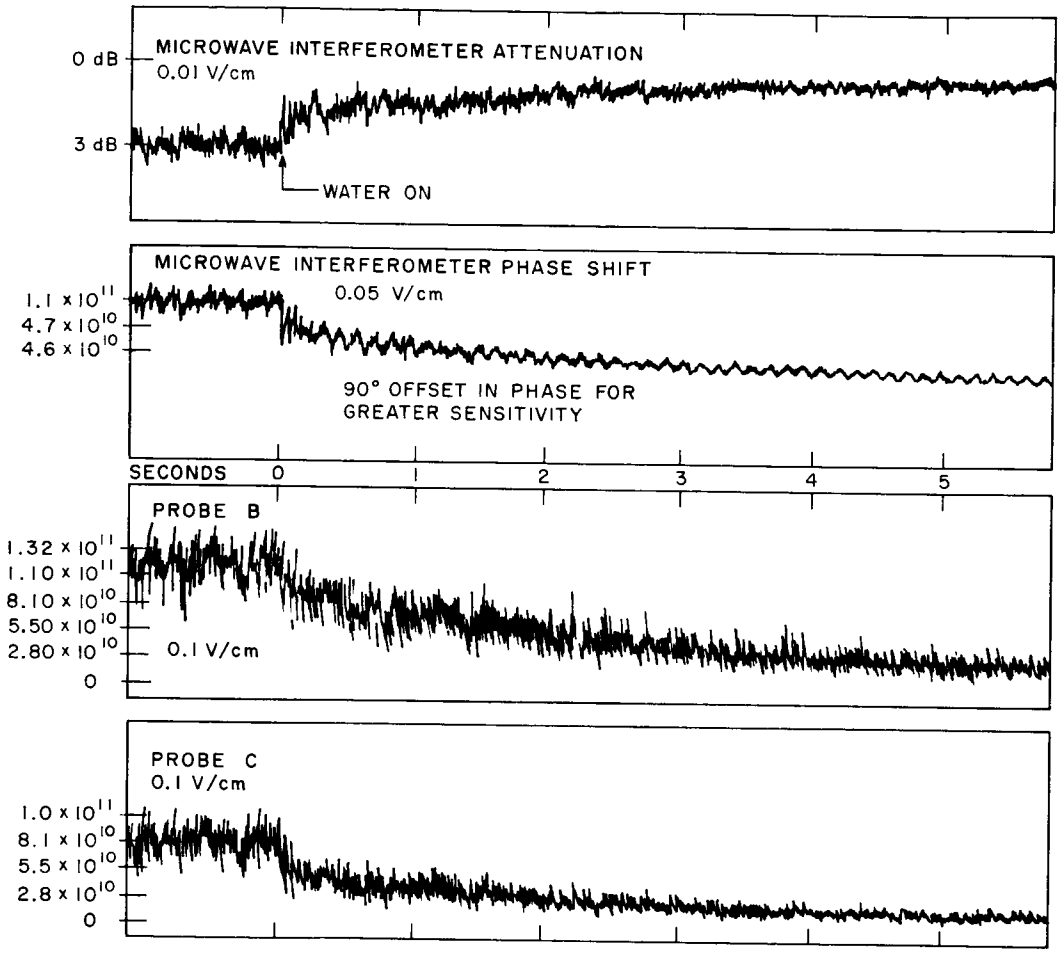

FIG. 39 TUR
LON
RES
(P_∞

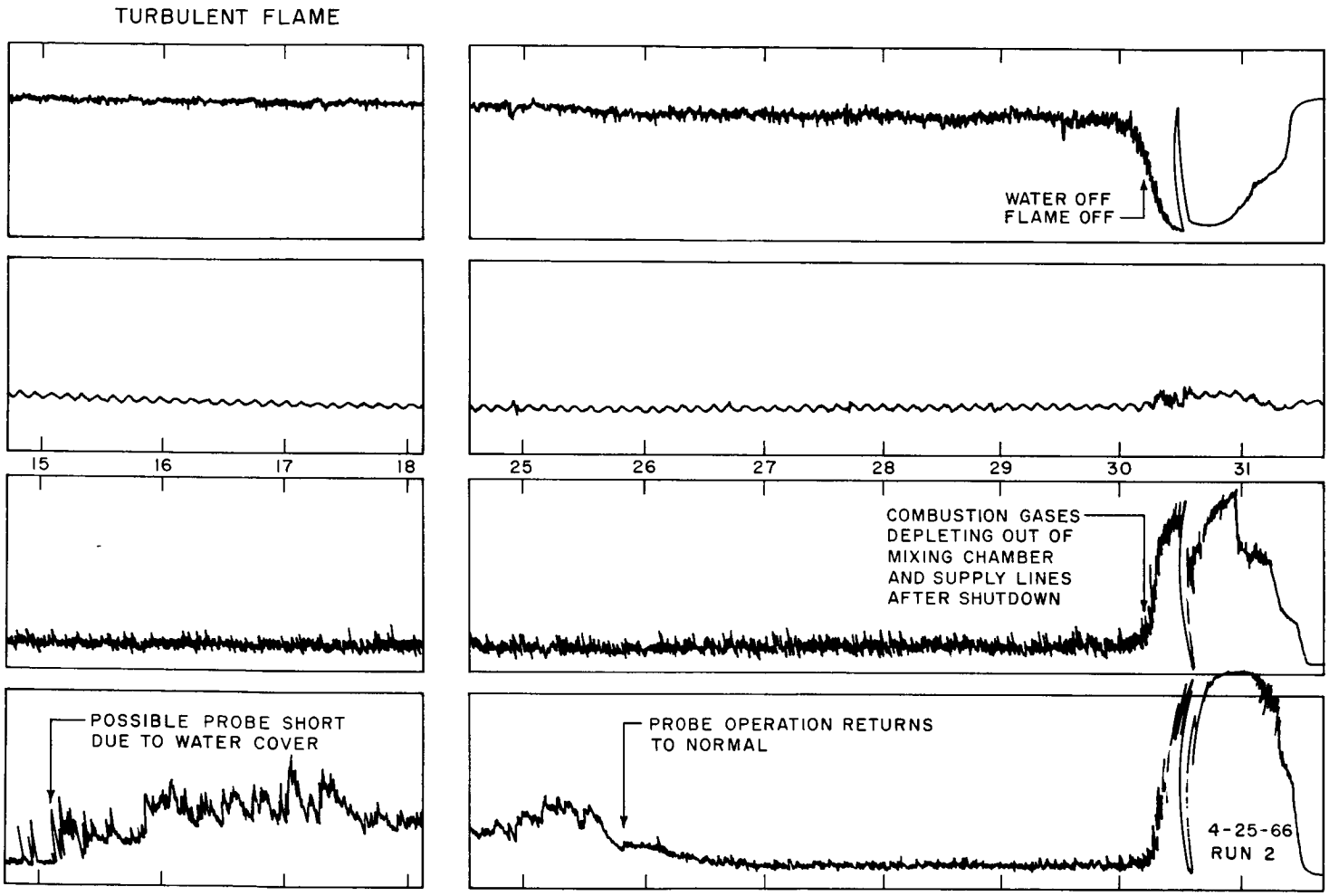

BULENT FLAME RECORD DISPLAYING
G-TERM COAXIAL ELECTROSTATIC PROBE
PONSE
~ 10 Torr, U_{max} ~ 230 m/sec, P_{inj} ~ 300 Psij)

FIG. 39

charge density after water injection was initiated was not as drastic as in the laminar flame experiment. At 1.5-gr/s water flow rates, Probe B current level, for instance, decreased only about 30%, while Probe C current level decreased about 70%. Again, at the low water flow rates, immediately upon initiation of water injection, the flame charge density temporarily decreased to zero, but it recovered more quickly to the aforementioned average levels than in the laminar flame experiment. This phenomenon seems to be associated with the transient injector characteristics, because it disappears at the larger injector flow rates.

Typically, after a few seconds of water injection the chamber pressure would increase, owing to limitations on the pumping capacity; the increase in pressure would in turn increase the charge density level in the exhaust jet. When additional pumping capacity was switched in manually, the observed charge density and the pressure would temporarily decline. These variations in average level of charge density were confirmed by all instruments.

In none of the above experiments did the electrostatic probes show any signs that probe operation was influenced by water injection.

b. Coaxial Electrostatic Probes

The coaxial electrostatic probes are similar to the standard probes except that the second electrode, a cylindrical tungsten mantel around the dielectric probe support, is in the immediate vicinity of the probe electrode (see Fig. 32). This configuration is the most likely to be shorted because of the close proximity of the two electrodes. Indeed, the brush recording shown in Fig. 39 indicates that a short may have occurred after 15 s on Probe C.

Note the turbulent fluctuations on all channels before water injection, and also the instantaneous but relatively small decrease in charge density after initiation of water injection. The subsequent steady decrease in charge density level is probably due to slowly decreasing chamber pressure. An additional vacuum pump was switched

into the system to hold the chamber pressure constant, but manual valve operation could not keep the pressure entirely steady.

At 14.8 s after water injection, coaxial electrostatic Probe C indicates an anomalous increase in probe current which is not confirmed by either Probe B or the microwave interferometer. The water mass flow rate was about the same as in the laminar flame experiment, i.e., 0.3 gr/cm^2/s. Note that the extraneous current disappears about 27 s after initiation of water injections.

The current overshoot at the end of the record corresponds to flame shut off. After the gas supply valves are closed, the gas supply still in the supply lines empties into the combustion chamber and the flame goes through a transient, hot, laminar stage. At flame shutoff, the chamber pressure had increased from the initial 10-torr level to 20 torr. Time limitations did not permit a rerun of this experiment.

In Fig. 40 the measured currents from Fig. 39 are reduced to charge densities. The same data reduction methods previously described have been applied here. Again good agreement is indicated initially between the microwave interferometer inferred charge densities and the charge densities obtained from the electrostatic probe measurements. The previously mentioned sudden increase in probe current about 15 s after initiation of water injection gives rise to the inferred charge density on Probe C which is unsubstantiated by the other instruments.

Note that the decrease in average charge density after water injection is not as pronounced in the turbulent flame as in the laminar flame experiment. (Compare Fig. 40 with Fig. 37.) This difference is explainable on the basis of shorter droplet residence times in the flame up to the probe station, owing to the increased velocity in the turbulent flame exhaust jet.

c. Electrostatic Wedge Probe

The electrostatic wedge probe consisted essentially of a 30^0 half-angle boron nitrate wedge. The ion-collecting electrode, a 0.150-inch long iridium wire, was located at the wedge leading edge. One side of the electrode was terminated in the insulator; the other end was

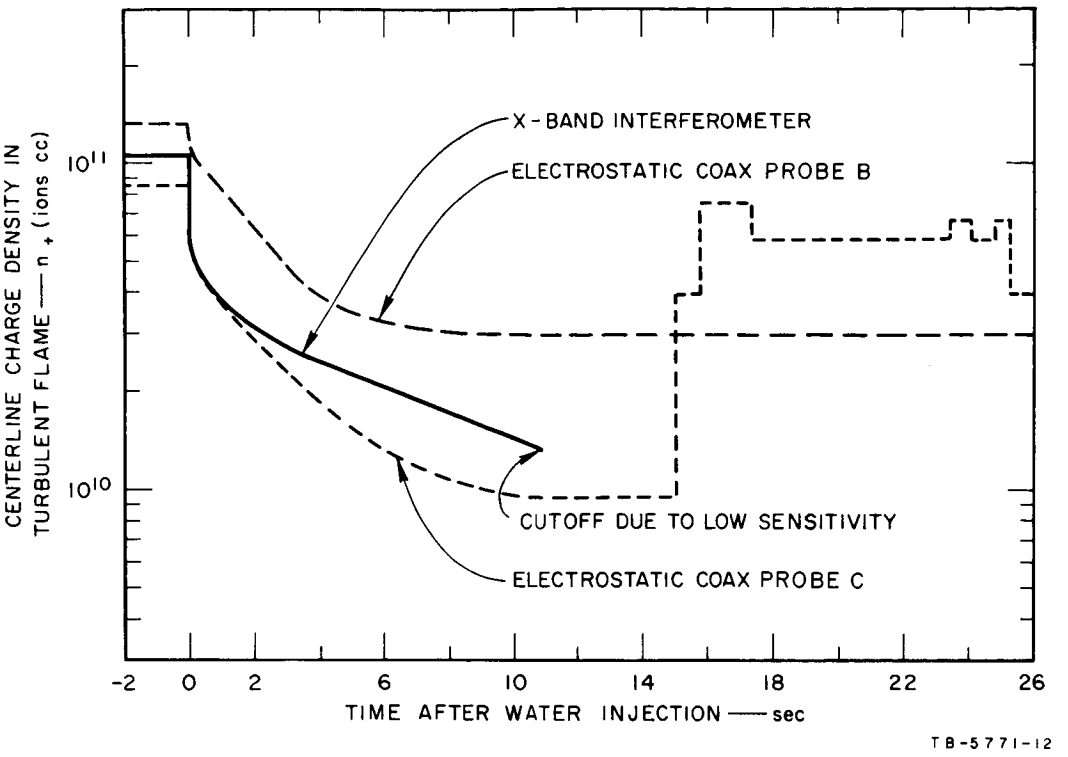

FIG. 40 ABSOLUTE CHARGE DENSITY LEVELS IN THE TURBULENT FLAME AFTER WATER INJECTION AS INFERRED FROM MICROWAVE INTERFEROMETER AND ELECTROSTATIC PROBE MEASUREMENTS

threaded through the dielectric. The second electrode consisted of two stainless-steel plates (shown in Fig. 32), terminating the wedge. The electrodes were separated by a distance of 5/8 inch. The electrostatic probe on the wedge was located in the standard Probe C position. The standard electrostatic Probe B was used as a control for comparison. Since the large wedge cross section in the immediate vicinity of the horns gave rise to significant errors in the microwave interferometer system, the microwave system was not used in these tests.

In the initial laminar flame checkout experiments without water injection, the wedge probe currents were proportional to the Probe B currents, but in the turbulent flame experiment the wedge probe behaved quite differently. In the hot laminar flame, the constant of proportionality between the wedge-probe and Probe-B currents was related to the differences in probe geometries, and as long as no leakage currents due to probe heating were present, the proportionality constant did not

vary. In the cooler turbulent flame, without water injection, the wedge-probe current would decay with time, as evidenced in Fig. 41.

Note the decay of the initial wedge-probe signal, relative to the steady level of Probe B. (Only the relative current levels should be considered here, since the capacitor followed the top envelope of the fluctuations rather than the average current level.) The decay of the wedge probe signal has been attributed to potassium salt condensing on the cold probe. As soon as the water spray is turned on, the wedge probe signal increases, indicating that the salt deposit on the probe has been washed off. This phenomenon was quite repeatable and constitutes another verification that water is impinging on the probes.

To keep the writing pen from splattering ink over the paper as it recorded the rapid fluctuation due to flame turbulence, 20-μf capacitors were connected across the recorder input terminals before the water injection was initiated. This permitted only the dc signal level to be recorded. Note that the beginning of the trace is made at a writing speed of 1 mm/s, and that the writing speed was increased to 25 mm/s once the capacitors were removed. The initial changes in Probe B current level are due to sensitivity changes, to prositioning the probes in the flame, and to removal of the probes from the flame in order to check zero current level. Once their water injection was initiated the probes were left in place.

In the turbulent flame, the temperature at the wedge station is about 1000^{o}C, and the large mass of the wedge never heats up sufficiently to prevent condenstation of the flame seeding material. To check this theory, the wedge was first heated in a hot laminar flame ($\sim$1500^{o}C) and then switched to the colder turbulent flame. The resulting probe response corresponds more nearly to the expected response characteristics as shown in Fig. 42. Upon water injection, the wedge response indicates a small initial decrease in signal level, followed by an increase to slightly higher than the initial level, from where the signal subsequently decays. Note that the wedge probe follows the standard Probe B rather closely with respect to relative response characteristics. If the heated wedge probe is left in the turbulent flame without water injection, the

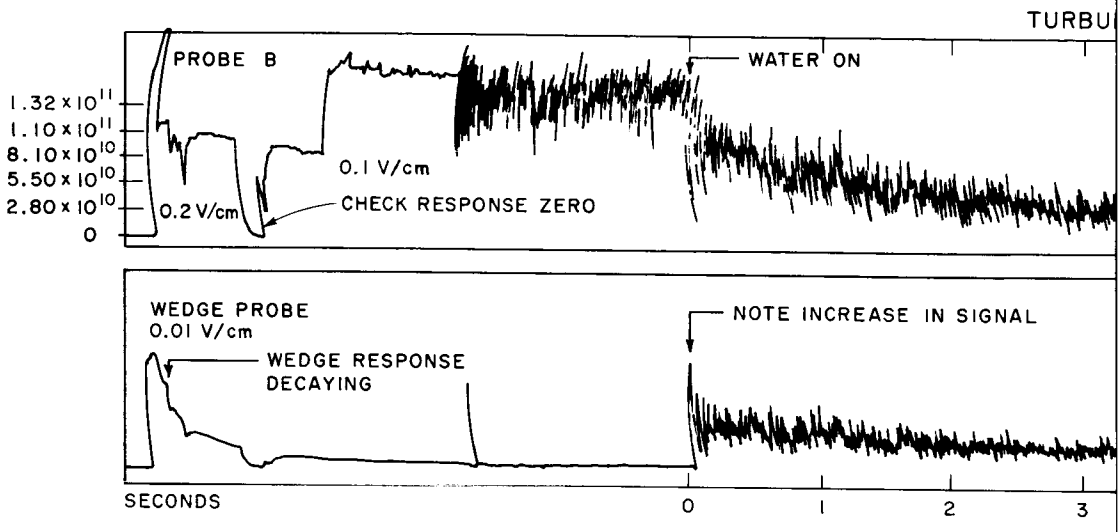

FIG. 41 EFFECT OF POTASSI
CONDENSING ON THE
IN THE TURBULENT
($P_\infty \sim$ 10 Torr, $U_{max} \sim$

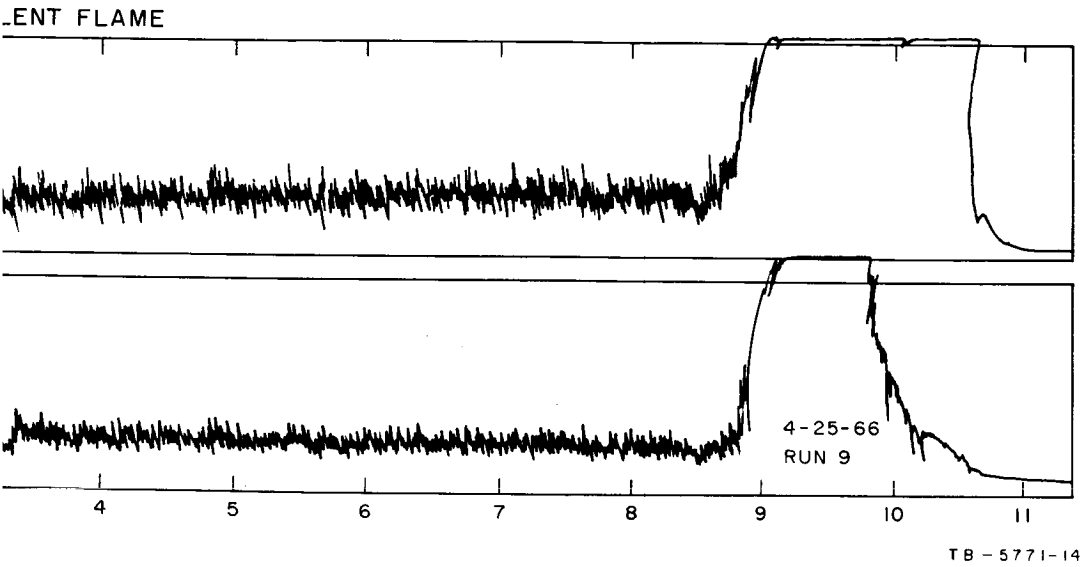

JM CHLORIDE VAPOR
UNHEATED WEDGE PROBE
FLAME
230 m/sec, P_{inj} = 300 Psij)

FIG. 41

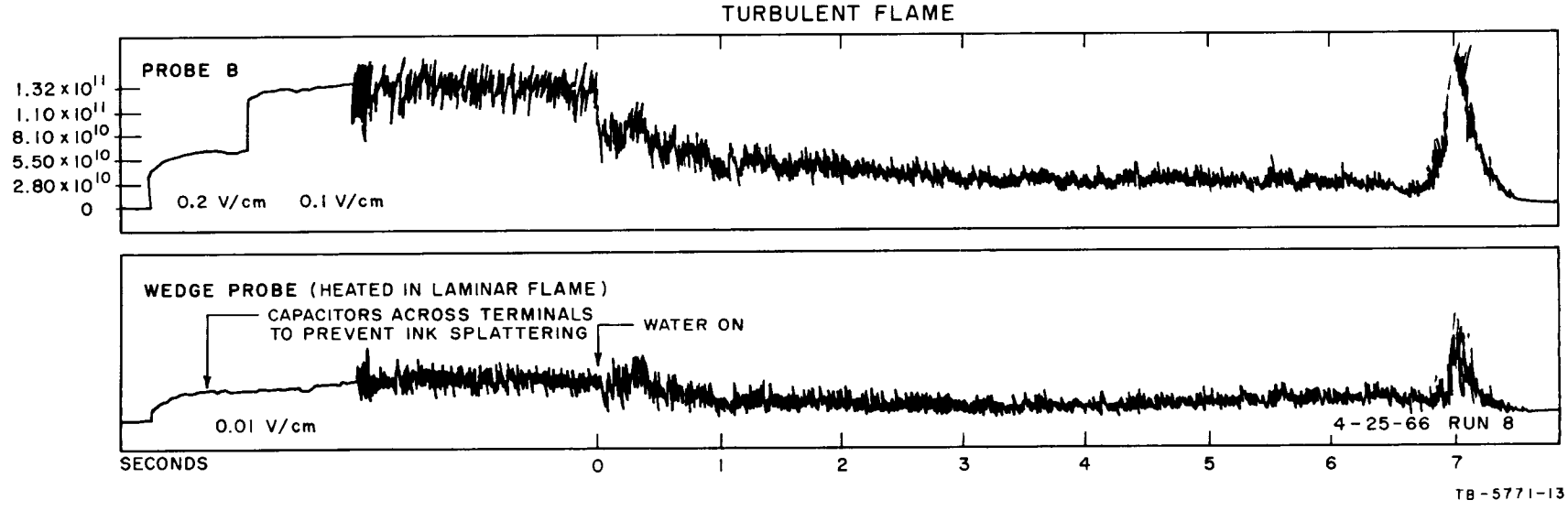

FIG. 42 TURBULENT FLAME RECORD, DISPLAYING ELECTROSTATIC WEDGE PROBE RESPONSE ($P_\infty \sim 10$ Torr, $U_{max} \sim 230$ m/sec, $P_{inj} \sim 300$ Psig)

signal level will eventually decay again. In Fig. 43 the relative responses of Probe B and the wedge probe are shown superimposed. Note the close agreement.

None of the wedge probe experiments exhibited any pronounced short circuit, although the wedge probe current generally seemed to increase relative to the Probe B current after about 5 s of water exposure. This phenomenon could not be sufficiently explained a priori. The injection water used was standard tap water, which was found to be highly conducting.

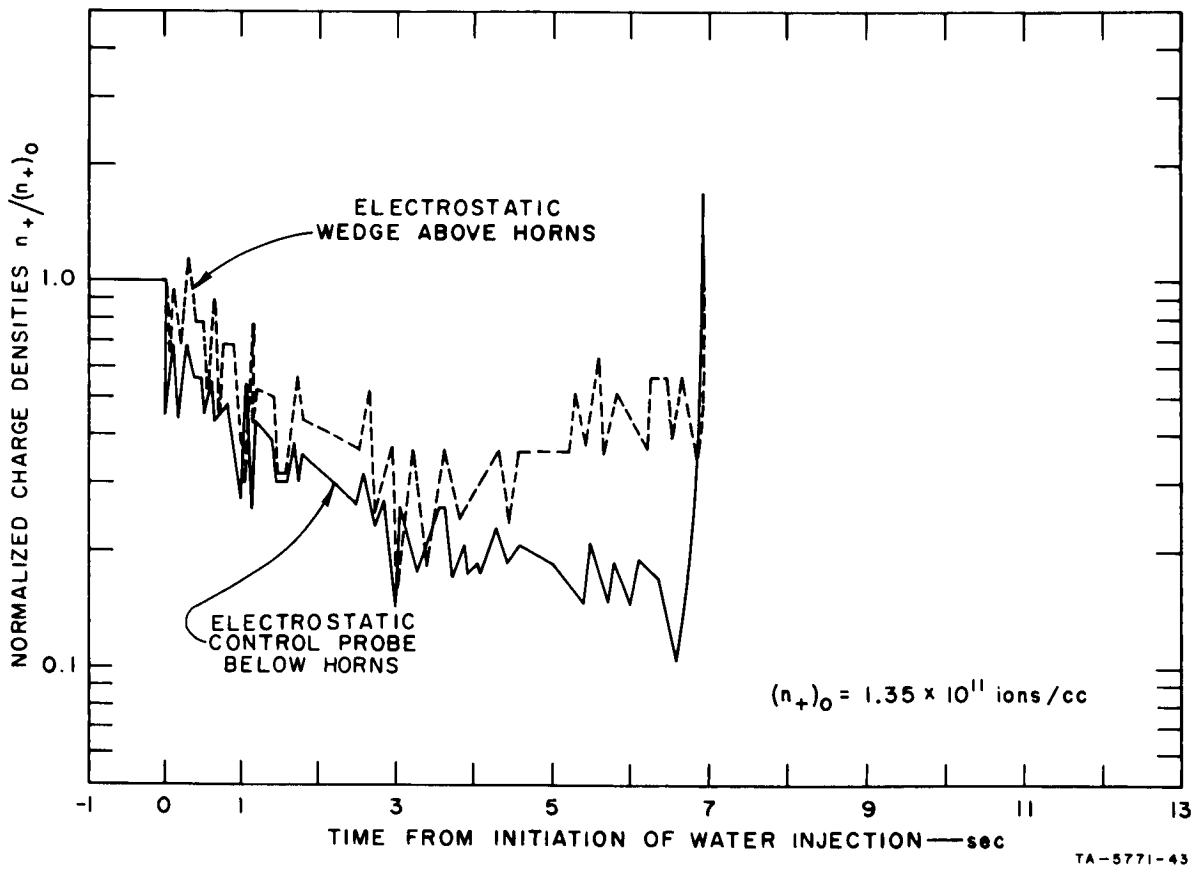

FIG. 43 ABSOLUTE CHARGE DENSITY LEVELS IN THE TURBULENT FLAME AS INFERRED FROM THE CYLINDRICAL AND WEDGE SHAPED ELECTROSTATIC PROBE ($P_\infty \sim$ 10 Torr, $U_{max} \sim$ 230 m/sec, P_{inj} = 300 Psig)

In Fig. 43 the normalized wedge-probe inferred charge density as a function of time is compared to the normalized Probe B response. Since the presence of the wedge probe did disturb the operation of the microwave interferometer system, the latter was not used in these tests. For Probe B the normalization charge density before water injection was 1.35×10^{11} ions/cc, while for the wedge the normalization charge density before water injection was estimated to be 4.55×10^{10} ions/cc. Comparison with cylindrical probe response in the same vicinity as the wedge probe indicated that the wedge probe reading was low by about a factor of 2. However, looking at the relative response characteristics, it is evident that the wedge probe response is in excellent correlation with the response of electrostatic Probe B. After about 4 s of running time, a slight increase in average inferred charge density is evident in the wedge probe but is not indicated by the Probe B. While this rise may represent some type of leakage current, the difference in probe current (see Fig. 41) is so small that no conclusion can be drawn.

D. SUMMARY AND CONCLUSIONS FOR WATER INJECTION EXPERIMENT

A preliminary investigation of the effects of adding water spray to a plasma on the operational characteristics of electrostatic probes has been completed. The limited time of four months for this phase of the experimental program necessarily restricted the scope of the work to observations of gross phenomena. The experiments were carried out in the exhaust jet of a seeded hydrocarbon flame at 10-torr ambient chamber pressure. The exhaust jet charge density was kept to around 10^{11} ions/cc in all experiments. The water mass flow rate incident on the probes was about 0.3 gr/cm^2/s. Three types of electrostatic probes were tested:

(1) A single cylindrical electrostatic probe with the burner as the second electrode

(2) A coaxial electrostatic probe with the outer cylinder as the second electrode

(3) A wedge type of electrostatic probe with a 0.01-inch-diameter iridium wire at the leading edge as the ion-collecting electrode and stainless steel plates at the sides of the wedge as the second electrode.

In all experiments except the wedge probe series, a microwave interferometer system provided a check on electrostatic probe operation.

The experimental results led to the following conclusions:

(1) The electrostatic probes do indeed intercept a significant amount of water flux. This conclusion was based on the following observations:

   (a) Cold-flow tests showed that the electrostatic probe at the spray center would be completely water-coated in a matter of seconds. The introduction of a cold oxygen gas flow having about the same velocity on the flame did not change this condition.

   (b) Rapid color fluctuations on the glowing electrostatic probe after the introduction of water spray into the laminar flame have been attributed to water impinging on the probe and flashing into vapor. The probe color changes are too rapid to be caused by simple heating or cooling conditions.

   (c) The wedge probe response decayed to low levels in the uncooled turbulent flame, presumably because of salt condensation on the probe. Immediately upon water injection, the wedge probe response increased to normal levels, indicating that the salt had been washed off.

(2) In only one experiment with coaxial probes (with both electrodes in close proximity and after prolonged water exposure) did we observe probe behavior which could possibly be attributed to the water droplets shorting the probe. In all other experiments the electrostatic probe results agreed well with the microwave readings.

(3) The addition of water to the flame substantially reduced the flame charge density at and beyond the water injection station. Typical recombination times to reduce the flame charge density by one order of magnitude were observed to be on the order of 2 ms.

(4) In both the laminar and turbulent flame experiments, excellent correlation in the relative responses of the microwave interferometer and the electrostatic probes was evident. Since the microwave interferometer system is sensitive only to changes in electron density, this result indicated that the response fluctuations represented variations in flame charge density.

As mentioned in Sec. IV-D, the operation of the electrostatic probe in a two-phase plasma flow depends on the actual magnitude of at least three parameters--the droplet concentration, the probe heating rate, and the interelectrode spacing--and in addition, probably the probe and liquid materials as well. In view of the limited scope of the present experiments, they cannot be considered conclusive, and further research on the subject is desirable under improved experimental conditions.

In particular, with respect to the RAM-C vehicle, it would be of interest to extend the present experiments to an air plasma environment. Also, the experimental probe environment should be varied over a larger range; i.e., variations of the liquid droplet concentration, ambient gas density, and flow Mach number should be systematically varied. In addition, independent experiments investigating the ion-electron recombination processes in the presence of liquid droplet coolants should be carried out.

V CONCLUSIONS

As a result of the work described in this report, a number of conclusions may be drawn:

(1) The RAM-C probe will give ion currents that are very similar to those obtained from a 10-mil-diameter cylindrical wire probe. Even at altitudes where shocks will form around the probe structures the two sensors agree to a factor of 2.

(2) Yaw angles up to 15 degrees produce negligible effects on the RAM-C probe ion current.

(3) For the RAM-C structure, the effect of changing the leading-edge angle with respect to the flow, from 90 degrees to 45 degrees, produced no changes in ion current that could not be handled in the theoretical analysis of wire probes in supersonic flow.

(4) Assuming that during the flight the gas density near the RAM-C probe is three times the ambient density, the probe currents can be interpreted using the free-molecular analysis presented in Sec. II down to altitudes of at least 170 kft. Accuracy will be better than a factor of 2.

(5) The probe operation at lower altitudes, where a stagnation region forms around the leading edge of the RAM-C probe, depends upon the state of the gas. If the gas is out of equilibrium such that the electron density is much higher than the equilibrium value, then the free molecular analysis will apply with errors of no more than a factor of 2. However, if the gas is in equilibrium, the free molecular analysis can lead to errors as large as an order of magnitude.

(6) Free-molecular theory can be used to interpret probe currents even when the probe radius is about three times neutral-neutral mean-free paths and when there are many collisions in the sheath. This result was obtained when the Mach number was between 2.5 and 3.5. This is a quite different result than would be obtained if the flow velocities were very small.

(7) Electron temperature measurements can be made using free-molecular equal-area probe theory, even when the probe is much larger than the mean-free path. When shocks form around the probe, the probe will measure the electron temperature of the electrons behind the shock.

(8) Probes with wedge-shaped electrodes can be used to measure the electron density in accordance with a simple theory interpreting the measured currents, even when the probe is large compared to the mean-free path. The assumption of frozen compression across the attached shock formed around the probes has been examined and shown both at initial shock-tube pressures of up to at least 1.0 torr. In the nonequilibrium flow at the rear of the RAM vehicle, it is likely that the frozen compression assumption will be appropriate. This type of probe will give more easily interpretable data than either a 10-mil wire or the present RAM-C probe at altitudes which correspond to $p_1 = 1.0$ torr in the shock tube. These probes are easier to fabricate than free-molecular wire probes and collect considerably more current.

(9) Angle-of-attack variations with the wedge-shaped electrode probes can be taken into account quite simply.

(10) The analysis for the wedge-shaped electrodes requires re-examination if ablation contaminants change the dominant ionization process.

(11) The experimental results from the water spray experiments lead to the conclusion that at low ambient pressure, the presence of water droplets does not affect probe operation if the following conditions are met:

(a) The heat transfer from the hot ambient gases is sufficient to continuously supply the electrostatic probe with the energy necessary for droplet evaporation

(b) The electrostatic metal probe has a heat capacity sufficiently large that the energy necessary to evaporate the droplets on contact constitutes only a small fraction of the total energy content of the probe

(c) The time interval between successive droplet impingements is sufficiently long to permit complete evaporation of the initial droplet and reheating of the particular probe segment

(d) The two electrodes are sufficiently far apart that, because of liquid evaporation, it is unlikely a continuous water sheet will be formed between the electrodes.

REFERENCES

1. W. E. Scharfman, "The Use of Langmuir Probes to Determine the Electron Density Surrounding Re-Entry Vehicles," Final Report, Contract NAS1-3942, SRI Project 5034, Stanford Research Institute, Menlo Park, California (June 1965).

2. F. O. Smetana, "On the Current Collected by a Charged Circular Cylinder Immersed in a Two-Dimensional Rarified Plasma Stream," Proc. Third Symposium on Rarified Gas Dynamics, Vol. II, pp. 65-91 (Academic Press, New York, 1963).

3. M. Kanal, "Theory of Current Collection of Moving Cylindrical Probes," JAP, Vol. 35, No. 6, pp. 1697-1703 (June 1964).

4. G. Hok, et al., "Dynamic Probe Measurements in the Ionosphere," Scientific Report FS-3, University of Michigan Research Institute, Reprinted under Contract AF 19(604)-1843 (November 1958).

5. J. G. Laframboise, "Theory of Spherical and Cylindrical Langmuir Probes in a Collisionless, Maxwellian Plasma at Rest," University of Toronto Institute of Aerospace Studies Report No. 100 (June 1966).

6. H. R. Bredfeldt, et al., "Boundary-Layer Ion Density Profiles as Measured by Electrostatic Probes," Technical Report 33, Contract SD-103 under ARPA Order 281-62, Project Code 7400, SRI Project 3857, Stanford Research Institute, Menlo Park, California (February 1966).

7. S. Feldman, "Hypersonic Gas Dynamic Charts for Equilibrium Air," AVCO Research Laboratory, Everett, Massachusetts (January 1957).

8. S. C. Lin and J. D. Teare, "Rate of Ionization Behind Shock Waves in Air; II. Theoretical Interpretations," Phys. Fluids, Vol. 6, No. 3, pp. 355-375 (March 1963).

9. I. Langmuir and H. Mott-Smith, "Studies of Electric Discharges at Low Pressures," General Electric Review, Vol. 27, Nos. 7, 8, 9, pp. 449-455, 538-548, 616-623 (July, August, September 1924).

10. E. O. Johnson and L. Malter, "A Floating Double-Probe Method for Measurements in Gas Discharges," Phys. Rev., Vol. 80, No. 1, pp. 56-68 (1 October 1950).

11. V. M. Zakharova, et al., Zh. Tckh. Fiz., Vol. 30, p. 411 (1960).

12. F. C. Cuddihy, I. E. Beckwith, and L. C. Schroeder, "Ram B2 Flight Test of a Method for Reducing Radio Attenuation During Hypersonic Re-Entry (U)," NASA TM X-902, NASA Langley Research Center, Hampton, Virginia (October 1963), CONFIDENTIAL.

13. W. F. Cuddihy, "Results of the Ram B2 Materials-Additional Flight Experiment (U)," Proc. of the NASA Conf. on Communicating Through Plasmas of Atmospheric Entry and Rocket Exhaust, NASA SP-52, NASA Langley Research Center, Hampton, Virginia (January 1964), CONFIDENTIAL.

14. I. E. Beckwith and J. K. Huffman, "Injection and Distribution of Liquids in the Flow Fields of Blunt Shapes at Hypersonic Speeds (U)," NASA TM-X-989, NASA Langley Research Center, Hampton, Virginia (August 1964), CONFIDENTIAL.

15. H. S. Rothman, "Electromagnetic Scattering from an Extended Laminar Plasma Column," Tech. Report 10, Contract SD-103 under ARPA Order 281-62, SRI Project 3857-5, Stanford Research Institute, Menlo Park, California (February 1963).

16. H S. Rothman, H. Guthart, and T. Morita, "Measurement of the Spectrum of Ionized and Neutral Density Fluctuations in a Thermally Produced Turbulent Plasma," Tech. Report 15, Contract SD-103 under ARPA Order 281-62, SRI Project 3857-5, Stanford Research Institute, Menlo Park, California (April 1965).

17. M. F. Heidmann and H. H. Foster, "Effect of Impingement Angle on Drop-Size Distribution and Spray Pattern of Two Impinging Water Jets," NASA TN-D-872, Lewis Research Center, Cleveland, Ohio (July 1961).

18. M. F. Heidmann, R. J. Priem, and J. C. Humphrey, "A Study of Sprays Formed by Two Impinging Jets," NACA TN-3835, Lewis Flight Propulsion Laboratory, Cleveland, Ohio (March 1957).

19. R. D. Ingebo, "Drop-Size Distributions for Impinging-Jet Breakup in Airstreams Simulating the Velocity Conditions in Rocket Combustors," NACA TN-4222, Lewis Flight Propulsion Laboratory, Cleveland, Ohio (March 1958).

20. R. D. Ingebo, "Study of Pressure Effects on Vaporization Rate of Drops in Gas Streams," NACA TN-2850, Lewis Flight Propulsion Laboratory, Cleveland, Ohio (January 1953).

21. H. H. Foster and M. F. Heidmann, "Spatial Characteristics of Water Spray Formed by Two Impinging Jets at Several Jet Velocities in Quiescent Air," NASA TN-D-301, Lewis Research Center, Cleveland, Ohio (July 1960).

22. H. R. Bredfeldt, "Evaluation of a Light Scattering Technique for Determining the Spray Characteristics of Impinging Liquid Jets," Tech. Report 648, NASA Grant NsG-99-60, Princeton University, Princeton, New Jersey (March 1964).

23. S. C. Kurzius and R. Ellison, "Effects of Water Droplets on Re-Entry Plasma Sheaths (U)," TP-123, Aerochemical Research Laboratories, Inc., Princeton, New Jersey (November 1965), CONFIDENTIAL.

24. D. E. Weissman, W. E. Scharfman, and H. Guthart, "Electrostatic Probe Measurements in a Short Mean-Free-Path Plasma," Tech. Report 1, Contract AF 04(694)-931, SRI Project 5938, Stanford Research Institute, Menlo Park, California (July 1966).